Powder Technology 447 (2024) 120109

Contents lists available at ScienceDirect

Powder Technology

journal homepage: www.journals.elsevier.com/powder-technology

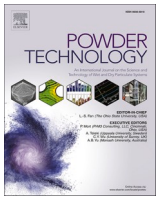

3D-measurement of particles and particulate assemblies - A review of the paradigm shift in describing anisotropic particles

X. Jia [a,*], R.A. Williams [b]

[a] School of Chemical and Process Engineering, University of Leeds, Leeds LS2 9JT, United Kingdom
[b] Heriot-Watt University, Edinburgh EH14 4AS, United Kingdom

HIGHLIGHTS

- Collection of evidence for why and how particle shape matters.
- Review of how shape description and measurement have changed in the past 30 years.
- Review of shape embracing computer models for particulates.
- Review of how AI has helped and speculation of how AI can help in the future.

ARTICLE INFO

Keywords:
Digital imaging
Discrete element modelling
Particle shape
Microtomography
Pharmaceutical dissolution
Packing
Consolidation

ABSTRACT

The goal of seeking advanced solutions to the descriptions of particle shape, packing and tomographic measurement were key areas promoted by Professor Reg Davies. In this paper we review and reflect on the revolution that has taken place over the last 30 years in our ability to describe and measure particle shape going beyond simple shape factors to their real morphologies of complex particles and particulate assemblies. The paper presents a comprehensive review of how shape has been described and some critical analyses in the form of extended tabulations. We show how digital approaches to particle descriptions can be used to predict the properties of particles and assemblies and their use in simulations of particle processing. We note the current status and prospects for the continued development of microtomographic systems to enable the measurement of particle shape in 3D and also the 3D imaging of complex particulate structures to enable property and processing predictions. Examples of these developments and critical appraisal of their utility will be given.

1. Introduction

Size and shape are the defining parameters of particulate materials. As Reg Davies was keen to point out at his numerous lectures, the industry had been making a good use of the single-number quantity commonly referred as 'particle size', starting to cope with particle size distribution (PSD), but having trouble to embrace particle shape information. This was in the early years of the 21st century. There were good reasons for this since commercial shape analysers were scarce in comparison with sizing devices, especially for real-time and/or inline use. Also shape was (and still is) more difficult to quantify by a single number for use in theoretical/empirical relationships and in correlations that underline quality assurance and control in powder handling and production. This is because within the same size range (e.g., classified by sieves), there can be many different shapes in the powder sample; particles can behave very differently depending on their shape; and which single-number shape factor is meaningful depends on what behaviour is of interest. It has long been recognised that for non-spherical particles, the measured 'size' is strongly dependent on how and along which direction the 'size' is measured, so much so that it would be idiotic (to paraphrase Reg's phrase) to talk about particle 'size' without referring to particle 'shape' at the same time! Otherwise, one runs the risk of nonsensical comparisons between sizes. Twenty years on, has the situation changed? The answer is a slowly but surely yes. In this review paper we present a brief and selective account of some major changes – how they happened and what impact they have brought – with an emphasis on computational models.

The foundational years of particle technology placed much emphasis

* Corresponding author.
E-mail address: x.jia@leeds.ac.uk (X. Jia).

https://doi.org/10.1016/j.powtec.2024.120109
Received 18 June 2024; Accepted 17 July 2024
Available online 3 August 2024

on establish robust methods to characterise what were obviously very complex systems. In the 1970s computational resources did not provide a practical basis for more complex approaches to be feasible. The approach was to seek to simplify the systems by reducing complexity through utilisations of equivalency to simpler forms. Shape characteristics were undertaken by equivalency to fixed know shape (sphere, rectangles) and distributions were fitted to convenient logarithmic and other known functions. On this basis classic books [1] and a range of US and British Standards for describing shape and size (described later in the paper), and instruments to measure these, were evolved. Systems behaviour was also taxonomised, for example in terms of the ways powder were fluidised [2–6]. Higher degrees of variations were recognised adopting more complexity science the 1990s with the use of fractal concepts, such as those of Kaye [7]. The famous trio of Davies, Scarlett and Kaye were ardent pioneers for the subject. Their passion and intellect gave rise to a strong academic and industrial legacy. The creation of standard based on simplification did, as is often the case, tend to cause drag on adoption of newer approaches since, naturally, new approaches needed to be calibrated with respect to existing and accepted standards. It may be argued that this has caused slowness of adoption and use of advanced methods presented in this paper, such arguments are not unique to particle science but a reality of engineering practice.

The review covers the following main topics. Section 2 exemplifies why and how shape matters. Section 3 reviews how shape is quantified while Section 4 focuses on how shapes are measured. Section 5 shows how shape info can be used in advanced computer models. Section 6 looks at AI prospect before conclusions in Section 7.

2. Why and how shape matters

It is a cliché to say that size matters. Given the inextricable link between size and shape, it is a fair statement that where size matters, shape too. If 30 years ago this was more a conviction, quantitative supporting evidence has expanded so much, especially in recent years, that, to paraphrase Reg's words again, one would be ignoring particle shape at one's own peril. Examples are abundant of how particle shape affects packing structure of particulates and hence properties that are structure-dependent. Since there are few – if any – properties that do not depend on the underlying structure, it is fair to say that, shape is as fundamental as size in determining particulate and powder behaviours. If we define 'particle' as "any entity that is small in the context or compared to its surrounding" and 'packing' simply as "putting together or arrangement (of particles) in a confined space", the concepts and applications of particle and packing go well beyond the traditional field of powder technology. Table 1 shows some examples where particle shape plays a direct role or an indirect role through its effects on the underlying structures, and also examples where shape affects properties at different levels simultaneously.

Unlike pure solids or fluids, for which scientists and engineers have by the first half of the last century been able to calculate and predict their properties, to a high enough degree of accuracy that design of equipment and plants can be done largely based on calculations and models, even though many are empirical correlations. The same cannot be said for particulate materials, despite that fact that over 2/3 of all industrial products are in this form at some stage of their product life [246]. The complexity and unpredictability are akin to social science in that behaviours of individuals matter, individual behaviours are so varied, causal relationships are often non-linear, and the worst of all, the number of individuals involved is so huge that it is impractical to include everyone with high fidelity in any (computer) model – existing or imagined. The pragmatic way to deal with this situation has been, and likely to continue to be, to focus on a small and manageable subset and hope that the subset is in a meaningful way sufficiently 'representative'.

For particle sizing, the concept of "equivalent size" makes size-related applications and comparisons easier, because the underlying shape is sphere – the most computationally friendly shape for particle-level analysis and modelling. There is no such concept as "equivalent shape", however, because if size was fixed, equivalent shape could be anything but spherical and it would only complicate things even further. If all particles were of the same shape, say spheres, the complexity and unpredictability would be lessened by many orders of magnitude. Given the importance of particle shape and its less-developed status quo (compared to particle size), it is perhaps fair to call particle shape a (if not the) last frontier of particle technology (**PT**).

3. Shape descriptors

Even twenty years ago, by some account (the authors of this review paper collected and counted shape descriptors in preparation for a training course on particle shape) no fewer than 100 shape descriptors had been proposed in publications. This is far more than the number of 'sizes' in use, and is a reflection of two facts. First, shape was (and still is) far more complicated and involved to quantify than size. Secondly, there was no standardised approach to *quantitative* shape description, everyone could define their own shape descriptors for the problems at hand if existing ones were deemed not fit for purpose. As a result, and for example, there are half a dozen definitions of "roundness" alone (see Table 2) and even more definitions of "sphericity" [247]. Note that some standards had been in circulation for qualitative terms (i.e., words) to describe shapes (see Table 3).

In fact, most of the shape descriptors used for powder particles today came from two groups outside the PT community: the geologists and the computer graphics scientists. They had the needs and, more importantly, the convenient means to do so. For example, geologists can often hold and measure the real and physical samples by hand; while computer scientists can have the virtual samples as computer graphics/images and of course the software to work with [338,371–379]. Since then, some new shape descriptors have been proposed [62,380–382]. Broadly, a descriptor describes shape at one of three scales, or level of details: the overall form, roundness/angularity, and surface texture/roughness, as indicated in Fig. 1. Table 2 categorises and summarises some of the shape descriptors. It is not meant to be an exhaustive list, the aim instead is to show diversity and variety. And wide diversity and variety are characteristic of a discipline still in its infancy.

Regarding the purpose and use of shape descriptors, four colloquial views are common:

1. *Why bother at all, just use a nominal size*. Such a view was prevailing among some practitioners, and indeed computer modellers, in the early days. Not because they did not realise the importance of shape, but more out of frustration for lack of convenient tools to make use of shape information.
2. *The actual shape is unimportant, all that is required is a number for comparison purposes*. This is a common, and valid, view among designers and users of process controls. Indeed, so long as a well-behaved correlation can be established, the relationship between the target and the control parameter need not be a causal one. Many publications on shape factors are in fact devoted to establishing correlations between shape factor(s) and properties of interest [382,62].
3. *It should be possible to regenerate the original shape from the descriptors*. People with this view tend to be computer modellers dealing with computer graphics, image processing and particle level simulations who can use a relatively small set of descriptors to recreate the original shape, and its variants.
4. *Why bother with shape descriptors, just use shapes as they are measured*. This view is held by the authors of this paper in the context of using 3D digital images as input to particle simulations (more details in Section 5). This is akin to using PSD: use of PSD makes mean size redundant since it is embedded in PSD.

The above list is broadly in chronological order. Examples for

approaches 2 and 3 are given in Table 2.

Many shape descriptors are calculated based on analysis of digital images. It should be emphasised that shape descriptors calculated from 2D projections can be very different from those calculated directly from 3D measurements of the same objects, although the two are often correlated [384–388]. It is easy to see why with an example: a cylinder's 2D projection can vary from circle to ellipse to pill-shape to rectangle; light scattering pattern depends on orientation of the cylinder at the time of measurement; and unless the cylinder is travelling in vacuum particle-fluid interaction means that the cylinder has a tendency to adopt a particular orientation while passing the sensing zone, e.g., parallel to the main flow in laminar flow regime and perpendicular in turbulent regime. Shape distribution in the same sample may be size dependent and the relationship can be indicative of the provenance, history and method of production of the sample (e.g., [389,390,391]). It should also be realised geometrically shape descriptors are invariant under translation, rotation and scaling but precise values of descriptors (and perimeter or surface area) calculated using (either 2D or 3D) image analysis (**IA**) obviously depend on the resolution (in other words, particle dimension measured in pixels or voxels) and, as a result and to some extent, on orientation of the shape in an image [392–398]. For example, a 3-pixel triangle cannot be treated as anything other than an equal sided right-angle triangle, regardless of the true shape of the particle or a spike in the particle's surface contour the 3 pixels represent. For this reason, manufacturers of particle sizers usually recommend a threshold (e.g., at least 5 pixels across) to reduce the impact of small ambiguous clusters; for shape analysis even larger threshold values (e.g., 20–50 pixels) have been suggested [399,400]. In practice, the threshold is obviously dependent on the shape and method of analysis. So long as the method (including shape representation, dimensionality and resolution) is consistent, the results are compatible and comparable.

When simple shape factors are used, there is usually a significant loss of information. A factor can only represent one aspect of the shape. Another problem is that for a given shape factor the same value may be obtained for widely different shapes. Hentschel and Page [401] have suggested that at least two shape factors are required, one for form (e.g., aspect ratio, $\frac{D_{min}}{D_{m}}$ne for surface texture (e.g., surface factor, $\frac{4\pi A}{P^2}$). Each is sensitive to a different attribute of shape: elongation and ruggedness. Many more [24,371,383,382,196] favour classification of shape descriptors into the three scale-dependent categories (i.e., sphericity for overall shape at large scale, roundness for corners at intermediate scale, and roughness for surface texture at small scale) or even four categories [385]. One from each category, or some combinatorial approach, should be used.

While there have been a long list of international and national standards for particle sizing [402], some progress has been made towards standardisation for shape description and only in specific areas. Table 3 lists some of the standards for particle shapes. It is worth noting that these standards are meant for some specific industries or materials, and their emphasis is on standardising the method, apparatus and procedure of measurement. This fragmented nature of the standards is again a reflection that shape is far more complicated and involved to quantify than size. This situation is likely to remain until, perhaps, advancements of advanced mathematical tools such as mathematical morphology [349,374,403–407] can give us a more unified way to describe all shapes.

In particle sizing, the question how many particles need to be measured for the obtained PSDs to be reliable and stable is usually answered by the equipment manufacturers (as the minimum amount by volume or weight) if the equipment is a purpose-built particle sizer. Various standards also recommend such numbers for different situations or applications and the minimum number is usual several hundreds. Lopez-Sanchez [408] demonstrated that the arithmetic mean, which many users so often automatically quote to report their results, may not always be the best one. For a specific application, when the means are correlated to some other property of interest and compared, the answer can reveal itself (e.g., [409]). The same questions are also legitimate for shape distributions, but the answers are far from being clear. The second question, which for shapes becomes which shape factor to use, is less of an issue because the user must make a conscious decision anyway since there are so many to choose from and none of them is a standard. To the first question, there is no standard answer although the number is likely to be higher than for sizing (10^3 vs 10^2). A pragmatic answer is to keep analysing more until the distribution curve no longer changes, or a preset statistical confidence is reached. In one example [410], 500 was quoted as the minimum and 1000–1500 was "the best". In another example [411], >6400 particles per sample were measured to obtain a 99% statistical confidence; this number is 10 times more than the usual for sizing. This is clearly tedious and time consuming but nonetheless robust.

One noteworthy use of shape descriptors is to help generate, either randomly or parametrically, a large number of model particles that retain certain pre-defined shape characteristics of the original real particles (or their packing structure) for simulations [277,412–419]. Fig. 2a & 2b show some examples. Thus, between the two extremes of using spheres for everything and using real shapes for all in the particle assembly [420], there is a mid-way house approach which is realistic to some degrees, yet fast, easy and free of noises often present in real-shape measurements, and hence currently more commonly used. It helps us to study shape effects through simulations [421–424]. Parallel to computer simulations, 3D printed model objects satisfying pre-defined shape descriptors and other properties have been used to study shape effects [425,46,426,427,184].

Like particle size, shape factors are often used for product quality control [438–446]; as part of product design and specifications [447–450]; and for industrial or medical diagnostic purposes [62,451–454].

4. Shape measurement techniques

Traditional shape factors such as aspect ratio and sphericity, and indeed sizes such as Feret diameters, also tended to originate from geologists – people dealing with rocks and pebbles – because they could easily hold, examine and measure the samples by hand. For powder technologists, their samples are small and they frequently have to resort to microscopy (optical, SEM or TEM) to examine the particles, thus shape descriptors they proposed tended to be image based to describe 2D projection areas. The issue of normalising the measured parameters according to the number of particles measured vs weight or volume is also key. The literature has examples of researchers who may use a descriptor sourced from particle counting and trying to compare with one derived from averaging volume, for which the results are very different. Later on, since the turn of the 21st century, X-ray CT technology allowed small particles to be scanned and reconstructed in full 3D, so characterisation can again be based on 3D forms. More recently, various 3D cameras or scanners have come on the market and be increasingly used to characterise 3D objects from a few mm upwards, they are not perfect but is the best thing one can hope for when imaging objects in-situ and in (almost) real-time. Examples of CT and laser scanned objects are given in Fig. 2c & 2d. and Table 4 summarises measurement techniques and associated shape descriptors.

It can be seen that particle shape characterisation has experienced three stages: it started with direct measurements of large 3D physical objects, then moved to analysis of 2D projections or images of small particles, and now coming back to computer aided measurement of 3D virtual objects (or reconstructed 3D images). From 3D to 2D back to 3D again, it is not exactly a full circle, but a spiral-up in terms of measurement techniques.

Computer modellers require real 3D shapes to be readily available in convenient formats, AI and advances in measurement technique and hardware make this possible. Therefore, it can be expected that the trend

of moving away from spheres towards using real/realistic particle shapes in computer models will continue. Section 5.1 demonstrates this trend, and shows that there is ample room for this trend to grow.

In the UK, the CCPi (Collaborative Computational Project in tomographic imaging) (https://ccpi.ac.uk) has been ongoing for years, providing access to CT scanners or synchrotron beamtime, user training and more importantly development of software toolbox (CIL – the open-source Core Imaging Library) for reconstruction and data analysis and visualisation. A similar CT user network NoCTURN (Non-Clinical Tomography Users Research Network) (https://nocturnetwork.org) exists in the USA. Its website maintains a list of CT labs around the world and the number currently (May 2024) is 197, and >80% of which are in Europe and North America. This is likely to be a fraction of the actual number. In the UK, in 2001 there were single digit number of CT machines for non-medical use, now the number is around 100. This is a reflection of how popular and commonplace CT has become as a means of material characterisation.

5. Shape-embracing computer models

5.1. General trends

With regard to particle shape, the advancement of shape-embracing computer models dwarfs the progress in the uptake of shape information in other areas (e.g., industrial control/production of particulate materials). Two snapshots of publications in the journal of Powder Technology from 2003 and 2023 can be used to illustrate the trends. When searching for a specific term, "shape" in this case (entered in two fields in the search form, "Find articles with these terms", and "Title, abstract or author-specified keywords"), on the journal's website, we have the following results. The search produced 30 articles from 2003 with only one paper containing the word "shape" in its title, whereas there were 103 hits from 2023 and 14 with titles containing "shape". Details are summarised in Table 5 below. In the table, "particle shape" is used to encompass form/morphology and surface roughness/texture of solid particulates, bubbles and even pores in structures made of particulates. Other quoted terms (namely, "characterisation", "modelling" and "effects") have particle shape either as an input (i.e., particle shape being a determining factor of a property) or as an output (i.e., particle shape or change in particle shape is a result of variations of process conditions). The statistics contain overlaps: a paper may appear simultaneously in more than one category, although most do not.

The trends are clear from Table 5. First, the number of publications pertaining to particle shape have quadrupled in the past 20 years, from 19 to 81. The increase in simulations that involve non-spherical shapes is even more dramatic, nearly 7-fold, from 6 to 41. There is also an increasing trend to investigate effects of particle shape on properties of interest by means of computer modelling. Indeed, most modelling papers were not about developing a model's capability to handle irregular shapes, but about using particles of more realistic shapes when simulating a behaviour or calculating a property. As we shall see later (Section 5.2), the number of computer models capable of dealing irregular shapes has not actually changed, only the popularity of some has increased, mainly in the form of commercial software packages.

The most notable change is the number of DEM simulations that use non-spherical shapes. In 2003, there were 9 DEM papers in Powder Technology, only one of which [550] used irregular shapes; in 2023, there were 160 DEM papers in the same journal, at least 26 of which involved non-spherical shapes. In percentage terms, however, the change is much less dramatic, 11% vs 14%. In a 2016 survey paper, Windows-Yule et al. [73] showed statistics, obtained from Google Scholar using keywords "discrete element method" or "discrete particle simulation", of DEM publications: In 2006 the number was close to 1000 and in 2014 just over 3000. Using the same search keywords for 2023, the number of hits is 10,475 (excluding citations and patents).

DEM (Discrete Element Method) [551], as the method of choice for particle-level simulations of particulate systems, has seen some notable advances. There appears to be a race towards realism in the following terms:

- Scale – Instead of thousands, it is possible to run DEM simulations with 2.4 billion particles (identical spheres of 100 μm diameter, in a real-scale, 1 m × 1 m × 2 cm, sandbox experiment) [552]. Real-time or quasi-real-time DEM codes that run on GPUs were developed soon after GPUs had showed their potentials for general purpose computations [553–556]. GPU based DEM simulations are very common now, routinely involving 10^5 or more particles and often of irregular shapes [557–559]. However, not everyone can afford, or have access to, the computing platforms and specialist software capable of fast handling so many particles. Thus, a more common approach to scale up is by coarse graining (or upscaling). Essentially, this approach uses a larger (super) particle to represent a group of smaller ones so that the number of (super) particles stays within a manageable range while simulating a dynamic process at a scale otherwise unattainable or too slow [560–565]. Like using equivalent-size or multi-sphere approaches for non-spherical shapes, upscaling is also using one thing to represent something else it is not, thus compromises must be made. There is no single standard way to upscale – how many smaller particles a super particle can represent, what properties or behaviour to preserve when deciding coarse graining parameters and how to calibrate are all case dependent and the choices can affect accuracy of the results [566–571]. Regardless of shape representation methods and computer models, it remains a challenge to simulate systems involving a very large (>1000) size ratio (e.g., refractory materials and concrete consisting of cement, sand and aggregates, with a size ranging from nano to cm, and with chemical reactions).
- Shape – The change, in both speed (of adoption) and variety, from sphere-only to irregular shapes has been dramatic in recent years. The need to cope with irregular shapes has also seen a rise in popularity of non-sphere based DEM simulators, as shown in Table 6. How shape is represented (Fig. 3) is fundamental as it has an impact on different aspects of the computer model, from shape fidelity, contact/overlap detection algorithm, coding complexity, run time or speed, to parameter calibration, and finally accuracy of the simulations [572–580].
- Multiscale morphology – Surface roughness has now been explicitly incorporated in DEM simulations for rough walls [581–583] as well as rough particles [584,585,421,586].
- Multiphysics – In addition to dynamic mechanical behaviour, other physical properties or effects of particles are being incorporated such as heat transfer [587,40,588] and charge transfer [589,590,591]. Most commercial and open-source DEM codes have some Multiphysics capabilities. The coupling of DEM with another computer method, chiefly CFD/FEM but also LBM/FDM, to model beyond spheres is on the rise [592,593], to incorporate in more detail of inter-particle forces and particle-fluid interactions [594–601], dissolution of moving particles [602–604], etc.
- AI involvement – AI is being used in several aspects of DEM type particles simulations, including drag force and terminal velocity estimations, collision/overlap detection, and possibly non-spherical shape reconstruction (see Section 6 for more details).

Extrapolating the above advances, and assuming computing power (or more importantly accessibility of the high computing power) is increasing at the current rate, with the help of AI to tackle the most time consuming parts of DEM modelling, including shape generation and reconstruction (see Section 6), contact/overlap detection (e.g., [563]) and estimation of contact force and drag force (e.g., [773]), it is not difficult to imagine that 10 years from now, simulations with real particle shapes will be as common as, if not more common than, the sphere-only ones. Therefore, the so-called last frontier of particle technology will have been broken down.

Quantum computing is particularly suited to many-body problems [782], albeit at present only of quantum-scale particles. Quantum-inspired laser computing is reportedly even more effective than both GPU supercomputing and quantum computing for some specific computational tasks (e.g., matrix multiplication, sorting through combinations) [783]. It may just be possible that one day equal-sphere based DEMs can, following the success story of GPU based DEM, be portable to run on quantum or optical computers.

5.2. Comparison shape-embracing computer models

Computer models capable of incorporating particle shape (among other particle properties) are broadly divided, by way of how particles are moved, into two groups: deterministic and stochastic. The former, which includes DEM, is by far the largest and typically for simulating a dynamic (time-dependent) process. Models can also be grouped according to how particle shape information is represented or incorporated in the model. It may be implicit or "unresolved" (e.g., DEM can use rolling friction for spheres to mimic in certain aspect the behaviour of non-spherical particles) or explicit or "resolved" (i.e., particles actually have non-spherical shapes). Table 6 shows pros and cons of different models in the context of simulating dynamic and quasi-static behaviours, formation of packing structures and structure-property relationships of particulate systems.

6. Prospect of AI

AI is making waves in every field of research and to everyday life, particle shape characterisation is no exception. Thus, no review can be complete without a look at AI contributions. The emphasis of this section is on shape recognition and reconstruction, leaving out AI generative design and content creation involving particle shapes (e.g., [416,784]) or AI property prediction based on shape/size metrics (e.g., [785]).

Using AI for face recognition/reconstruction is maturing and a major success story for AI [786–789]. There are billions of people, each with a distinct face. Face recognition has two parts. The first part is to tell a human face from the rest in a photo, this is equivalent to recognising a particular shape/texture from any other shape/texture in images of particles. The second part is to attach an ID to a face. An equivalent of this part is doing detailed shape/texture calculations about the particles. Comparing to the task of particle shape/texture recognition, face recognition is perhaps an easier task in the sense that all (normal) human faces conform to one basic template (i.e., the shapes and relative sizes of face outline, two ears, two eyes, one nose and one mouth are well defined), but the legal consequence of wrong identification is much more serious. Apparently, there are several quintillions (10^{18}) of sand grains [790], probably many times more particulates, on Earth. Strictly speaking, no two are identical in every aspect. However, precision and accuracy required for particle shape/texture recognition may be much less than required for human face recognition because the purposes are different. Also, AI does not need to recognise something in order to reconstruct it. It is therefore hopefully that a similar success can be expected for particle shape recognition, provided that sufficient and similar effort can be put in. AI developed for other disciplines or applications [500] could well be adaptable and useful for particle shape and structure.

Table 7 gives some examples of using machine learning (ML) for shape recognition and reconstruction. None of them is ready-to-use for powder particles but they show potentials and inspirations for the shape of things to come.

For computer modellers, a dream has been that putting a pinch or handful of particles (deemed enough for a typical particle-level simulation) through a machine, by the time the particles pass through and come out of the machine, we would already have them characterised and reconstructed in full 3D, ready for use as input to our models. In principle, it is possible for a parallel CT setup with hardware reconstruction to achieve this in real-time. An example for large objects is 920 CT – a RTT® (Real-Time Tomography) device for airport security (RapidScan [844]). However, the cost would simply be too high for routine particle shape measurements. On the other hand, most image-analysis (IA) based particle sizers can capture and analyse thousands of particle images in a matter of seconds (i.e., as good as real-time). Can such images be used to reconstruct the particles in 3D? Mathematically, a key difference between CT projections and particle sizer captured images is that the former are from known or preset angles but the latter are unknown or random. Nevertheless, looking at the images before the shading/texture information is removed (e.g., Fig. 4a), human eyes and brain can often form a good idea of what the particles look like in 3D, although human brain is not as good at assigning precise values to describe the shapes. If the former ability is acquired through a machine vision technique such as SfS (shape from shading) and/or ML (machine learning) (as exemplified in Table 7), and the latter is automatically taken care of by the use of computers (since the computer assigns numbers to everything it works on), it may be possible, to use AI to reconstruct 3D shapes out of the images captured by existing particle sizers. Then, the computer modeller's dream is realisable in the foreseeable future!

7. Concluding remarks

The review suggested a number of conclusions that embrace practical actions, cautions and opportunities, as follows:

The speed of advance has been remarkable in the last decade: At fundamental and methodology levels, none of the advances reviewed here has come as a surprise, since they all existed 20 years ago. However, the speed at which the advances, especially in tomographic imaging and GPU assisted DEM, have been taken up and applied in recent years is nothing short of 'astonishing'.

Shape description and its application is diverging rather than converging: On the one hand, it continues to develop along the conventional path of determining explicitly one or a few numbers to describe shapes for a particular purpose (e.g., for comparison, product specification, quality control, etc). On the other hand, with the help from AI and increased computing power, image based recognition and/or reconstruction of shapes are expected to be used more and more. The latter does not require preexisting and explicit shape factor values to work, the required statistics can be obtained from raw input data through an AI tool trained for a particular purpose.

Forward facing standards that embrace modern digital standards are needed: One might argue with the diversity of approaches enabled by digital methods there is a need to revisit the issue of modern digital standards for shape definition for industrial application. The situation with standardisation is likely to remain for the foreseeable future, but new mathematical tools (e.g., mathematical morphology) and/or increased prevalence of simulations involving real shapes, may give rise to fresh ways to characterise shapes such that standardisation may be possible.

New and/or faster measurement techniques can be expected to continue to appear: For example, femto-photography, with its trillion frames per second camera, can capture the light as it travels [845,846], and has been demonstrated to be able to capture and recover 3D shape around a corner (i.e., out of the direct line of sight, using light reflected off walls/obstacles). It is conceivable that one day such technique could be used to validate contact force models by imaging an evolving particle contact at a single DEM time step ($\leq$ nano-second) level.

Sphere based DEM models will continue to dominate and scale-out: For example, EDEM and PFC-3D are expected to expand in the range and scale of applications and the use of sphere-composites for non-spherical shapes will be even more prevalent, especially if the process of optimising sphere composite to represent shapes can be automated (and even standardised). Mesh-based DEM is catching on, as evidenced by the recent acquisition of Rocky DEM (once an academic niche) by Ansys (a

global engineering software company). Image or voxel based DEM-style models (e.g., DigiDEM) or physics engines (e.g., Atomontage Engine) are finding niche applications such as packaging of nuclear waste and virtual reality computer games. With so many different models to handle shapes, a set of standard benchmark test cases would be really helpful, but it will be difficult since it cuts across so many disciplines or interest groups. Dosta et al. [592] made a start but more should be done. Although there is still no hope for particle-level simulations to match industrial scales except for some special cases [847], with (near) real-time 3D shape reconstruction to provide 3D particle input to DEM style models, a DT (digital twin), possibly implemented in VR (virtual reality) environment, can be expected in the not too distant future, to match lab scale setups. DEM has already been used to create a DT, albeit in a time-delayed fashion in most cases, at small (lab) scales [848–855]; and VR representation for particle systems is also not unheard of [856, 857]. This (lab-scale DT/VR) is still a huge triumph for particle-level models because they can then replace expensive physical tests, especially in difficult-to-reach or extreme conditions, and they can provide much more info than physical measurements can usually manage. Therefore, the best of DEM with real particle shapes has yet to come.

Use of AI so far has been geared towards consumer and high value applications: Its use in particle technology, or shape measurement/reconstruction, is still limited. This is a challenge but also a great opportunity academically and commercially. AI's ability to cope with shape complexity is beyond doubt. While real-world training datasets are difficult and/or time consuming to obtain, artificial or synthetic training sets are relatively easy to generate using software (e.g., DigiPac), with 3D graphics, for singular, clustered, or packed particles. Proof of concept should be easy to do. Real-world applications will require large datasets of real particles, taken with real equipment. It is only a matter of time before this happens – once people realise its potential. Following AlphaGo which demonstrated that machines can outperform humans in highly skilled (but trainable) games, we now have AlphaFold 2 [858] to help solve the protein-folding problem and AlphaFold 3 [859] to generate biomolecular complexes (e.g., DNAs, RNAs and even ligands) to accelerate progress of solving real-world problems such as breaking down single-use plastics [860] and creating new malaria vaccines [861]. With millions of users globally, Google estimates that its free and easy-to-use AlphaFold Server can potentially save many millions of research-years in time and trillions of dollars in cost (https://deepmind.google/technologies/alphafold/). Perhaps one day, something similar will appear to help particle technologists the way AlphaFold Server helps biologists: give a description of the requirements, AI will generate the shape to meet the requirements and, what's more, predict its interactions with others (e.g., collisions, contact forces, drag forces, etc), taking over the most difficult and computationally expensive part of DEM, or even making DEM as we know it redundant if AI can rapidly and correctly predict the properties or phenomena that DEM is used to investigate in the first place. Earlier this year (March 2024), Devin – the first AI software engineer – has been released (https://www.cognition.ai/introducing-devin) by a start-up company for free access to create computer code for some real-world software problems collected from GitHub, beating GitHub's own Copilot, Anthropic's Claude 2 and OpenAI's GPT-4. In the future, DEM software will no longer be the purview of (specialist) computer programmers, everyone can have their ideas coded up by AI and tested on the (cloud) computer. GPT-4o, which to ChatGPT is equivalent to adding GUI to a batch DEM program, and alike will make it easier for humans to use AI as a helping tool. From now on, prompting skills (or prompt engineering) will be the new and must-have (human-machine) communication skills. With AI, things will happen much faster, if they happen at all, at a pace unseen in the human technological history.

Table 1
Examples of direct and indirect influence of particle shape on properties of interest.

Properties of interest	Roles of particle shape	Examples
Packing & structure-property relationships	• Shape is a determining factor for the maximum packing efficiency. Random close packing (**RCP**) of equal spheres has a generally accepted maximum bulk packing fraction of 0.64 [8,9]. With a finite (and relatively small) number, or in a given container, the answer is more complicated even for equal spheres [10,11]. • If the spheres are slightly squashed to become spheroids with a height/width ratio of 0.7, the maximum packing fraction increases to 0.72 [12]. This is close to the limit by ordered sphere packings such as HCP (hexagonal close packing) and FCC (face-centred cubic packing), both have a packing efficiency of 0.74 [13]. This level of packing efficiency can also be reached by RCP of some spheropolyhedra of high (~0.9) sphericity [14] or in polydispersed packing [15]. • Most physical properties are structure-dependent. Indeed, in our own experience in providing people with packing structures (either simulated and/or CT scanned), more than half the people who are interested in packing structure are interested because of the properties of interest that they know or believe are structure-dependent in some way. • Shape affects microstructure of the packing including packing density and details of contacts [16–21], which in turn affect mechanical and thermal/electrical conductivity properties. For example, packing of round particles are more resistant to compression while packing of angular particles to shear. • Porous media made of particulates are examples of packing structure. Particle shape affects morphology of the pores and topology of the pore network, which in turn affects pass-ability of fluids and/or particles through the pores.	• RCP principles are useful guide for designing metal alloys since achieving optimal packing of atoms or ions is essential for desired material properties [22]. • The shape of particles influences mechanical strength, compressibility, shear resistance, thermal conductivity of particle assemblies as powder, sand or soil 23–66. • Shape of filler particles (and volume fraction) can substantially change electrical and magnetic properties of nickel/polyethylene composites [67]. • Flowability of granular material is affected by particle shape [25,68–75]. • In granular materials, random packing of spheres plays a role in understanding jamming transitions [76–79]. • RCP concepts help explain transition from liquid-like state to a rigid solid in amorphous materials like glass [80]. • Bin packing and packing optimisation help optimise container utilisation in shipping containers, product packaging, storage bins and silos, and nuclear decommissioning [82–92]. • In civil engineering and geotechnical studies, how granular materials packing is crucial, affecting construction, foundation design and stability [27,93–99]. • Slusser [100] listed five ways particle size affect pharmaceutical product quality: compression, dissolution, bioavailability, flowability and shelf life. Particle shape is involved directly or indirectly in all five. In pharmaceutical manufacturing, achieving optimal packing density of powders used for pills and tablets impacts drug dissolution rates, bioavailability, and dosage consistency [101–106]. • Colloidal particles in suspensions exhibit RCP behaviour [107,10]. Understanding their packing density is essential for designing stable emulsions, paints and coatings. • Biological cells, tissues and organelles often exhibit random packing. RCP informs our understanding of cell packing in tissues, blood vessels and organs [108,109]. • Designer cells can be made to act like self-renewing living machines (e.g., Xenobots), and a crucial step is tissue layering and shaping

(*continued on next page*)

Table 1 (*continued*)

Properties of interest	Roles of particle shape	Examples
		[110,111]. Making synthetic particles or cells to mimic living cells is a hot topic [112,113]. • In 3D printing, two aspects are closely related to shape. Particle shape affect flow-ability and spread-ability of the powder [114,70], which impacts quality of the printed parts. The second aspect is efficient use of the print tray space to maximise the number of parts printed in one batch [115,116], which is a special packing problem and linked to the cost of the printed parts. The special requirements include: parts should not be in an arbitrary orientation, and there must be gaps between the parts. • Permeability and performance of filters (as porous media) are affected by the shape of particulates that are in the suspension or making up the cake and/or the filter itself [117,118]. • In solid-fluid separation (e.g., in a cyclone), particle shape plays an important part in performance [119]. • Solids fraction, contact statistics, uniformity or voids distribution, pore shape and pore network structure, tortuosity and permeability of packing as porous medium are all particle shape related [120–134].
Segregation & Mixing	• Segregation can happen due to any difference that affects relative mobility of particles when they are in relative motion. Although size difference is the most cited cause, differences in shape, density, composition, cohesion, etc. can all induce segregation. • Mixing is the opposite of segregation and is more often the desired state than segregation. Segregation is a major contributor to the "meagre" (60%) operating efficiency of most solids processing operations in industry [135]. • The two usually co-exist and are easily turned to one another. The two are so related that mixing can be, and frequently is, described by scale and intensity of segregation [136,137].	• The Brazil nut effect (and its reverse) is synonymous to size-segregation [138–144]. However, particles of the same 'size' but different shapes can also segregate [145,146]. • Separation by means of jigging is an example of segregation by density and/or by size/shape and other properties that affect hindered settling velocity of particles [147–150]. • Segregation in heaps and silos is another example where shape, among other things, matters [145,25,151,152]. • More simulation and experimental studies of segregation of non-spherical particles can be found in the literature [153–164]. • Powder mixing usually involve non-spherical particles and has been extensively studied for decades experimentally and numerically [74,165–184].
Size measurement	• It is because of shape that different sizing techniques can produce different results for the same powder [185–197]. • Sizing by sieving is not a robust method for a mixture of very different shapes. For example, needle-shaped particles can pass through the same mesh as round particles, so long as they have the same second largest linear dimension, but the two groups clearly have different sizes and behave differently. • Sizing by light diffraction method [198] can show apparent bimodal size distribution for mono-sized needle-like particles [199,200] or a broadened peak for rod-like particles [201]. • Shape-dependency of sizing techniques can cause confusion, uncertainty, or wrong interpretation, especially when dealing with a mixture of different sizes and shapes [202–204].	• In sieving, the 2nd highest dimension determines if a particle can pass through a given mesh [1]. • Obviously, irregular shapes generally are more difficult, or take longer, to pass through the sieve than round particles [205]. In other words, the volume of particles retained on a sieve varies with shape as well as size [206]. • Single particle optical counters used to be popular for PSD measurement. For particles much smaller than the wavelength of light, the measured size is very close to volume-equivalent diameter; whereas for particles much larger than the wavelength, the measured size is more correlated with the particle's projected area [207].
Particle-particle (P—P) interaction related properties or phenomena	• Even among particles of the same material, shape affects the nature (e.g., point contacts vs surface contacts) and the number of contacts in powders.	• Effective thermal conductivity is affected by particle shape in a packing. • Thermal conductivity of nanofluids depends on shape of nanoparticles. • Chemical reaction kinetics depend on exposed surface area and its distribution in confined space (e.g., packed column reactors). • In 3D printing, flowability or spread-ability of powder critically affects quality of the printed parts [208]. • Shear resistance at the initial (re-arrangement) stage mainly depends on characteristics of particle (surface) contacts. • Irregular shaped river rocks lose their angularity due to abrasion faster than the rocks lose their size – the so-called shape-size paradox [209]. • Irregularly shaped particles in chocolate affects its texture and mouthfeel. • In concrete production, particle shape affects aggregate properties, impacting the final product's strength [99,210].
Particle-surface (P–S) interaction related properties and phenomena	• P-S may be considered an extension of P—P interaction if the two are made of the same material; but more often they are of different materials. • P–S interaction gives rise to the so-called "wall effect", meaning the packing structure (and hence structure-related properties) near the wall is different from that of the bulk. How thick this wall-effect layer is depends on particle shape (and whether it is a mixture). • Shape and surface characteristics of virus particles affect their affinity to membrane of tissues, thus toxicity. • Asbestos are cancerous because their fibrous shape makes them easily trapped in the lung once inhaled, causing long term damage. • Particle shape impacts the sensory experience of food products.	• It is well known that inhalation of fibrous particles (e.g., asbestos) can cause respiratory diseases and lung cancer [211]. • All virions consist of a nucleic acid genome and a protective layer of proteins (called a capsid). By shape or morphology, viruses are classified into four groups: filamentous (i.e., long and cylindrical), isometric or icosahedral (i.e., roughly spherical), enveloped (having a membrane surrounding the capsid), and head and tail. The shape of a virus play an important role in determining if and how it can infect the host [212]. • Shape of nanoparticles is a determining factor of their cytotoxicity [213,214]. • While particle size has long been recognised to affect mouthfeel of chocolate (e.g., particles below 20 um give a silky feel and 2–3 um particle size difference can be detectable by the tongue as a different level of smoothness) [215], the shape of the chocolate piece has also been shown to have an impact on its oral perception [216]. • Coating uniformity is affected by particle shape.

(*continued on next page*)

Table 1 (*continued*)

Properties of interest	Roles of particle shape	Examples
Particle-fluid (P—F) interaction related properties and phenomena	• Particle shape is a determining factor for drag force. Also, asymmetry in shape means that drag force on a particle is (relative) flow direction dependent. • Particle shape influences dissolution (and more generally chemical reaction) kinetics because from mass transfer point of view spatial distribution of the exposed surface (where dissolution/reaction occurs) affects how quickly the dissolved phase is dispersed, through diffusion and/or convection, away from the reaction sites. For facetted crystals, growth and dissolution rates are different for different facets, thus not only the overall dissolution speed is shape dependent but also the shape itself changes during growth/dissolution.	• Particle deposition rate, detachment rate, and surface coverage are shape dependent. Spheres differ significantly from other shapes (e.g., rod-like particles, spheroids) in these terms [217–224]. • Drag coefficients are shape dependent [225,226]. • Particle motion and settling in fluid is shape-dependent [227–234]. • Overall rate of dissolution is particle shape dependent [235–237]. • If the dissolution rate is directional or facet-dependent, as is usually the case for crystals, different faces recede at different velocities [238]. • Particle shape affects drug delivery efficiency [239,240]. • Particle shape also affects functionality of dietary fibre concentrates [241]. • Particle shape affects heat transfer performance of particle laden nanofluids [242,243] or heat loss of particles or even buildings [244,245].

Table 2
Particle shape descriptors.

Terms	Category	Purposes and links with properties	Comments
Acicular, angular, crystalline, dendritic, fibrous, flaky, granular, irregular, modular, spherical.	Qualitative	General terms used for powder particles as defined in BS 2955 Glossary of terms [1,248].	Qualitative terms are descriptive and easy for the reader to perceive the shape being referred to. However, they are subjective, ambiguous and arbitrary, and need to be used in conjunction with some quantitative terms to make comparative sense.
Platy, rod-like, blocky, cubical, needle-like, prismoidal, sponge, rounded, tabular, equant, columnar, blade, etc.	Qualitative	Additional descriptive terms suggested for powder particles [249].	
Lamellar, tabular, equant, columnar, acicular. *Paired up with* Isometric, tetragonal, hexagonal, etc.	Qualitative	Used in pairs, for crystalline particles in pharmaceutical context [250].	
Shape factors based on Feret, Martin and project area diameters [251–254]	Quantitative Geometrical 2D	• Particle sizing based on image analysis (IA), but many commercial particle sizers and shape analysers use these to report shape factors along with PSD.	• Feret diameter is also called calliper diameter. It is easy to hand measure with a calliper but not unique. • Martin diameter is logical as a geometrical concept, but not as easy to hand measure, and cannot be precisely determined if the particle image has a low resolution (while the other two can still be precisely determined). • Feret and Martin diameters are direction dependent and not unique, their maxima and minima are more often used. • Projected area diameter is calculated from solid-pixel count, thus in practice the most well-defined among the three. • Although Feret diameter applies to 3D, all three are generally used to describe 2D projections of the 3D particles.
Feret diameter (d_F), also called calliper diameter, is the distance between two parallel planes that bound the particle in any given direction. For 2D projection of the particle, it is the distance between two parallel tangential bounding lines. For a 2D convex projection, the average Feret diameter over all directions is $\overline{d_F} = \frac{P}{\pi}$ by Cauchy's theorem, where P is the perimeter of the area.			
Martin diameter, for a 2D projection area, is the chord length that bisects the area along any given direction.			
Projection area diameter is the diameter of a circle with the same area (A) as the projection: $d_a = \sqrt{\frac{4A}{\pi}}$			
These relationships always hold: $d_{Fmax} > d_a$ *and* $d_{Fmin} < d_a$			
Aspect ratio: $\psi_A = \frac{d_{Fmin}}{d_{Fmax}}$			
Straightness (for fibres): $\frac{d_{Fmax}}{\textit{fibre length}}$			
Curl index (for fibres): $\frac{\textit{fibre length}}{d_{Fmax}} - 1$			
Wadell series [255–257]	Quantitative Geometrical 3D and 2D	Proposed in the context of geology but widely applied in other fields as well.	• In practice, roundness and sphericity values had typically been estimated using charts that were developed in the 1940s–1950s. Studies [260–262] showed that only with proper training and experience can users obtain correct and consistent results. This would be as expected for any manual operated measurements. They demonstrate the needs for developing automated computer methods and standardisation. • Computer methods, based on image analysis, for shape factor calculations, usually for specific types of particles, and of course not limited to traditional shape factors, have indeed been developed
Sphericity or Carman's shape factor: $\frac{\textit{surface of equal volume sphere}}{\textit{surface of the particle}} = \left(\frac{d_v}{d_s}\right)^2$			
Circularity: $\frac{\textit{perimeter of equal area circle}}{\textit{perimeter of particle projection}} = \frac{d_a}{d_p}$			
Roundness: $\frac{1}{N}\sum_{i=1}^{N}\left(\frac{r_i}{R}\right)$ where r_i is radius of curvature at corners, R radius of the maximum inscribed circle, and N the number of edges (corners).			
Lees [258] defines degree of angularity in a similar way – summing up the contribution from each corner, but instead of local curvature of the corner, angle of the corner (α_i) and distance (x_i) of the corner tip from the centre of the maximum			

(*continued on next page*)

Table 2 (*continued*)

Terms	Category	Purposes and links with properties	Comments
inscribed circle is used: $(180-\alpha_i)\frac{x_i}{R}$ An even more detailed definition of shape factor was proposed by Podczeck [259]. Using image analysis of a particle's projected outline, it is easy to calculate the area (A), the perimeter (P), the minimum Feret diameter (d_{Fmin}), Feret diameter (d_{sp}) perpendicular to (d_{Fmin}), the maximum Feret diameter (d_{Fmax}), deviation from square $H_1 = \frac{A}{d_{Fmin}d_{sp}}$, from circle $H_2 = \frac{A}{\left(\frac{\pi}{4}\right)d_{sp}^2}$, from triangle $H_3 = \frac{2A}{d_{Fmin}d_{sp}}$ and elongation $H_4 = \frac{P}{d_{Fmax}}$. The shape factor is then defined as $NS = NC + H_4H_3 - H_2H_1$ where NC is the number of characteristic corners. Using IA, NS and PSD can be obtained at the same time and NS is more sensitive to small shape changes than other commonly used factors, but it does not evaluate sharpness of the corners and does not work well if the shape is irregular and has more than a few (say 5) corners.			(sometimes with modified or new definitions), bundled with equipment, and continue to be improved (e.g., [259,263–294]. • Corresponding to "mean size", a definition of "mean shape" has been proposed [295]. Yu et al. [105] showed that active pharmaceutical ingredients (API) with a low molecular weight (<500 *Da*) have a typical median aspect ratio between 0.6 and 0.8. This corroborates the concept of mean shape. Using a mean size/shape obviously makes comparisons simpler and easier, but beware the pitfalls of using averages – they hide the range and variability of the raw data thus can be misleading or misinterpreted.
Krumbein [296,297] Sphericity: $\varphi = \left(\frac{C}{B}\right)\left(\frac{B}{L}\right)^2$ Roundness: Surface texture: where L = longest dimension of the particle, B = breath measured perpendicular to L, C = thickness of the particle	Quantitative Geometrical 3D	• Zingg's classification of pebble shapes was described by Krumbein [297].	• The dimensions are different from Heywood's definitions.
Heywood series [298] Elongation ratio: $n = \frac{L}{B}$ Flakiness ratio (or flatness): $m = \frac{B}{T}$ Projection area: $A = \frac{\pi}{4}d^2 = \alpha BL$ Volume: $V = \beta d^3 = pAT = p\alpha BLT$ Shape factor: $\beta = \left(\frac{\pi\sqrt{\pi}}{8}\frac{p}{\sqrt{\alpha}}\right)\left(\frac{1}{m\sqrt{n}}\right)$ Zingg's index: $F = \frac{LT}{B^2}$ Space-filling factor: $f_v = \frac{LTB}{V}$ Schulz's index: $k = 100\left(\frac{L^2B}{V}-1\right) = 100\left(\frac{L}{T}-1\right)$ All expressed in terms of Heywood's limiting dimensions: L = length, B = breath, T = thickness of the bounding box of the particle lying on the side of maximum stability.	Quantitative Geometrical 3D	• Angular and tetrahedral when $\alpha = 0.5-0.8$ and $p = 0.4-0.53$ • Angular and prismoidal when $\alpha = 0.5-0.9$ and $p = 0.53-0.9$ • Sub-angular when $\alpha = 0.65-0.85$ and $p = 0.55-0.8$ • Rounded when $\alpha = 0.72-0.82$ and $p = 0.62-0.75$ • Shape factor β has two bracketed terms, the first describes form, the second proportion. • Zingg's is the most widespread classification system for pebble shapes in geology [299,300]. For example, pebbles on the seaside tend to have F < 1 (oblate), whereas stones on river banks tend to have F > 1 (prolate), spheres or blades have F = 1. • Space-filling factor is linked to resistance to fracture of grinder particles. • Schulz's index is linked to ballast for roads and blast furnace clinker.	• Originally designed to quantify shapes of rocks and pebbles – those that can be hand-held and hand-measured. The dimensions are uniquely defined if the particle has only one side of maximum stability. • In particle imaging devices, such as Malvern G3, particles also tend to land on a side of some stability – not necessarily side of maximum stability if adhesion is strong compared to particle weight – these shape factors can be similarly defined and calculated.
Hausner [301] Elongation ratio: $\frac{L}{W}$ Bulkiness factor: $\frac{A}{LW}$ Surface factor: $\frac{C^2}{4\pi A}$ Contour ratio: $\frac{C}{\pi D}$ where L and W are length and width of the enveloping rectangle of minimum area. A is the project area of the particle, C its perimeter, D the area diameter of the projection.	Quantitative Geometrical 2D		Surface factor is square of contour ratio. Contour ratio is reciprocal of circularity.
Sugimoto et al. [302] Degree of circularity (form):	Quantitative Geometrical	Used in pair to form a matrix to describe projections ranging from smooth circle ($\phi = 1$ *and* $\varsigma = 1$) to rough edged ellipses (e.g., $\phi = 0.75$ *and* $\varsigma = 0.825$)	Can simultaneously describe form and texture, albeit in 2D only. The concept should be extendable to 3D.

(*continued on next page*)

Table 2 (*continued*)

Terms	Category	Purposes and links with properties	Comments
$\phi = \frac{diameter\ of\ equal\ area\ circle}{major\ axis\ length\ of\ equal\ area\ ellipse}$ Surface roughness (texture): $\varsigma = \frac{perimeter}{perimeter\ of\ equal\ area\ ellipse}$	2D		The real shapes are forced to conform to some underlying templates which are regular and symmetrical shapes (i.e., ellipses).
Tsubaki and Jimbo [303,304] $\Psi_{ac} = \frac{d_a}{d_c}\quad \Psi_{aF} = \frac{d_a}{d_F}\quad \Psi_{aR} = \frac{d_a}{d_R}$ $\Psi_{cF} = \frac{d_c}{d_F}\quad \Psi_{cR} = \frac{d_c}{d_R}\quad \Psi_{FR} = \frac{d_F}{d_R}$ $\Psi_{\bar{F}a} = \frac{d_{\bar{F}}}{d_a}\quad \Psi_{Stv} = \frac{d_{St}}{d_v}\quad \kappa = \left(\frac{d_v}{d_{St}}\right)^2$ $d_{\bar{F}} = \frac{d_{F_{min}} + d_{F_{\pi/2}}}{2}$ $E(d_R) = \frac{1}{\pi}\int_0^{2\pi} R d\theta_R \qquad \sigma_R = \sqrt{\left[E(R^2) - \frac{E^2(R)}{E(R)}\right]}$ $E(d_F) = \frac{1}{\pi}\int_0^{\pi} d_F d\theta_R \qquad \sigma_F = \sqrt{\left[E\left(d_F^2\right) - \frac{E^2(d_F)}{E(d_F)}\right]}$ where d_a is project area diameter, d_c perimeter diameter, d_FFeret's diameter, and d_R unrolled diameter.	Quantitative Geometrical 2D	Nine new parameters in three groups are defined to describe 2D projections of particles. When two or three of them are used together in a diagram, fine details or small changes in shape can be distinguished.	Very detailed, and with image analysis software tools, they should be easily calculatable. Yet, they have not caught on and widely used in the set's entirety.
Mikli et al. [305] Aspect ratio: $AS = \frac{a}{b}$ Elongation: $EL = log_2\left(\frac{a}{b}\right)$ Dispersion: $DP = log_2(\pi ab)$ Roundness: $RN = \frac{P^2}{4\pi A}$ Roundness factor: $RNF = \frac{P}{d_A}$ Irregularity parameter: $IP = \frac{D}{d}$ Spike value: $SV = h\ cos\left(\frac{\theta}{2}\right)$ Spike parameter – linear fit: $SP = \frac{1}{n}\sum\frac{1}{m}\sum\frac{SV_{max}}{h_{max}}$ Spike parameter – quadratic fit: $SPQ = SV_{av}$ where a and b are major and minor diameters of Legendre ellipse that fit the particle's project, d_A diameter of equal area circle, d and D diameters of inscribed and escribed circles, θ is angle of a spike in the contour, h protrusion height of the spike, m number of valid SV for a given step size, and n number of different step sizes used.	Quantitative Geometrical 2D	• For metal powder particles produced by mechanical methods such as milling. Angularity factors characterising the spikes are linked to particles' ability to abrade and erode.	• Precise values of shape factors can be worked out using image analysis tools. Each shape can be described by multiple factors for different aspects. • For example, a perfect ellipse corresponds to $DP = 0$; a star shaped particle with an elliptical fitting profile has $DP = 0.732$; a twig like particle has $EL = 3.818$; a square has $RN = 1.273, RNF = 1.128, IP = 1.414$ and $SPQ = 0.707$.
Russ [306] Form factor: $4\pi\frac{Area}{Perimeter^2}$ Roundness: $\frac{4\ Area}{\pi\ MaxDiameter^2}$ Aspect ratio: $\frac{MaxDiameter}{MinDiameter}$ Elongation: $\frac{FibreLength}{FibreWidth}$ Curl: $\frac{Length}{FibreLength}$ Convexity: $\frac{ConvexPerimeter}{Perimeter}$ Solidity: $\frac{Area}{ConvexArea}$	Quantitative Geometrical 2D	• For shapes in the context of computer image analysis.	• With digital (binary) images of isolated shapes, precise values of shape factors can be worked out using image analysis tools. Again, each shape is describable by multiple factors for different aspects.

(*continued on next page*)

Table 2 (*continued*)

Terms	Category	Purposes and links with properties	Comments
Compactness: $\frac{\sqrt{4\frac{Area}{\pi}}}{MaxDiameter}$ Modification ratio: $\frac{InscribedDiameter}{MaxDiameter}$ Extent: $\frac{NetArea}{BoundingRectangle}$			
Sneed & Folk [307]; Benn & Ballantyne [308]; Graham & Midgley [309] A shape is a point in a TRI-PLOT which is a three-axis triangle with "Blocks" (sphere), "Slabs" (oblate) and "Rods" (prolate) at the three vertices, and ratios $\frac{c}{a}, \frac{b}{a}, \frac{a-b}{a-c}$ as axes. Here a, b and c are bounding box dimensions. It shows how close a shape is to the three typical shapes (sphere, oblate spheroid and prolate spheroid). Kaye et al. [310] Plotting chunkiness and fractal dimension against particle size in a 3D plot, powders with different characteristics are visually and easily separated into cluster(s) in the plot.	Quantitative Geometrical 2D/3D	• The widespread Zingg diagram [300] is simple and easy to use but limited to 4 classes (blade, disc, rod and sphere). Sneed and Folk [307] used a triangular diagram to include 10 shape classes. • Making it easier to visually separate particles of different properties or to group them according to properties.	• Interesting way to describe shapes, can simultaneously show 3 ratios in one plot. • Ratios vary linearly, resulting in even distribution of particle forms across the diagram without distorting the shape continuum. • Simultaneously show different aspects of particles, makes it easy to visually separate particles into groups, and see the correlation or interdependency between them [283,311].
E-classification [312] Instead of measuring lengths, this method involves hand experiment (with the shape and a flat surface) and counting the numbers of stable (S), unstable (U) and saddle type (H) equilibria. Given the Poincare-Hopf relationship, S + U-H = 2, for convex shaped pebble shapes, only two of which need to be counted.	Quantitative Geometrical 2D/3D	• Based on static equilibrium points, for pebble and crystal shapes, the so-called E-classification is "more sophisticated" yet "considerably faster in practice than the classical Zingg method". • Extendable for crystals where the number of faces (F), vertices (V) and edges (E) satisfy the Euler's rule, F-V-E = 2.	• Works with whole numbers (counts). • Field-work friendly and quick. • Can cover polyhedral shapes which cannot be extracted from the Zingg system. • There can be many more E-classes (depending on S and U numbers), but a simplified version involves only 4 E-classes (e.g., flat shapes belong to E(I), elongated shapes to E (IV)). • Hand-sized, convex shaped objects only.
Miscellaneous, a collection from Powder Technology Handbook by Gotoh et al. [313] Volume shape coefficient: $V = \phi_v d^3$ Surface shape coefficient: $S = \phi_s d^2$ Specific surface shape coefficient: $\phi = \frac{\phi_s}{\phi_v}$ Carman's surface coefficient: $S_v = \frac{6}{\phi_c d_v}$ where S_v is volume specific surface area, d_v equivalent volume diameter. Centroid aspect ratio (CAR): $\frac{MaxLengthThroughCentroid}{PerpendicularDimensionThroughCentroid}$ Anisometry: *axial ratio of equivalent ellipsoid* Rugosity: $\frac{Perimeter}{PerimeterOfSmoothCircumscribingProfile}$ Surface factor: $\frac{Perimeter^2}{4\pi\ Area}$ Bulkiness: $\frac{Surface}{MinAreaOfEnvelopingRectangle}$ Bulkiness factor: $\frac{VolumeOfEquivalentEllipsoid}{ParticleVolume}$	Quantitative Geometrical 2D and 3D	• A diverse range, complementary to other existing shape factors.	• Not attributed to a specific pioneer but in common use.
Fractal dimensions and fractal based descriptors If a property A (e.g., mass, perimeter) of a structure is measured using a yardstick B (e.g., radius of gyration, stride), and the relationship follows a power law as $A \propto B^{\delta}$ and δ is not a whole number, then the structure can be described as fractal and δ is the so-called fractal dimension.	Quantitative Geometrical 2D and 3D	• For self-similar, finger-like structures, e.g., aggregates of colloidal particles [314,71,315], viscous finger in a Hele-Shaw-Cell [316], manganese oxide at the joint surfaces in sedimentary rocks [317].	• Powerful tool to describe certain type of complex structures. • Mass based fractal dimensions and perimeter based fractal dimensions are different in value for the same fractal structures, mass fractal dimensions are usually larger. • Based on the fractal concept, a 2D fractal structure has a defined area

(*continued on next page*)

Table 2 (*continued*)

Terms	Category	Purposes and links with properties	Comments
			but not perimeter; a 3D fractal has a defined volume but not surface. The implication is that measurement results for perimeter length or surface area are scale-dependent. Such measurements should be reported together with the measurement conditions, much like how 'size' should be reported for irregular shapes.
Fourier analysis, spherical harmonics, Hilbert-Huang transforms [268,290,318–337] In the simplest form, the (R,θ) Fourier method [318,319] can describe, in closed form, a 2D profile as: $R(\theta) = a_0 + \sum_{n=1}^{N}[a_n cos(n\theta) + b_n sin(n\theta)]$ provided that the radius R is uniquely defined for every angle θ (i.e., there is no re-entrant angle where the profile doubles back on itself) and the centroid, acting as the origin of (R,θ) coordinates, can be accurately determined. Both restrictions can be relaxed or removed if complex Fourier analysis is used [338], which in effect replaces (R,θ) with a (x,y) pair of coordinates: $x_m + iy_m = \sum_{n=-\frac{N}{2}}^{\frac{N}{2}}(a_n + ib_n)\left[cos\left(\frac{2\pi nm}{M}\right) + isin\left(\frac{2\pi nm}{M}\right)\right]$ In the above $n = 1, 2, 3, \ldots, N$ is the index number of descriptors, $m = 1, 2, 3, \ldots, M$ the index number of (x, y) points. In practice, M is chosen to be a power of 2. Garboczi [322,339] proposed a 3D equivalent of the Fourier series, using a truncated spherical harmonic (SH) series defined on a unit sphere, to describe the contour of a particle in 3D: $R(\theta,\phi) \approx \sum_{n=1}^{N}\sum_{m=-n}^{n} a_{nm} Y_{nm}(\theta,\phi)$ $Y_{nm}(\theta,\phi)$ is called a spherical harmonic function, easily calculable for given (n,m,θ,ϕ). Once $R(\theta,\phi)$ is determined from 3D image of the particle, the coefficient a_{nm} can be calculated as an integral using $R(\theta,\phi)$ and complex conjugate of $Y_{nm}(\theta,\phi)$. In most cases, N up to 30 is considered sufficient [340]. SH is a very popular method for describing shape and shape distribution and for mass production of shapes for simulations. Liu et al. [341] adapted the so-called Hilbert-Huang transform (HHT) to decompose particle geometry into a HHT series that (like a Fourier series) represent geometry at different scales. Based on this, they proposed a "complete and generic" descriptor system to characterise irregular shapes, covering sphericity, roundness, fractal dimension and a new structural index. The math and computational process behind it are complicated but a free software is made available on GitHub (https://github.com/yfliu088/GMAP).	Quantitative Geometrical 2D and 3D	• A relatively small set of Fourier descriptors are required to reconstruct shape to a varying degree of accuracy: more descriptors mean more details. • Lower order descriptors ($n = 1$ to 4) describe the overall shape, while higher ones are for texture or local roughness details. $N = 10$ *to* 15 are usually sufficient for a highly complex shape [342] and $N = 3$ may be enough to approximate morphology of a sand particle [268]. • Fourier analysis formulation is clearly limited to 2D profiles (i.e., 2D images or projections of 3D particles). • SH is designed to describe surface contour of a solid 3D object, i.e., small holes – if they present – should be should be filled before the analysis. • SH representation has been used to help with in-depth comparison of different angularity indices for irregular particle shapes and surface roughness [343,344].	• These transforms work best for smooth contours, not so well for contours with sharp angles since more parameters are required and the fitting is only approximate. • Can be used to recover shapes [330] as well as characterising them. • Pena et al. [345] extended 2D Fourier descriptor theory to 3D and used it to reconstruct individual particles for use in simulations.
Polygonal harmonics and facetted crystals ([346,347]) Recognising the difficulty of Fourier analysis in dealing with "very jagged and highly reentrant" particle cross-sections, Young et al. [348] used polygonal harmonics to characterise such particles. In the second half of 1990's, a French group proposed at least half a dozen descriptors specifically to describe crystal shapes (in 2D and pseudo-3D), based on results from a series of morphological dilation and erosion [349,350] or from Apollonian packing of squares to completely cover the surface of faceted particles observed by reflection [351]. Using the concept of Minkowski addition, Reinhold and Briesen [352] showed that a complex crystal shape can be decomposed into a set of simpler shapes for which any	Quantitative Geometrical 2D and 3D	Specifically for facetted shapes that are best described as polygons or polyhedrons (e.g., crystals and faceted objects)	• Like all modern shape descriptors, they tend to be only obtainable by a computer program (i.e., not easily done by hand), and not as intuitive as the traditional shape factors. On the other hand, they tend to be much more quantitatively discriminating for the shapes they are designed to use. • Reinhold and Briesen [352] commented that "Although the concepts are developed for faceted crystals only, the framework may apply to a much broader class of convex particles." Could the idea be

(*continued on next page*)

Table 2 (*continued*)

Terms	Category	Purposes and links with properties	Comments
geometric measure (e.g., volume, surface area, sizes) can readily be computed. The original crystal is a linear (algebraic) sum of the simpler shapes.			developed to cover non-convex or more general shapes?
Dynamic shape factors Davies [353] defined a dynamic shape factor based on terminal velocity ratio and demonstrated, for falling spheroids in viscous flow, how the shape factor is related to aspect ratio: $R = \frac{a}{b}$ and $K = \frac{V_s}{V}$ where a is major axis, b minor axis of a spheroid, V Stokes velocity of the spheroid, V_s Stokes velocity of equal volume sphere. Furuuchi et al. [354] proposed a method to use measured electrical conductivities of the continuous phase (K_c) and of the suspension (K_s) of known solids fraction (ϕ) to determine dynamic shape parameter (M) defined in terms of geometric aspect ratio and demonstrated their method for disks and needles. $\frac{K_c - K_s}{K_s} = \frac{3M+2}{3M(2-M)}\frac{\phi}{1-\phi}$ (for ϕ between 0.05 and 0.1) $M = \frac{(2y - sin2y)}{2sin^3 y}cosy$ $\frac{a}{b} = cosy$ (for a < b) $M = \frac{1}{sin^2 x} - \frac{cos^2 x}{2sin^3 x}ln\left(\frac{1+sinx}{1-sinx}\right)$ $\frac{b}{a} = cosx$ (for a > b)	Quantitative Dynamic 3D	• As R increases from 1, K lines become increasingly separated in a K-R plot for prolate and oblate spheroids. • In (a/b) vs M plot, different shapes (e.g., disks, cylinders, oblate and prolate spheroids) show clear separations in trend curves.	• Effects of particle-fluid interactions are the most exploited when determining dynamic shape factors. More examples are given in [355–358]. • Like aerodynamic size, these parameters can better capture or link particle shape with a dynamic response. However, they cannot be used, like static geometry-based shape factors, out of the context where they are determined.
Geometry descriptors for pores in porous media [129] Porosity: complement of packing fraction Pore size distribution: particle size distribution Mean empty space: average pore size Constrictivity: depends on the ratio of diffusing particle size to pore size but defined for the entire porous medium rather than a single pore Tortuosity: definition varies according to context (e.g., hydraulic, electrical, diffusion, thermal) but all used to predict transport properties of porous media	Quantitative Geometrical 2D and 3D	• Porosity, constrictivity and tortuosity are three parameters often used in empirical relationships to describe transport processes like diffusion, fluid flow (permeability), and thermal conductivity [127,359,360,218,361,362,363,63].	• Another way to geometrically quantify a particle assembly (or packing or agglomerate or cluster) is to treat it as a porous medium and focus on the voids (pores) instead of the solids. In concept, since the porous structure can be inverted such that pores become particles and particles voids, the pores can be quantified just like particles. In practice, the pores are in most cases so interconnected that there is often no natural boundaries to separate individual pores apart for analysis. Thus, separate sets of descriptors are used to describe the pores and the particles. Nevertheless, the two are highly correlated or equivalent to each other. For example, packing fraction and porosity are complementary and so are correlation functions (e.g., radial distribution function); particle and pore size distributions are related and so as mean particle size and mean empty space; specific surface area is identical; tortuosity distribution for the pores and force chains for the solids are both a reflection of their respective connectivity. • Much like particle size for irregular shapes, pore size is not a well or uniquely defined quantity, because pores have irregular shapes and because except for the closed pores the boundaries that separates the pores are somewhat artificial and arbitrary and so what constitutes a pore can vary from one analysis to another. Thus, like PSD, pore size distribution depends on how the pore size is defined, measured and calculated [364,365]. • Given a 3D image of a piece of porous medium, calculating

(*continued on next page*)

Table 2 (*continued*)

Terms	Category	Purposes and links with properties	Comments
			tortuosity [364,366] using simulated MIP (mercury intrusion porosimetry) may not be less effort/runtime than simulating flow through the medium using LBM [367,368,369], but the latter gives much more information. Thus, tortuosity as a means to estimate permeability is no longer as prevalent as it used to be. • Voronoi tessellation as tool to create pore network in sphere packing has been extended to deal with packing of arbitrary shapes [370].

Table 3
Standards for particle shape description.

Standard	Year	Coverage
Qualitative		
BS2955	1993	A list of terms for general particle technology including types of particles, particle size and shape. Also methods for measuring suspensions, emulsions, surface area, and porosity.
ISO 9276-6:2008	2008	Rules and nomenclature for the description and quantitative representation of particle shape and morphology.
ASTM standard F1877–16	2016	Procedures for characterising particles with specific focuses on the morphology, number, size, and size distribution of particles. An appendix in the standard includes a classification scheme for describing particle morphology.
Glossary of terms	Various	Terms used for particle shape. NIST used to have a glossary available on their website, but not anymore. Some portals have booklets or lists of commonly used terms for particle shapes (e.g., https://www.bulksolids-portal.com/pdfs/8431-pdfUK.pdf)
Quantitative		
BS EN ISO 19749:2023	2023	Methods for determining nanoparticle size and shape distributions using SEM.
EN ISO 14688-1:2017	2017	Geotechnical investigation and testing – Identification and classification of soil. Contains a section for particle shape.
ASTM D 2488-09a	2016	Standard Practice for Description and Identification of Soils (Visual-Manual Procedure). Very strict about what terms to use and when to use (or not to use) them. Only three terms are defined for shape (flat, elongated, flat and elongated).
BS EN 933–3:2012	2012	Reference method for determining flakiness index of aggregates. This is a European Standard on tests for geometrical properties of aggregates.
BS EN 933–4:2008	2008	Reference method for type testing and dispute resolution when determining the shape index of coarse aggregates.
ASTM D8090–17	2017	Standard test method for particle size and shape analysis of paints and pigments using dynamic imaging methods.
ASTM F3571–22	2022	Standard Guide for Additive Manufacturing – Feedstock – Particle Shape Image Analysis by Optical Photography to Identify and Quantify the Agglomerates/Satellites in Metal Powder Feedstock
ASTM D4791–10	2010	Standard test method for flat particles, elongated particles, or flat and elongated particles in coarse aggregate
ASTM D3398–00	2000	Determination of particle index of aggregates as an overall measure of particle shape and texture characteristics.

Table 4
Shape measurement techniques.

Technique	Typical resolution	Applicable sample size range	Purposes and applications	Comments	Typical cost of hardware
			Direct measurement of (often) **static** sample for geometrical description		
Hand measurement (3D)	0.5 mm	mm – m	Static, geometrical, 3D based, descriptors such as the Heywood series in Table 3.	Shape descriptors started with geologists using hand measurements. It remains their method of choice for field work in many cases.	A ruler can be had for less than $1 and a calliper for as little as $10 (although $10K+ callipers are also available).
Optical microscopy or imaging (2D)	μm	μm – mm	• Geometrical descriptors, mostly 2D but can be 3D if operated in stereo or tomographic mode. • For particle size/shape analysis, dynamic and/or digital image analysis is more common now. Imaging and analysing moving particles makes the equipment more expensive but the saving in time and effort is well worth the extra cost. • Examples of using optical tomography for shape characterisation are available [455,267]. • Tomographic phase microscopy [456] uses phase shifting laser with variable illumination angle to map refractive index in cells and tissues. It can be used to track cells structural changes over time.	• A favourite tool for people dealing with powders or granular materials [457]. Inner structures are missed unless the particles are semi-transparent and containing sufficient contrast. • Automated IA is the norm among commercial particle sizers and shape analysers [276,458]. • Simultaneous sizing, specific surface area and shape characterisation through image analysis (IA) [459]. • Using structural light can help eliminate/reduce errors due to textures/shadows in image-based particle sizing and shape characterisation [460]. • There had been attempt to make use of light diffraction pattern, with Fourier analysis, to obtain shape information [461].	A size measurement microscope can easily cost $6K or more.

(*continued on next page*)

Table 4 (*continued*)

Technique	Typical resolution	Applicable sample size range	Purposes and applications	Comments	Typical cost of hardware
				• Using a CFD model based design, Weirich et al. [462] developed a 3D light scattering sensor to measure sphericity index of aerosol particles (0.5–5 μm) in a setup not so different in concept from Coulter counter – allowing only one particle to pass the sensing zone at time.	
SEM (2D) and FIB-SEM (3D)	0.5 nm	nm – mm	• SEM is a surface imaging technique, relying on reflected electrons from the sample surface. It can be used provide information about surface morphology, topology and roughness of solids [463,464]. The outlines of particles can be analysed as if they are project areas to calculate static, geometrical, 2D based, shape descriptors. • Stereo SEM takes images from different sample tilt angles. It is possible to reconstruct a digital elevation model from these stereo images to allow 3D characterisation of irregular shaped particles [465,466] or structures [467]. • Some SEMs can have a focused ion beam (FIB) in addition to electron beam. Ions (typically gallium ions) are much heavier than electrons and can cut through the surface of a sample, allowing FIB-SEM combo to image inside the sample up to nanoscale depth [468]. For a thicker sample, the process involves layer-by-layer milling and imaging. Compared to X-ray μCT, FIB-SEM offers higher resolutions (nm vs μm) and often used to image porous structures [469,470]. When data from both CT and FIB-SEM are fused, larger samples can be imaged with more details and better accuracy than either alone can provide [471,472].	• Can be used for size/shape characterisation of pores as well as particles. • SEM photos may look like real (optical) photos, containing shades and contrast variations resembling shadows, to reveal surface morphology, but it must be realised that surfaces react to photons and electrons differently. • SEM images do not have focal depth like normal photos, as SEM images are essentially maps of depth-integrated response to electrons of surface points, but they have something equivalent, depth of field, and it is narrow, meaning surface features being imaged cannot be more than several pixels in height. This is usually a problem but can be taken advantage of, by fusing images taken at different depth, for 3D analysis of particles [473]. • Combining stereo images and shape-from-shading (SfS), it may be possible to reconstruct at least the visible part of the 3D structure [474–480].	An SEM can cost anything between $10K and a few millions.
TEM (2D) and ET (3D)	0.5 Å	Å - μm	• TEM uses transmitted electrons to create an image, thus can provide information about the inner structure of the sample. Typically used for studying crystal defects, impurities and nanoscale structures. • Stereo TEM, like stereo SEM, takes multiple images to obtain 3D information of smaller (e.g., nm) structures [481,482]. More often used in STEM (scanning transmission electron microscopy) mode [483,484,485]. By exploiting 1D crystalline defects, STEM can be used in tilt-less mode, which is orders of magnitude faster than the standard title-arc mode, for reconstruction of complex curvilinear structures [486]. • ET (electron tomography) can be used to image 3D structure of macromolecular and cellular sized particles [487].	• Reconstruct structure in 2.5D from a tilt series of 2D projections. • Real-time reconstruction and 3D data analysis are now possible using tomviz - an open-source, cross-platform software (tomviz.org) [488].	A TEM can cost anything between $500K and several millions.
X-ray μCT (3D)	μm	μm – cm	• CT uses penetrative X-rays to create 3D images of density since attenuation through the material being imaged is related to atomic number of chemical compositions in the material. • With full 3D virtual sample available, particle sizing as well as shape descriptors can be calculated, provided the resolution is high enough for the sample being analysed [489,490,491,329]. • In terms of 3D shape/morphology analysis of real powder particles, CT provides the gold standard or ground truth, for others to use for AI training and for shape validation purposes. The 3D-CNN in Table 7 is an example. • Sub-micron resolution, or nano-CT, is available [492].	• Overall form, surface texture as well as internal structure can all be obtained at once. Internal structural info is useful for predicting body based properties such as heat transfer, breakage, etc. • Measure pores [501–507] as well as particles; and help build pore network models [508]. • Usually for static images, but can in principle be used to track dynamic process if X-ray shadow images (rather than reconstructed tomograms) can be used, since each projection takes milli-seconds to acquire. Some CT scanners (e.g., Nanotom) are designed to be easily set up to operate in this mode. • For particle sizing and shape analysis, it is important to ensure that particles are physically and adequately separated. A	A desktop or lab scale CT scanner for material characterisation (i.e., non-medical use) usually costs $400K or more.

(*continued on next page*)

Table 4 (*continued*)

Technique	Typical resolution	Applicable sample size range	Purposes and applications	Comments	Typical cost of hardware
			• Phase contrast X-ray CT maps the real part of the refractive index of the material being imaged, making it more suitable for imaging relatively low density materials such as crystals, soft tissues [493,494]. • Multi-energy or multi-tube voltage X-ray CT [495] can help when dealing with difficult-to-detect material contrast in samples. • A more recent development [496] combines CT with XRD (X-ray diffraction) to create images with enhanced ability to identify materials (e.g., explosives and narcotics) that have similar densities as benign everyday materials (e.g., plastics, light metals). • A latest development [497] makes it possible to use synchrotron X-ray scanning tunnelling microscopy (SX-STM) to capture signature of a single atom. This could possibly be developed to image particles in terms of chemical composition as well as geometrical structure. • ML (machine learning) is a promising tool to help reduce the time and effort for analysing the samples as particle assembly [498,499] or as porous medium [500].	usual trick is to sprinkle particles on a cotton ball or a polymer foam spacer or graphite nanoparticles as spacers, so that they can be easily distinguished in the tomograms [509,340]. Otherwise, segmentation and extraction of individual particles from the tomograms (of a packed bed of particles) can easily be more time consuming than sample mounting and scanning combined. There are tools to help with this task, but their effectiveness is shape dependent. Watershed based segmentation methods work best for convex shapes and can cope with mildly concave shapes [510,511]. Markov chain template matching method can be used for any shape in a mono-shape packing (e.g., DigiUtility) but extremely time consuming. Other specialist tools are available [512–517]. Machine learning (ML) tools are also becoming available [498,518–523]. • Commercial CT scanners now come bundled with, or at least allow their raw CT data to be processed by third-party, GPU-enabled reconstruction software, reducing reconstruction time from hours to minutes.	
Synchrotron tomography (3D)	μm - mm			• Maybe an overkill for shape characterisation, more useful for in-situ tracking time evolution or dynamics of a particulate system in close to real-world environments [524,525]. Its X-ray source purity and power, and parallel beam (as opposed to fan or cone beam), mean faster and higher quality imaging compared to those from cheaper desktop CT scanners [526,527]. • Real time reconstruction on GPUs is a reality but the high cost of computing hardware means that it is only available at present in some synchrotron and medical facilities [528,529,530]. Deep learning based reconstruction has the potential to make real-time reconstruction more widely spread [531].	Phase 1 of UK's Diamond Light Source costed $330M (£263M). Only one of its several beamlines is required for tomographic imaging. Beamtime or access is by application and free for scientific use.
NMR or MRI (3D)	μm - mm	mm - cm	• NMR or MRI (nuclear magnetic resonance imaging) is a useful tool for monitoring chemical reactions or dissolution in flow through a porous medium or packing [532-535].	• NMR specifically applies to nuclei with odd number of nucleons, typically ^{1}H and ^{13}C, thus best suited to bio (carbon) or water based samples.	
Partial capture of shapes (3D)	μm - mm	mm - cm	• Several techniques exist to allow particles (or more generally a geometric scene) to be scanned from one side. The working principles are diverse and varied, but the devices are all designed to capture only a half of the particle's geometry at a time, thus often referred to as 2.5D techniques. Examples include confocal microscopy [536–539] structured light microscopy and tomographic phase microscopy for small particles, profilometry and laser scanning for large particles. Zheng et al. [540] showed how to correct shape factors obtained from half particle geometry. • Bujak & Bottlinger [541] described a method to capture free-falling particles from three orthogonal directions and reconstruct particle in 3D sense. • Ziegel et al. [542] developed statistical procedures for estimating shape and orientation of arbitrary 3D particles, via volume tensors, from sections of the particles.	• The method demonstrated by Bujak & Bottlinger [541] may be regarded as a simplistic parallel optical tomography with just 3 projections. Many details are missed, but it should still provide more information than from IA of a single 2D projections. • Sectioning and histology are often used for biological and mineralogical analyses where size and shape are a by-product rather than the main purpose. • Optical means (e.g., holography, confocal and other microscopy) that require focus suffer from limited depth of field. • Unless the hidden side is known to be different (e.g., from a depth image of a human face to 3D head reconstruction), symmetry is frequently assumed when reconstructing a full 3D object from the 2.5D data.	A holographic microscope can cost as little as $250.

(*continued on next page*)

Table 4 (*continued*)

Technique	Typical resolution	Applicable sample size range	Purposes and applications	Comments	Typical cost of hardware
			• Digital holographic tomography (DHT) [543,544] is an optical tomography technique. Imaging is based on contrast in absorption and refractive index in the sample. Unlike a X-ray μCT where the sample rotates, in DHT the sample is stationary but the illumination light beam rotates on top of the sample, thus it is 2.5D but much faster than X-ray μCT. It is useful for imaging small, light, semi-transparent particles – the kind that X-ray μCT may struggle with.		
Full 3D scanners and cameras (3D)	0.1 mm	cm – m	• 3D cameras and scanners are commercially available to allow 3D object, structure or scene to be captured. Depending on the model, mode of operation and object size, sub-mm resolution can be achieved. • Turchiuli & Castillo-Castaneda [455] showed a make-shift 3D scanner for diary powder particles. • Smartphone photogrammetry, based on techniques such as SfM (structure-from-motion), has been used to capture and characterise, in field conditions, 3D cm-sized particles [545,546,396] or rock joint roughness [547,548]. • With Apps like polycam (https://poly.cam/), any smartphone with a camera can be used to capture images around an object and reconstruct it when operated in photo (grammetry) mode, or scan and reconstruct a 3D scene when operated in LiDAR mode on phones equipped with a LiDAR sensor (e.g., iPhone Pro).	• Point clouds tend to be imperfect (noisy) and incomplete (missing surfaces) as it can capture visible surfaces. It is possible to patch missing parts up in some situations using AI [549]. • Can easily be turned into voxels, thus can be used directly as input to voxel-based computer models. • Tools exist, often bundled with hardware, to extract geometry from point clouds, thus computer models (e.g., FEM, FDM) that take CAD data for structure input can also use them. • Limited to exposed (i.e., optically accessible) surfaces.	3D camera/scanner costs $500 or more.

Table 5
Classification of "shape" relating publications in Powder Technology in 2003 and 2023 respectively.

	2003	2023
Number of hits from the search	30	103
Total number of papers in the year in Powder Technology	316	932
Number of hits with a title containing the word "shape"	1	14
Number of hits not directly relating to "particle shape"	11	22
Number of hits focusing on "characterisation"	5	10
Number of hits focusing on "modelling" – DEM related	1	26
Number of hits focusing on "modelling" – Others	5	15
Number of hits focusing on "effects"	10	46

Table 6
Comparison of particle-shape embracing computer models.

Model basis	Shape representation	Typical use	Features	Comments	Software examples
Dynamic models for particulate systems/processes					
DEM (sphere based)	Spheres, other shapes are approximated by clumping spheres together.	Dynamic behaviour of powder particles	• Sphere is the simplest (fastest) shape for collision/overlap detection in a particle-level simulation. • Sphere based DEM has multiple, well established contact force models for different situations. • Relatively easy to parallelise (as a typical particle-based system). Commercial software can now run on GPUs, thus significantly reduces the running time. • Very large user base and excellent user support. • A small number of primary spheres can be used to approximate almost any shapes [605–613] • Multi-sphere model vs bonded-particle model: spheres can be clamped together to represent a rigid body, or the primary particles can be grouped using intra-granular bonds which can handle tension, compression, tangential forces, bending torque, and torsion torque. The former is faster but the latter can deal with soft, flexible, deformable or crushable objects [614–617]. Grohn et al. [618] presented a comparative case study between the two models for powder compression under cyclic loading.	• Difficult to truly represent sharp corners or edges, or flat and smooth surfaces. • Shape fidelity is increased by using more spheres but more spheres means more computing time. • Contact force models used in DEM usually assume small overlaps between the spheres. Using many small spheres to represent a (large) shape can reduce the amount of overlaps the simulation can handle, unless special measures are in place to deal with large (e.g., larger-than primary sphere) overlaps. There may also be discrepancies in the nature of contact (e.g., point contact vs line contact vs face contact) and number of contacts. Therefore, simply using more primary spheres does not automatically guarantee more accurate results [573,619–623]. • Finding the optimal balance between the two conflicting requirement is still largely a trial-and-error exercise by the user. • If used to simulate breakage of agglomerates, the results are affected by the initial composition since primary spheres do not break, only the bonds between them are allowed to break. • Before conducting a full-scale DEM, it is necessary to calibrate, through essentially a retrofitting optimisation process, some micro-parameters (e.g., rolling and sliding friction, and restitution coefficients, Young's modulus, Poisson's ratio) so that sphere-based DEM can match certain key macro-properties (e.g., angle of repose) of the real (non-spherical) thing at a small scale. Given its importance, the issue has been addressed and re-addressed many times and the latest developments appear to be towards standardisation, automation and use of machine learning techniques [572,624–631].	EDEM (www.altair.com/edem) PFC-3D (www.itascainternational.com) Granularworks® (www.granuleworks.com) ThreeParticle/CAE (www.becker3d.com) MercuryDPM (www.mercurydpm.org)
DEM (non-spherical, equation described shapes)	Primary building blocks are non-spherical but still equation-based and parametrically defined. Introduced to DEM by Williams and Pentland [632] in 2D and extended to 3D by Cleary et al [633,634], superquadrics [635], including superellipsoids and supertoroids, have become a common method to represent different shapes in DEM simulations. In its general form, it is defined as	Dynamic behaviour of a mixture of different shapes. Particle packing.	• YADE is a generic DEM code [636], featuring object-oriented programming thus easier to plug-in user's own simulation code. SudoDEM [637] is built on YADE but include non-spherical primary building blocks such as poly-superellipsoids, superellipsoids, cylinders, cones, polyhedrons. • SDEM [638,433] can deal with a wide range of shapes represented using superquadric (symmetrical and convex), multi-superquadric (clamping together several superquadric shapes), poly-superquadric (splicing together parts of superquadric shapes) and level-set method (for shapes with sharp corners and cracks). • There are numerous examples of superquadrics based DEM simulations [639,640). In comparison, SH based DEM examples [641,642,643,644] are not as many. There is a practical reason for that, most SH based	• While flexible, open-source codes do have a steep learning curve compared to commercial ones. • Require specialist contact detection algorithms [645–658]. • May be less computationally efficient than sphere based models for similar shapes [659]. • Superquadrics can have sharp corners/edges but the ones used in DEMs tend to be limited to smooth surfaced with rounded corners and edges.	YADE-OPEN DEM (open-source) (www.yade-dem.org) SudoDEM (open-source) (www.sudodem.github.io)

(*continued on next page*)

Table 6 (*continued*)

Model basis	Shape representation	Typical use	Features	Comments	Software examples
	$\left\|\frac{x}{a}\right\|^r + \left\|\frac{y}{b}\right\|^s + \left\|\frac{z}{c}\right\|^t = 1$ where (r,s,t) are positive real numbers. They cover a very wide range of shapes that resemble cubes, octahedrons, cylinders, tablets, capsules, doughnut. Spherical harmonics (SH), developed by Garboczi [322] for star-shaped particles (see also Table 2), is another popular means to represent shapes in DEM simulation.		simulations are for real particles and they need to be digitised first (e.g., by CT scans).	• Alaniz et al. [660] has demonstrated an iterative re-composition method to turn multi-views of an 3D object into a poly-superquadric model. Liu et al, [430] showed a probabilistic approach to fit point clouds to superquadric models. The reconstructed models can be used in superquadric DEM simulations. • Soltanbeigi et al. [661] showed how multi-sphere and superquadric representations compare in DEM simulations.	
DEM (3D image based) [662,663,664]	Voxel based, 3D images as from CT scans or computer generated	Dynamic behaviour of particles of different shapes. Particle packing.	• Can use real particle shapes, as real as machines can measure. • Collision/overlap detection is as simple as checking for double (or multiple) occupancy in the underlying lattice grid. • Contact force is proportional to overlap volume which can be calculated at sub-voxel level if required. • Computing time is not dependent on shape complexity, but on number of solid voxels. Thus, a fractal structure can be handled as quickly as equal-volume spheres. • Use voxels as the basic building blocks, and relationships between voxels in a simulation are easier and faster to handle than spheres (or any other building block shapes). A flat panel TV screen can display any moving objects or scene but the pixels never change their locations, only their colours. Image based DEM models like DigiDEM operate in the same way in a 3D lattice grid. When particles move/rotate, grid cells do not move/rotate, only the voxels change their locations in the grid. This is a key difference between voxel-based approach and others (that use building blocks to make arbitrary shapes), and the main reason why it is faster in handling complex shapes. • Output (packing structure) can be used directly as input for grid based property calculation programs such as FDM and LBM.	• Even modest scale simulations routinely involve 40–50 million voxels. • Extremely demanding of computer resources especially RAM. • Poor scalability: doubling the size of a sub-group of particles in a vector or geometry based DEM makes no difference in RAM or CPU requirements, but 8× more voxels will need to be used in DigiDEM with the pro-rota increase in computing time and RAM. • Unlike a typical particle-based or grid-based system for which parallelisation paradigms are well-developed, DigiDEM algorithm works in a mishmash of both, and cannot make effective use of either to parallelise. • For packing simulations, DEM models need to run for orders of magnitude more (time) steps, but do not necessarily take proportionally more CPU time, than stochastic models. This is because, (1) stochastic models need to take remedial steps to correct for trial moves that end up in overlaps, thus their per step CPU time is much longer than DEM's; and (2) with interaction forces being the guide, DEM is more efficient in finding resting positions for particles than models that move particles randomly. • Using voxels also makes it easy to handle multi-component particles, as each voxel can be assigned different properties. • The image based DEM (iDEM) by Zhang & Tahmasebi [664] uses nodal points on particle surface to calculate overlaps, so it is not a voxel-based one.	DigiDEM (www.structurevision.com)

(*continued on next page*)

Table 6 (*continued*)

Model basis	Shape representation	Typical use	Features	Comments	Software examples
DEM (polyhedron based)	Polyhedrons (both convex and non-convex shapes, or cluster of polyhedrons)	Dynamic behaviour of particles of different shapes. Particle packing.	• Excels when true sharp edges or corners and flat surfaces need to be preserved. • Easy to link with existing CAD programs since the underlying data structures are compatible (both for grouped vertices). • Vertex based, thus also relatively easy to parallelise and can run on GPUs (e.g., [171]).	• While DigiDEM couples with LBM when needed, iDEM with conventional CFD. • Cannot faithfully represent curved smooth surfaces. • Requires special methods to detect and process collisions and overlaps [665–667, 171,668,669]. • More time consuming than sphere-based DEM for similar situations. • To reduce the computational burden, Illana et al. [670] use fully resolved shape where shape effects are critical (e.g., at narrow orifice) and volume-equivalent, property adjusted spheres elsewhere (e.g., in the bulk), and achieved 340% speedup in their hopper flow test case without accuracy loss. This is however only useful for cases where shape-critical regions are small relative to the domain. Otherwise, the speed advantage is lost. • However, a ray tracing DEM scheme may come to the rescue to speed up mesh based DEMs [671].	Rocky (www.ansys.com) BlazeDEM-GPU (open-source) (github.com/erfanrazi/blazedemGPU)
DEM (NURBS-based)	Arbitrary rounded shapes	Dynamic behaviour of particles of different shapes.	• NURBS stands for non-uniform rational B-splines, consists of control points connected by curves rather than straight line segments (as in mesh), thus can more accurately describe shapes with curved surfaces. • NURBS is already used by some commercial software (e.g., Aviso, Simpleware) for CT data processing, so shape models from CT data can be easily imported to NURBS DEM [672,673]. • NURBS based DEM models have been reported in the literature (e.g., [674–676].	• It used to be a popular method in computer graphics due to its smaller memory requirement and superior scalability (compared to mesh), but subdivision surfaces (i.e., finer mesh) have made NURBS obsolete because mesh is easier to create and process.	
DEM (element based)	Varied (spheres, super-quadrics, polyhedrons)	Particle fracture and breakage	• FRM (fragment replacement method) [677,678,679] starts with whole particles, then use stress or force distribution to decide where fracture or breakage should take place, and replace the broken parts with discrete elements (of spherical or irregular shapes). • BEM (bonded element method) ([680], 2001) can bond polyhedral elements to form particles and simulate their fracture/breakage. • Image based DEM [681] can simulate all three modes of breakage (splitting, chipping, and fragmentation) with non-planar fracture surfaces because the breakage criteria are applied at voxel level in 3D image.	• FRM is more computationally efficient than BEM because the number of fragments only increases when breakage happens, but the result is dependent on failure criterion used. • BEM elements do not fracture or break (although they are allowed to change shape), thus the results are dependent on size/shape of the elements and how they bond. Also, BEM carries a rather high computational cost.	
DEM (Miscellaneous)	Various (e.g., sets of points or curves)	Dynamic behaviour of particles of different shapes.	• Level-set (LS) based DEM examples include [682–688] for arbitrary shapes with sharp corners and/or changing topology; NURBS (non-uniform rational B-splines) DEM [672,673] which can seamlessly incorporate CT scanned irregular particle shapes as CT data processing programs (e.g., Aviso, Simpleware) output resolved shapes in this format; Metaball-Imaging DEM [689] for blobby looking objects.	• Shape representing models in this category are common in compactness, sophistication, complication and versatility for hard to describe, naturally occurring shapes, compared to other DEM models. They all originated from early days of computer graphics, aiming to accurately represent irregular shapes with a minimal set of parameters. • Good at accurate representation of shapes with smooth and curved surfaces but complicated collision and overlap detection, and can be computationally expensive (e.g., demonstration cases generally involve a small number of particles).	LS-DEM (level-set DEM)

(*continued on next page*)

Table 6 (*continued*)

Model basis	Shape representation	Typical use	Features	Comments	Software examples
MD and pulse-based DEM (sphere based)	Sphere	Hard sphere	• In the early days of DEM, MD (molecular dynamics) style model [690] was a strong competitor. Both used spheres, although soft spheres in DEM and hard spheres in MD. Both now can use spheres to assemble non-spherical shapes in simulations. • LAMMPS [691] is an open-source, user-extendable, MD based particle simulator, well-known for its massive parallelisation and ability to handle large numbers (e.g., billions) of particles, with a few built-in non-spherical shapes (e.g., ellipsoidal and polyhedral, line, and triangular particles) and can of course use rigid assembly of spheres for other shapes. • LIGGGHTS is another open-source code, based on LAMMPS but, as the name suggests, specifically improved for general granular and granular heat transfer simulations. User-extendable, can work with other simulation engines for co-simulation (e.g., CFDEM for CFD-DEM; ParScale for intra-particle transport). Now includes superquadric shapes. Can also be used to simulate particle growth or shrinkage [692].	• Steep learning curve, especially if code modification is required, for specific applications. • Not designed to be user-interactive, GUI-based, and do not have built-in sophisticated tools for data analysis of results. • Aspherix® is a successor of LIGGGHTS, commercial, with GUI and post-processing tools hence easier to use. Includes both multi-sphere and bonded particle models for non-spherical shapes. Includes Multi-physics models, can simulate mass transfer and chemical reactions.	LIGGGHTS (open-source) (www.cfdem.com/liggghtsr-open-source-discrete-element-method-particle-simulation-code) LAMMPS (open-source) (www.lammps.org) Aspherix (www.aspherix-dem.com)
MPM (point based) and Peridynamics (PD)	Points	Particle deformation, breakage and fracture	• FEM and MPM share the same continuum mechanics framework and constitutive models, MPM can simulate what FEM can, with less accuracy or otherwise more time consuming, but without the problems associated with mesh distortion and the need for remeshing, making it particularly suited for simulation large deformations of objects [693–700]. • Peridynamics [701–706] is also point based, and specially formulated to deal with fractures of solids such as particles [701,707].	• Both methods are mass point based thus compatible and convertible, their relative strengths can be combined and exploited by a hybrid such that PD deals with the cracks while MPM the rest [708,709,710]. • MPM has the same flexibility as 3D image based DEM in handling arbitrary shapes. DEM and MPM are complementary, the former is well suited for problems with large displacements (and can handle large number of particles), the latter with large deformations. A hybrid of the two has the potential to handle a large number of deformable irregular shapes with DEM efficiency and MPM accuracy. In fact, examples of DEM-MPM combination have already been reported, where MPM is used at individual particle level [699,711], or to represent the surrounding continuum medium [712,713,714,715]. • Similarly, PD and DEM can combine to take advantages of both for breakage problems [716,].	PeriLab (open-source) (https://github.com/ElsevierSoftwareX/SOFTX-D-24-00031)
Models for **packing** of irregular shapes					
DEM [717–723,647]	Any	Packing is a by-product of dynamic simulation of particle assembly – when particles are allowed to naturally settle down (i.e., virtually lose all their kinetic energy).	• Can simulate any shape. • Can easily study influence of process conditions (e.g., vibration, stirring, or in a rotating drum). • DEM can be used in a hybrid mode to increase the runtime efficiency for packing [724]. Randomly placed particles are allowed to grow and move around. The DEM procedure identifies, deals with and reduces the overlaps more efficiently than the traditional MC procedure.	• Tend to take longer than specialist packing models. • DEM relies on overlaps for contact forces, and overlaps tend to result in an overestimate of the packing fraction. • Overlaps also makes it difficult for the packing structure to be used directly for CFD/FEM simulations as their re-meshing routines often require input geometric entities to be air-tight and non-overlapping.	

(*continued on next page*)

Table 6 (*continued*)

Model basis	Shape representation	Typical use	Features	Comments	Software examples
DigiPac [725,726,727,728,729]	Voxel, or poly-cubes	Stochastic, purpose-built packing model for arbitrary shapes	• DigiPac is voxel-based packing model for arbitrary shapes using random-walks to move particles around. • A similar model described by Byholm et al. [727] with better speed performance. • Remond & Gallias [726] compared full and semi-digital packing models and show that the semi-digital approach performed better when particles were small (as measured in pixels).	• DigiDEM is a DEM version of DigiPac. • The main difference between full and semi-digital models is that in semi-digital model, particle positions are real numbers rather than integers. • Real number positions and displacements are also employed in DigiDEM.	
Other non-DEM models	Varied	Non-DEM based models for packing	• Examples of non-DEM packing models for non-spherical shapes include Nolan & Kavanagh [730] using sphere-composite, Lee et al. [731] for ellipsoids, Abreu et al. [732] for spherocylinders, Lee et al. [733] for convex polyhedrons, Pérez Morales [734] for spherocylinders but extendable to general shapes, Liu et al. [713] for superellipsoids, Salemi & Wang [735] for asphalt aggregates using an image-based FEM approach, Rémond et al. [728] for non-convex cut pieces of a hollow cylinder.	• Non-DEM models had been popular, but are now giving way to DEM models.	
Models for **property-structure** relationships					
FEM	Mesh	Calculation of contact forces between non-spherical particles [736,737,738,210].	• Compared to FDM, FEM is typically much more computationally efficient because it employs non-uniform sized mesh grid (fine grid where it matters and coarse grid for the rest) resulting in much fewer grid cells to compute.	• Remeshing entailed by structural deformation/fracture can be expensive. • Detailed but limited to a small number of contacting objects.	LS-DYNA (www.ansys.com)
FDM	Grid cells or voxels	Various (e.g., heat transfer, dissolution)	• Relatively easy to formulate and to code by anyone with engineering training, and to incorporate multi-physics. • DigiDiss is a dissolution model for irregular shapes or complex structures [236,739]. • DigiTherm calculates effective conductivity of packing of arbitrary shapes or CT scanned porous media [740].	• Natural fit with lattice grid, or voxel based, structure models from CT scans or simulations.	
SPH	Particles		• Meshless, Lagrangian particle-based, good at simulating free-surface flow in confinement of complex geometry and through porous media; solid mechanics; multi-phase flow; and fluid-structure interactions [741].		LS-DYNA (www.ansys.com)
LBM	Lattice grid cells or voxels	Flow in/around complex geometries such as porous media [742,743]	• Being a lattice grid based numerical model, Lattice Boltzmann Method (LBM) can easily handle any shape or structure which is voxel-represented.	• Often used to calculate permeability of porous media [744,368] or drag force in LBM-DEM simulations, but LBM alone can simulate particles suspended or settling in fluid [745,746,747].	OpenLB (open-source) (www.openlb.net)
DEM **coupling** with another model					
FEM-DEM or FDEM (mesh based)	Mesh	Deformation and fracture of geo-objects (e.g., rocks). Packing.	• Can simulate fracture and fragmentation without the need to seed (whereas a pure FEM model would need to). • Open-source, general purpose, 2D and 3D, FEM-DEM solid mechanics codes are available [748,749,750]. • Can deal with arbitrary shapes [751,752,753,754,755].	• Not easily extendable to powders (involving 10^3 or more objects) due to computational costs.	Solidity (open-source) (www.solidityproject.com) OpenFDEM (openfdem.com) PFC/FLAC3D (www.itascacg.com/)
CFD-DEM coupling	Mesh for CFD	Particle-fluid interactions	• The are a large number of examples of CFD-DEM coupling for a variety of applications [756,757,758,596,759,760,761,762,763,764,765,748].	• The most common instances of DEM coupling with another model is with CFD. • The vast majority of CFD-DEM simulations use CFD cells that are large enough to contain several DEM particles	EDEM+Fluent

(*continued on next page*)

Table 6 (*continued*)

Model basis	Shape representation	Typical use	Features	Comments	Software examples
LBM-DEM and DNS-DEM coupling	Lattice grid based	LBM is a FDM style, grid based, numerical model for fluid flow, suitable for cases involving boundaries of complex geometry such as porous media and irregular shapes [766,689]. DNS is similar in resolution and capability in dealing with arbitrary shapes, but based on different (and more conventional CFD style) formulation [767].	• Both LBM and DNS operate at a sub-particle resolution, i.e., an individual particle is usually represented by many grid cells, thus can easily deal with arbitrary shapes. • Drag force is calculated as a result of LBM or DNS, thus effects of particle shape, (relative) flow speed, regime and direction are all taken care of automatically. • of relative there is no need to employ any shape-dependent drag force formula. • LBM is a FDM style implementation of the kinetic theory ideas to compute fluid flow at a scale closer to DNS than CFD. A DEM-LBM model of particles typically operates with a 2 to 4 orders of magnitude finer mesh grid than DEM-CFD. In DEM-LBM a particle is divided into 10s–100s grid cells (voxels) across, whereas in DEM-CFD, a CFD cell contains multiple particles. Thus, DEM-LBM embeds particle shapes explicitly but typical DEM-CFD considers shape effects implicitly. However, there has been examples where CFD is used at a sub-particle scale [768].	• Extremely computationally demanding • In DigiDEM example, the LBM part takes >95% of the total runtime, even with GPU support. • There is a conflict that needs special resolution: while DEM is dependent on overlaps to calculate contact forces, LBM must have a gap between colliding particles to properly calculate flow and drag forces. • If LBM alone is used for particles in fluid (e.g., [745,746]), this would not be an issue since particles do not overlap. • Examples of LBM and DEM coupling include [600,769–771].	DigiDEM (www.structurevision.com)
AI involvement					
AI involvement	Varied	If there is a pattern to exploit, AI can possibly help. [772]	• AI can potentially help reconstruct 3D shapes from single or multiple views of the objects (see Table 7 for examples). • In particle simulations, collision/overlap detection is usually the most computationally expensive step. CNN (convolutional neural network) has been shown to help with this step and achieved a speedup by orders of magnitude for spheres [773]. Lai et al. [774] gave an example for irregular shapes. • CNN has also been used to predict constrained modulus for granular soil [775]. • ANN (artificial neural network) has been trained to predict drag force on individual particles in suspension [776] or terminal velocity [777], which should be useful for DEM simulations. • It is possible to predict fluid-particle flow fields using ANN and LSTM (long short-term memory) with significant (~40%) saving in simulation time [778]. • Chen et al. [779] gave an example where ML is used to predict what is happening inside a hopper from limited discharge data, thus doing the job that DEM is typically used for. Admittedly, DEM in this case provided the training dataset.	• Requires a large amount of data and huge amount computing power for the training. • Making such data available often means that the problem being helped with by the AI must already be solvable (for simulations) or measurable (for experiments) another way. • Like empirical correlations, training and thus application of AI is usually case specific. • Similarities between DEM and NN (Neural Network) in AI are striking. Particles in DEM correspond to perceptrons (neurons) in NN, each controlled by its own set of parameters (properties) and each plays a small yet non-negligible role, in a defined and non-linear way (particles by Newton's laws, perceptrons by say sigmoid function). Particles interact with each other, so do neurons. And it is the interactions that determine their respective collective behaviours. Applied forces (including gravity) in DEM correspond to input data to NN. DEM simulated powder behaviour corresponds to AI predicted pattern. Both are good at finding and exploit (hidden) patterns, and both can be used generatively. Even their advancement paths are similar (i.e., sluggish for decades then growing exponentially), albeit not to the same scale. A crucial difference is that while neurons and their links are fixed, particles move and interact dynamically. Thus, after training AI is quick to respond but DEM takes hours if not days to run. It remains to be seen if the similarities could be exploited to create a new breed of DEM.	MFiX (for training data provision) (mfix.netl.doe.gov) TensorFlow (for AI model building and training) (www.tensorflow.org) PyTorch (a popular alternative to Tensorflow) (www.pytorch.org)

Table 7
Machine Learning methods useful for characterising and reconstructing 3D particle shapes.

Model	Features	Comments
Conventional (geometric model-based) 3D reconstruction methods that may be helped or replaced by AI [791]	• SfS (shape-from-shading): Assuming that the light conditions are known and the object has a smooth and continuous Lambertian surface (i.e., reflecting light equally in all directions), with a single image, SfS algorithms estimate, from pixel intensity gradients, surface normals at each pixel, then integrate the normals to recover depth information, and obtain a 3D representation of the shape [792,793]. • SfM (structure-from-motion): Given a sequence of images taken from different viewpoints, SfM involves feature extraction, feature matching across the images, estimating camera poses, triangulating the features to create a 3D point cloud [545,396]. • SLAM (simultaneous localisation and mapping): This in a way is an extension of SfM but attempts to work out camera pose and create a 3D map of the environment simultaneously, often in real-time, with details and accuracy being increased by processing successive images of the same environment as the camera moves around [794,795].	• The emphasis here is not how the images are obtained in the first place, but on how they can be processed to obtain 3D shape information. • SfS can fail if the Lambertian assumption is not met or due to ambiguities arising from non-ideal lighting conditions. Although SfS is not on its own a ML model, it has increasingly found help from AI [796,797,798,799]. SfS can also be used in conjunction with stereo imaging to obtain shapes [800], as also exemplified in Table 4 under SEM. • SLAM is typically used in robotics applications but could conceivably be used for autonomous 3D images of large rocks etc.
3D-R2N2 [801] Pix2Vox [802,803]	• Voxelised reconstruction of 3D object from a single or multiple (photo) images from arbitrary (random) viewpoints. (http://3d-r2n2.stanford.edu/) • 3D-R2N2 stands for 3D recurrent reconstruction neural network. It "learns a mapping from images of objects to their underlying 3D shapes from a large collection of synthetic data using 3D-Convolutional LSTM which allows attention mechanism to focus on visible parts in 3D". • An improvement of 3D-R2N2, in terms of consistency of output, long-term memory of important features in early input images, and training speed, has been made by Xie et al. [802], called Pix2Vox (https://github.com/hzxie/Pix2Vox). Its follow-up, Pix2Vox++ [803], is not only context-aware (i.e., objects do not need to be isolated from the background first) but also multi-scale (i.e., not fixed at 32^3 as 3D-R2N2 is, and can be easily extended to 64^3 or 128^3).	• Training and testing datasets are available from ShapeNet – a huge collection of well-categorised images of some everyday objects such as chairs, tables, cars, aircrafts, etc. • One can make one's own training/testing datasets for powder particles from CT scans, CAD or some specialist particle generators (e.g., DigiUtility, Matlab Fourier analysis shape generator, etc), and store the data in the open-standard format used by ShapeNet. • The original 3D-R2N2 was implemented based on a particular Python library (Theano) which is out of date now. Implementations based on newer libraries (e.g., PyTorch, TensorFlow) are available from GitHub, all with GPU support. • Since the output is in voxel format, it can be directly used by 3D image based particle-level simulation models such as DigiPac and DigiDEM. • According to Xie et al. [802], ML methods based on RNNs (recurrent neural networks), including 3D-R2N2, suffer from three problems: (i) permutation variance, i.e., quality of output is dependent on the order of input images; (ii) long-term memory loss, i.e., important features from early input images may be forgotten; and (iii) time-consuming training because input images are processed sequentially rather than in parallel. Newer models (e.g., Pix2Vox, DeepMVS and AttSets) overcome or lessen the above problems by adopting different approaches. • Other networks proposed for reconstruction of 3D object from a single or multiple images include LSM [804], 3DensiNet [805], DeepMVS [806], RayNet [807], AttSets [808].
NeRF [809,810] NeuS & NeuS2 [811–813] Geo-NeuS [814] Depth-NeuS [815] SDFusion [816]	• Introduced by Mildenhall et al. [809], NeRF (neural radiance field) models quickly gained popularity as a view synthesis method. It uses volume rendering with typically implicit neural scene representation to learn the geometry and lighting of a 3D scene [810]. NeRF is self-supervised (i.e., needing only multi-view images of a scene as input, 3D/depth supervision not required); the poses can be estimated using SfM; and the result is photo-realistic. • However, extracting high-quality surfaces from NeRF representation is difficult because of insufficient surface constraints in the representation. To resolve this problem, NeuS [811] represents surface as a zero-level set of a signed distance function (SDF) and uses a new volume rendering method to train a neural SDF. The result is better quality surface reconstruction, especially for objects or scenes with complex structure and self-occlusion. NeuS2 [813] is a significant improvement in accuracy and speed over NeuS. • NeRF and NeuS lack explicit multi-view geometry constraints, meaning they usually fail to generate geometry consistent surface reconstruction. Geo-NeuS [814] fills this gap by directly locating the zero-level set of SDF network and explicitly perform multi-view geometry optimisation. This gives results that look cleaner and smoother. • NeuS predicts depth information, which is not required by NeRF, by learning RGB image features through a network. Geo-NeuS uses interpolation and SfM supervision to help with the prediction. Inevitably the predictions contain errors. Depth-NeuS adds the depth information as input to improve surface reconstruction.	• Note that, on its own, NeRF is a view generator but it does not explicitly reconstruct the surface of an object/scene. • Self-supervision of NeRF and NeuS is particularly attractive feature if these methods are used for 3D reconstruction of particles. • Due to high demand of computing resources, many ML based 3D reconstruction networks limit the output to 32x32x32 volume, which is restricting for particle simulations. • Cheng et al. [816] proposed SDFusion that uses a new encoder-decoder to compress 3D shape information, thus making it easy to scale up to 128x128x128 resolution. • Zheng et al. [817] addressed this problem by using depth SDF representation and incorporating an implicit template shape so that shape prior contained in the template can be utilised for the reconstruction to retain more complex topology and shape details than pre-existing networks like 3D-R2N2 or Mesh R-CNN. • NeuS combines implicit surface representation and radiance field to achieve surface reconstruction through volume rendering without the need to calculate the exact surface. Since it represent the entire space within a single network, large scale reconstruction is not feasible. Li et al. [521] proposed Vox-Surf, a hybrid of a neural implicit surface representation and an explicit voxel representation to overcome the limitation. However, the method requires multi-view images, and the trained network is scene specific and cannot be used for other scenes without retraining.

(*continued on next page*)

Table 7 (*continued*)

Model	Features	Comments
ShapeClipper [818]	• This method "learns high-quality reconstruction through single-view supervision without known viewpoint and can reconstruct shapes of various objects". It is based on CLIP, a neural network that learns visual concepts from natural language supervision [819]. • The paper [818] also listed several other single-view methods for object shape reconstruction. They differ in supervision (fully-supervised, weakly supervised, image supervision, shape supervision), whether it is view point free or not, and how shape is represented: by occupancy function [820], by point cloud [821], by depth [822], by SDF [823], by mesh [824–827].	• CLIP allows useful information to be extracted from natural langue text such as "round table" is not just a tag but both the adjective and the noun give clues about the shape and such additional information can be made use of. For example, it makes it easier to find similar shapes to the input across the whole training dataset and use them to regulate shape learning. • According to the creators of ShapeClipper, it does not work as well for occluded or deformable shapes.
3D-CNN [828,781]	• Can generate 3D shapes from a limited number of 2D projections [781] or 2D slices/sections [516]. • Examples of using 3D-CNN (and other AI techniques) to extract bio shapes are given by Esteva et al. [829] and Li et al. [830]. • Mask R-CNN has been used to reconstruct 3D rocks from video tracking of 2D random projections [831], or to track 3D rod-like particles in a suspension [499]. • Using AI to reconstruct 3D porous structures from 2D slices have been demonstrated [832–834].	• Results from IA of 2D images are not the same as from 3D reconstruction (e.g., circularity vs sphericity). • This latest development shows that AI can not only reconstruct 3D objects from 2D projections but also characterise the 3D objects in terms of shape descriptors (sphericity, elongation, aspect ratio, flatness, etc), requiring much fewer 2D projections than traditional CT method (e.g., 8 for AI vs 1440 for CT). On the other hand, AI relies on learned experience through training (usually with a huge amount of data), only works for shape categories it has been trained for and only produces an approximation, whereas CT works for any (new) shapes and provides ground-truth quality result. • AI is almost 6× as fast as Fourier method (4 min vs 23 min to generate 220 particles). However, if the results are used as input for DEM simulations, the time difference at the particle generation stage is negligible because the runtime of DEM is often many hours if not days; and the Fourier method is actually preferred because it provides the ground truth in the first place.
ResNet [835] and derivatives	• Introduced by Microsoft Research, ResNet and its variants (e.g., ResNet50) are among the most popular (with over 230,540 citations in under 8 years) CNN architectures because they ease the training of deep networks. Deep networks often suffer from the vanishing gradient problem (i.e., as the gradient is backpropagated through layers, it can become so small as to slow or even prevent convergence during training). ResNet residual learning framework addresses this problem by allowing gradients to flow through the layers without significant attenuation.	Examples of networks that use ResNet as the backbone, for 3D reconstruction from a single image, include: • PPR-CNet for face reconstruction [836]. • PushNet to reconstruct 3D shapes in point cloud format from a single colour image [837]. • Mesh R-CNN from Facebook [838] combines voxel generation and triangular mesh reconstruction to generate 3D mesh structure of an object from a 2D single-view image. Mesh R-CNN-LS adds a Laplacian smoothing to it to constrain triangular deformation for a better and smoother 3D mesh [839]. • Hybrid 3DU-GNet [840] uses VGG-ResNet framework for depth analysis. The hybrid 3D U-Net and graph network generates a point cloud of an object from a single-view object image and accurately predicts its volume.
NVIDIA Kaolin tools (https://developer.nvidia.com/kaolin)	• Not an AI 3D shape reconstructor per se but the toolkit allows 3D shapes to be represented and rendered in an AI friendly way, to help others develop AI tools for 3D shape reconstruction. • One example is DIB-R (an interpolation-based differentiable rendering framework) that can be used to reconstruct 3D object with realistic geometry, texture and colour (lighting/shading) from a single image [841]. • Another example is NGLOD (neural geometric level of detail), which combines neural networks, SDF (signed distance function) based shape representation, and efficient rendering techniques, for real-time rendering with high-fidelity surface details of difficult structures such as 3D fractals (Fig. 4b) [842].	• Open source, free for research use. • Optimised for NVIDIA GPUs.
NVIDIA Neuralangelo [843]	• Turns images from a video clip into a detailed 3D reconstruction of the object or the scene, using NVDIA Instant NeRF to help capture fine textures. (https://blogs.nvidia.com/blog/neuralangelo-ai-research-3d-reconstruction/).	• A sequence of images from a video clip can be used to work out relative positioning of viewpoints from an arbitrary starting point. • Can make use of textures of complex materials in its reconstruction, and works with video clips captured using smartphones. This means that anyone with a smartphone can start to digitise, in-situ, rocks or any sizeable objects in front of them. • It is a 3D surface rendering tool and excels in capturing surface geometry or texture. Could be useful for model validation and for digital twin setup, given its 3D scene rendering ability.

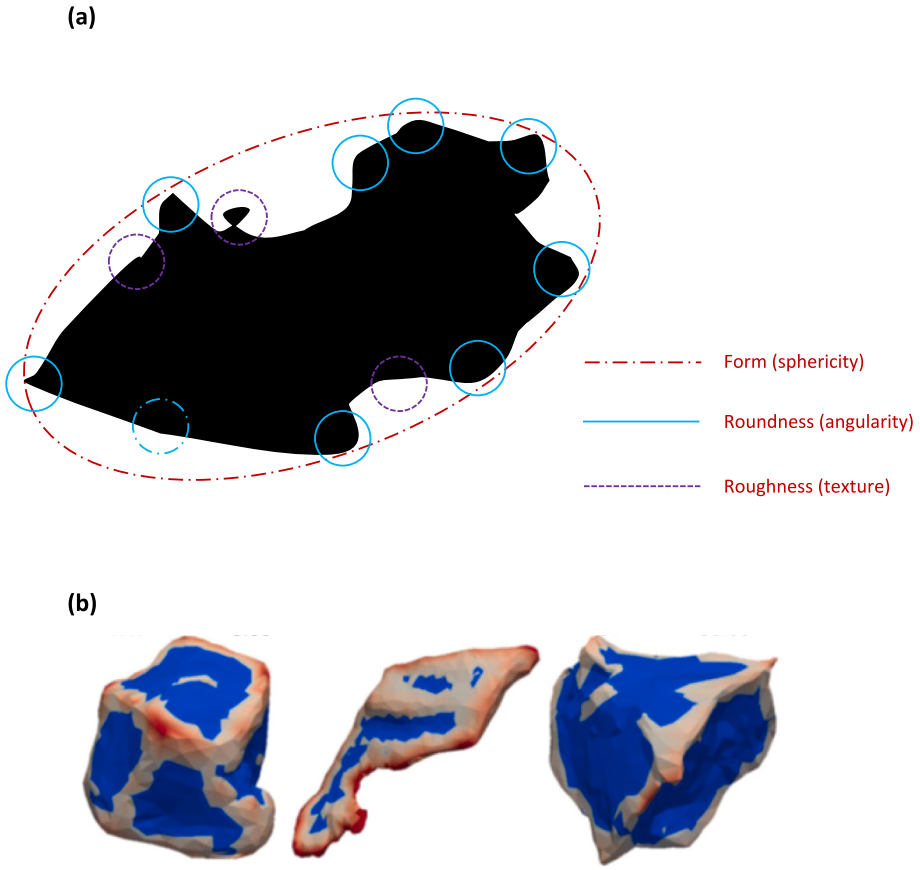

Fig. 1. Three scales that shape descriptors are used to describe (a) in 2D (following examples of [62,383]) and (b) in 3D (from [282]).

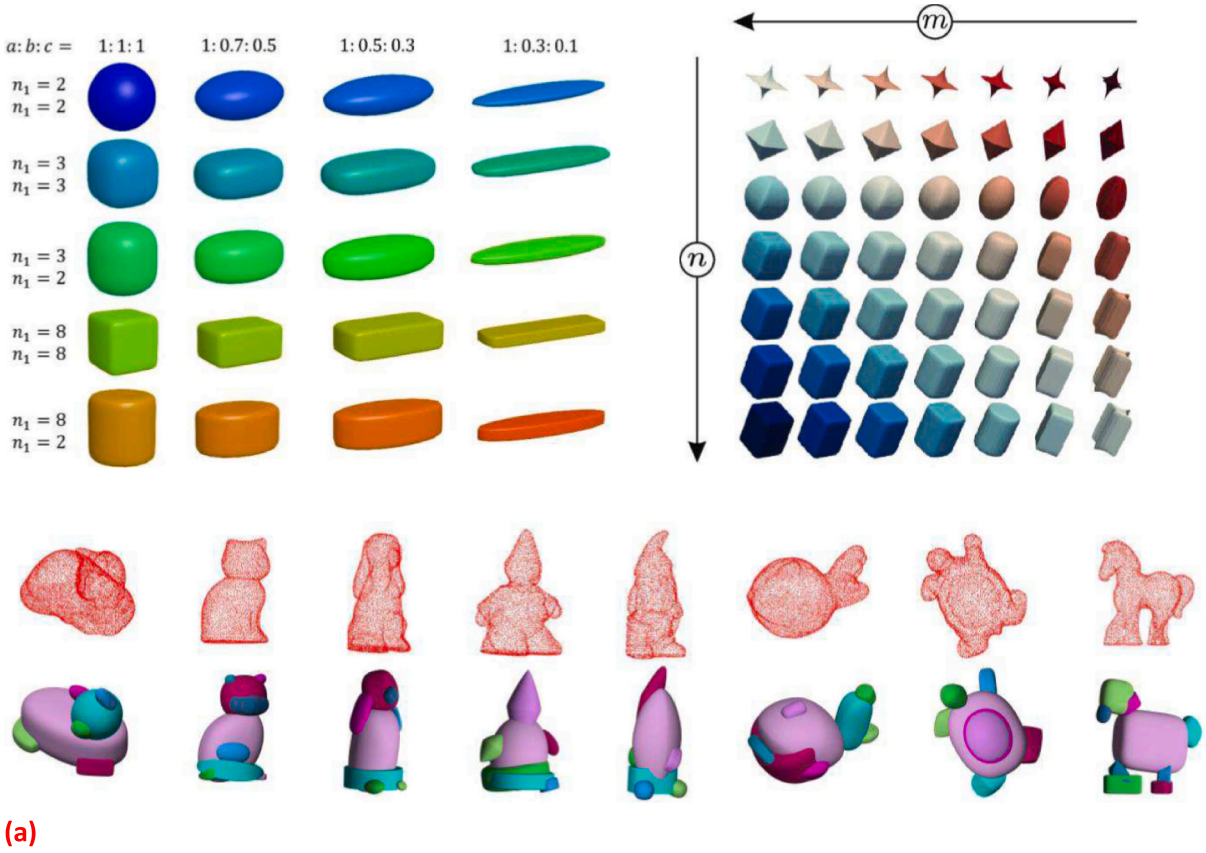

Fig. 2. Examples of shapes that particle-level simulation models can handle. (a) Superquadrics based. A typical single-superquadric shape is smooth, symmetrical, either rounded or sharp edged, either solid or toroidal. They can be combined (as in multi- or poly-superquadrics) to represent more complex shapes. (b) Spherical harmonics based. Typically star-shaped, smooth but textured. The ripples are more often an artefact of using high order terms than a representation of real surface roughness. (c) X-ray CT scanned. The raw data are voxelated (and directly usable by DigiPac/DigiDEM) but can be meshed up and smoothed in post-processing (for input to other DEM models). (d) Point clouds from 3D camera or laser scanning. They are typically imperfect and incomplete. The raw form can be used directly by DigiPac/DigiDEM, or usable as template for multi-sphere approximation, or meshed up for others. (Sources of images [29,340,428–437].

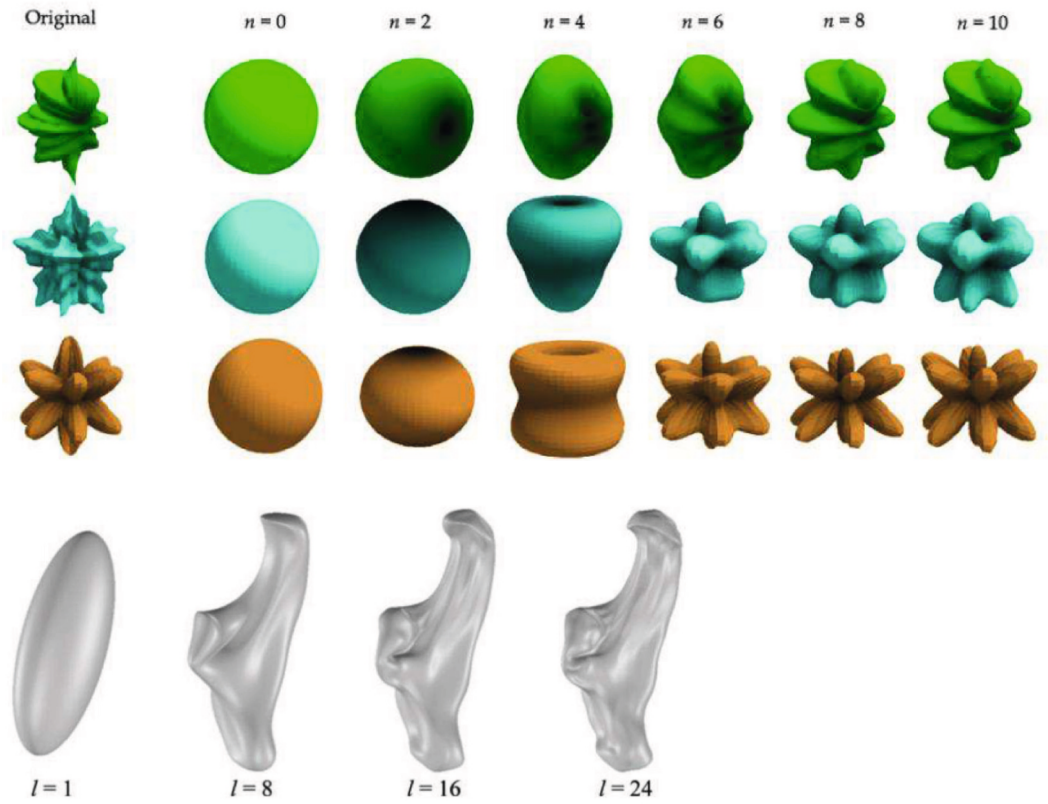

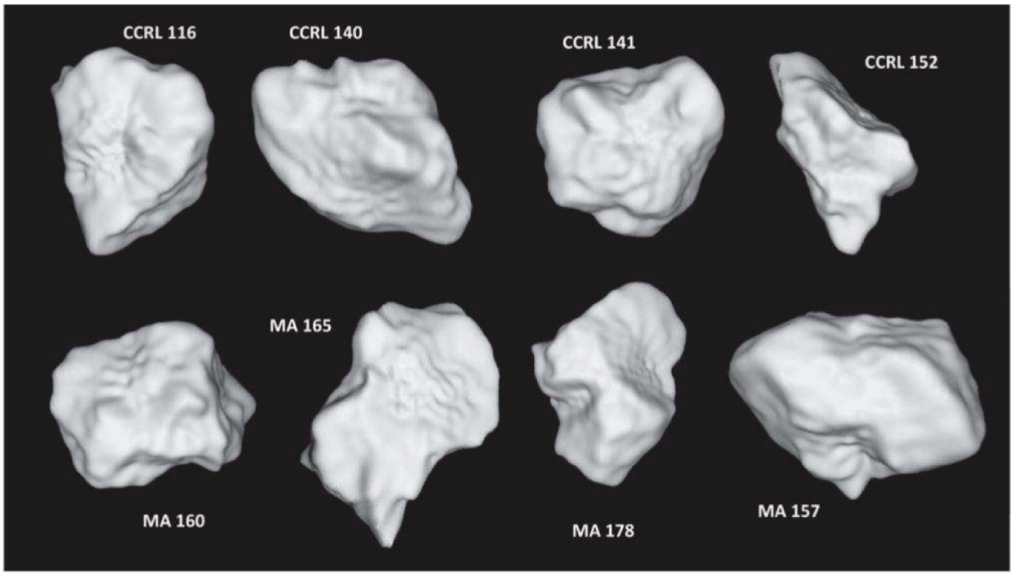

(b)

Fig. 2. (*continued*).

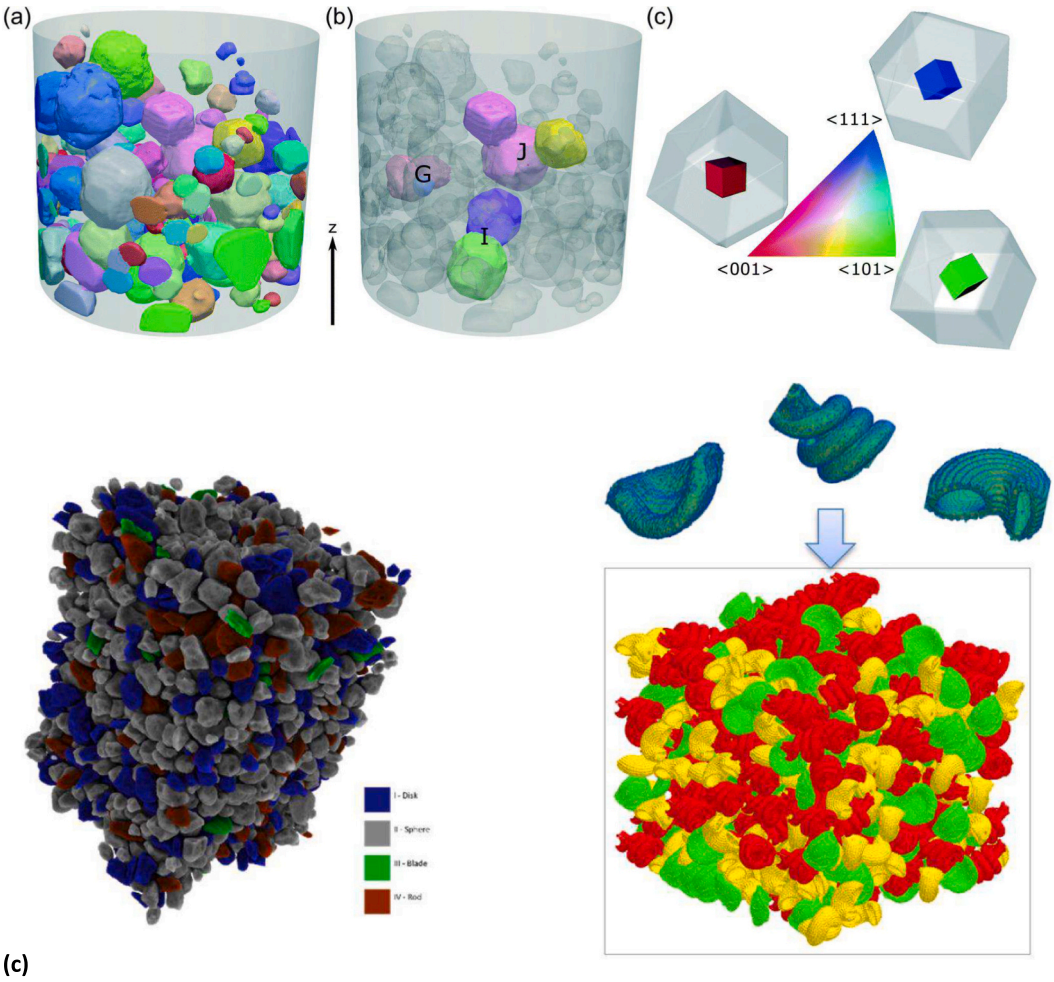

Fig. 2. (*continued*).

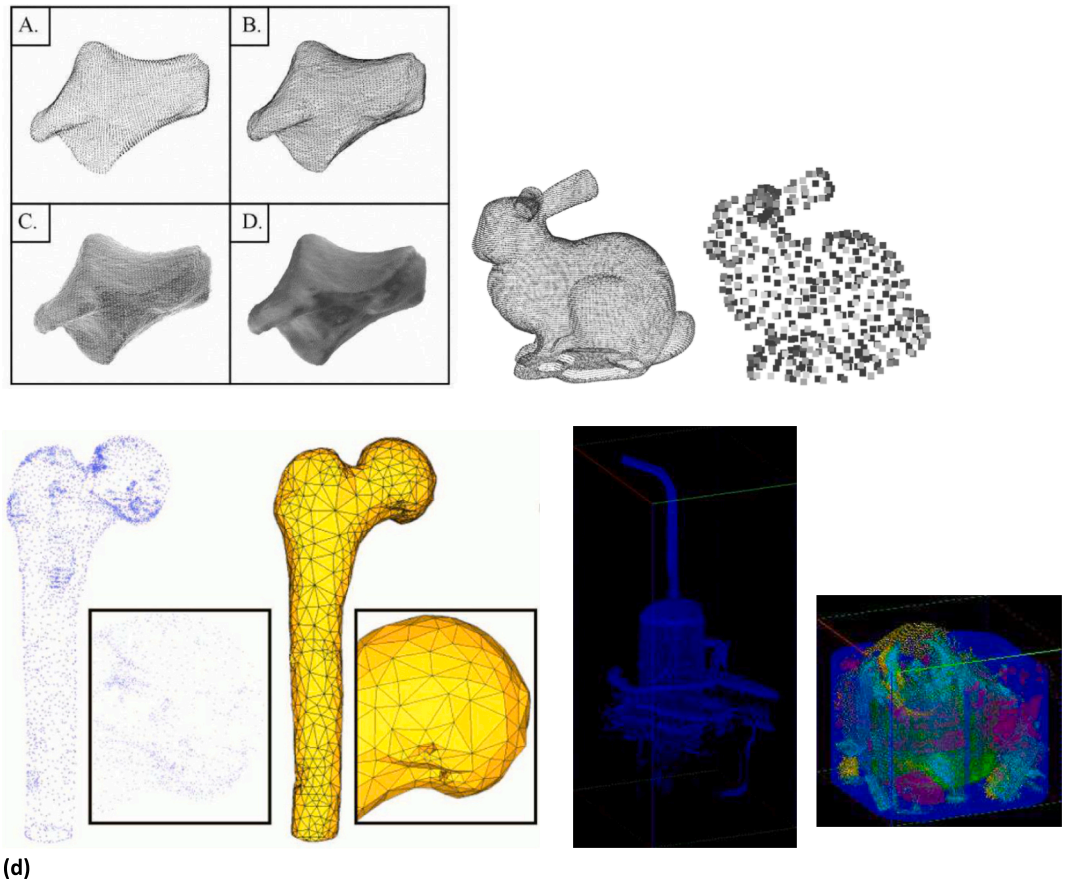

Fig. 2. (*continued*).

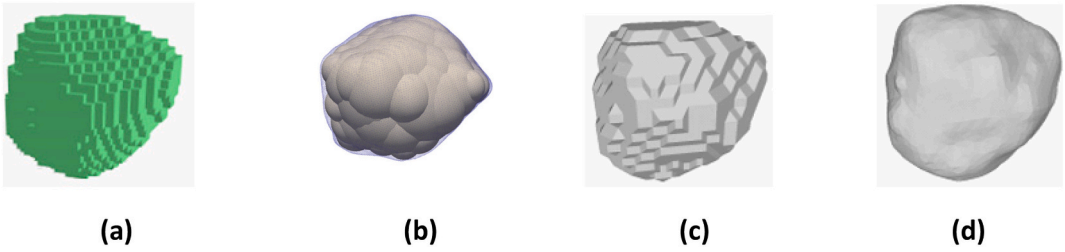

Fig. 3. Shape representations used in computer models (a) 3D image or voxel-based (directly from a CT scan), used in DigiPac/DigiDEM; (b) multi-sphere representation, usable by EDEM/PFC3D; (c) a mesh representation, usable by Rocky; (d) a smoothed version by SH or superquadric, usable by SDEM or SuperDEM. (Sources of images: [780,781]).

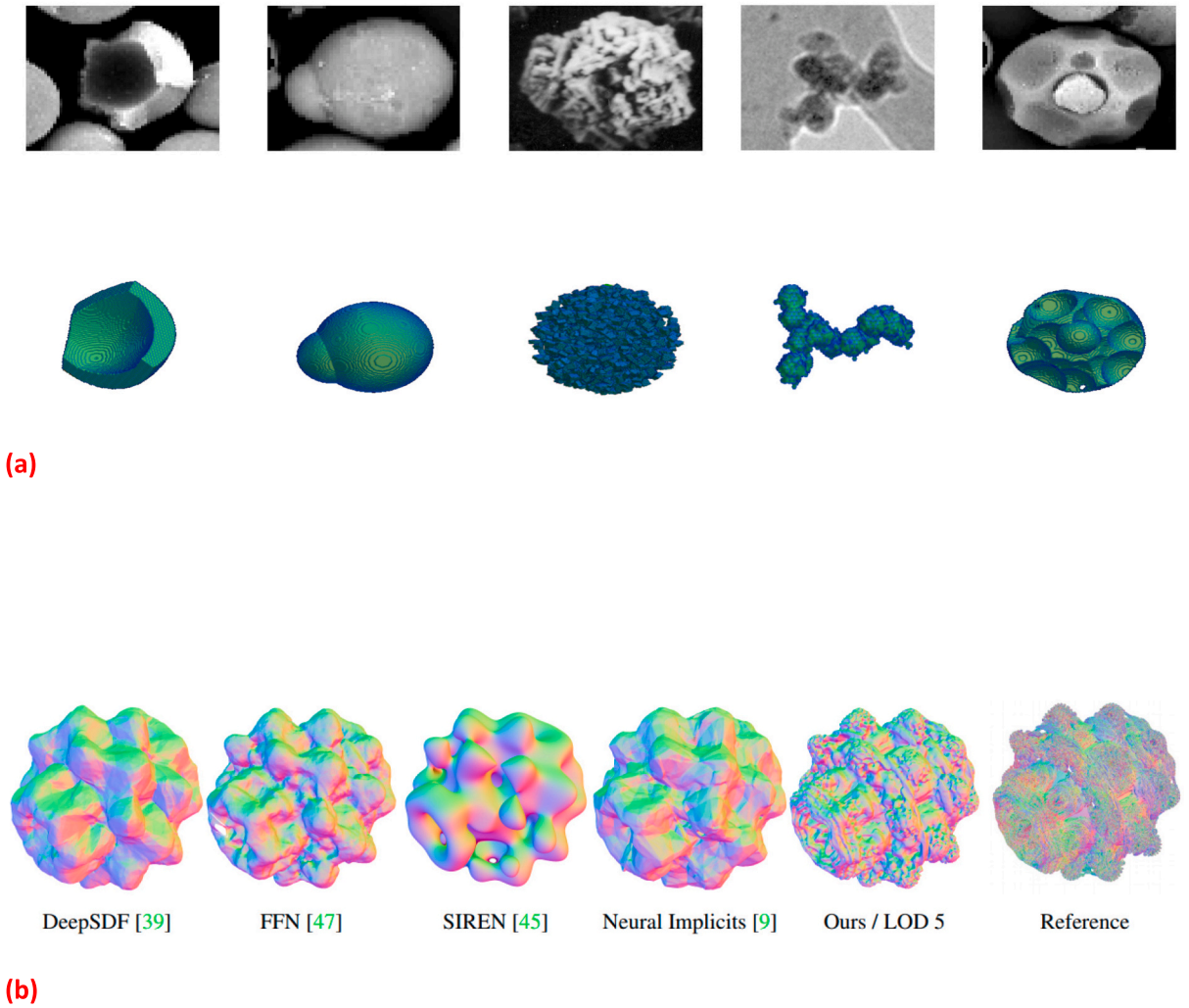

Fig. 4. (a) Given SEM or photo images of irregular shapes, with the right tool (e.g., DigiUtility or CAD), it is possible to manually construct/assemble a usable mimic for simulations. Can AI take over this tedious task? (b) Examples of AI reconstructed shape (a Mandelbulb fractal structure reconstructed using different methods [842]).

CRediT authorship contribution statement

X. Jia: Conceptualization, Writing – original draft, Writing – review & editing. **R.A. Williams:** Conceptualization, Writing – original draft, Writing – review & editing.

Declaration of competing interest

The authors declare that they have no known competing financial interests or personal relationships that could have appeared to influence the work reported in this paper.

Data availability

No data was used for the research described in the article.

Acknowledgements

The authors are honoured to express their personal gratitude to Reg Davies and co-pioneers of particle technology that brought a sense of fun, ambition and industrial focus to our research.

References

[1] T. Allen, Particle Size Measurement, 4th edn, Chapman & Hall, 1990. ISBN: 041235070X.
[2] R. Cocco, Jia Wei Chew, 50 years of Geldart classification, Powder Technol. 428 (2023) 118861, https://doi.org/10.1016/j.powtec.2023.118861.
[3] D. Geldart, Types of gas fluidization, Powder Technol. 7 (5) (1973) 285–292, https://doi.org/10.1016/0032-5910(73)80037-3.
[4] O. Molerus, Interpretation of Geldart's type A, B, C and D powders by taking into account interparticle cohesion forces, Powder Technol. 33 (1) (1982) 81–87, https://doi.org/10.1016/0032-5910(82)85041-9.
[5] J.P.K. Seville, C.D. Willett, P.C. Knight, Interparticle forces in fluidisation: a review, Powder Technol. 113 (3) (2020) 261–268, https://doi.org/10.1016/S0032-5910(00)00309-0.
[6] T. Yehuda, Haim Kalman, Geldart classification for wet particles, Powder Technol. 362 (2020) 288–300, https://doi.org/10.1016/j.powtec.2019.11.073.
[7] B.H. Kaye, A Random Walk through Fractal Dimensions, Verlagsgesellschaft mbH, VCH, 1994, ISBN 9783527290789, https://doi.org/10.1002/9783527615995.
[8] T. Aste, D. Weaire, The Pursuit of Perfect Packing, IoP Publishing, 2000. ISBN: 0750306483.
[9] J.H. Conway, N.J.A. Sloane, Sphere Packings, Lattices, and Groups, 3rd edition, Springer-Verlag, New York, 1999.
[10] S. Marín-Aguilar, F. Camerin, S. van der Ham, et al., A colloidal viewpoint on the sausage catastrophe and the finite sphere packing problem, Nat. Commun. 14 (2023) 7896, https://doi.org/10.1038/s41467-023-43722-0.
[11] B. Yu, X.Z. An, R.P. Zou, R.Y. Yang, K. Kendall, Self-assembly of particles for densest packing by mechanical vibration, Phys. Rev. Lett. 97 (2006) 265501, https://doi.org/10.1103/PhysRevLett.97.265501.

[12] P. Weiss, Candy science: M&Ms pack more tightly than spheres, Sci. News 165 (Feb 14) (2004) 102. https://www.sciencenews.org/article/candy-science-mms-pack-more-tightly-spheres.
[13] T. Hales, M. Adams, G. Bauer, et al., A formal proof of the Kepler conjecture, For. Math. Pi 5 (2017) e2, https://doi.org/10.1017/fmp.2017.1.
[14] Y. Yuan, Lufeng Liu, Wei Deng, Shuixiang Li, Random-packing properties of spheropolyhedra, Powder Technol. 351 (2019) 186–194, https://doi.org/10.1016/j.powtec.2019.04.018.
[15] Y. Yuan, Lufeng Liu, Yuzhou Zhuang, Weiwei Jin, Shuixiang Li, Coupling effects of particle size and shape on improving the density of disordered polydisperse packings, Phys. Rev. E 98 (2018) 042903, https://doi.org/10.1103/PhysRevE.98.042903.
[16] K. Dong, Chuncheng Wang, Aibing Yu, Voronoi analysis of the packings of non-spherical particles, Chem. Eng. Sci. 153 (2016) 330–343, https://doi.org/10.1016/j.ces.2016.07.013.
[17] M. Fan, Su Dong, Xiangsheng Chen, Monodisperse and polydisperse packings of equiaxed concave particles: Effects of angularity and roughness, Powder Technol. (2024) 119924, https://doi.org/10.1016/j.powtec.2024.119924.
[18] X. Jia, R. Caulkin, A. Williams, Z.Y. Zhou, A.B. Yu, The role of geometric constraints in random packing of non-spherical particles, Europhys. Lett. 92 (6) (2010) 68005, https://doi.org/10.1209/0295-5075/92/68005.
[19] A. Miyazaki, T. Yada, K. Yogata, et al., A newly revised estimation of bulk densities and examination of the shape of individual Ryugu grains, Earth Planets Space 75 (2023) 171, https://doi.org/10.1186/s40623-023-01904-6.
[20] J. Tian, Enlong Liu, Effect of particle shape on micro- and mesostructure evolution of granular assemblies under biaxial loading conditions, Comptes Rendus Mécanique 346 (12) (2018) 1233–1252, https://doi.org/10.1016/j.crme.2018.08.013.
[21] B. Zhao, X. An, Y. Wang, Q. Qian, X. Yang, X. Sun, Dem dynamic simulation of tetrahedral particle packing under 3D mechanical vibration, Powder Technol. 317 (2017) 171–180.
[22] F.C. Frank, J.S. Kasper, Complex alloy structures regarded as sphere packings. I. Definitions and basic principles, Acta Cryst 11 (1958) 184–190, https://doi.org/10.1107/S0365110X58000487.
[23] S.J. Antony, Matthew R. Kuhn, Influence of particle shape on granular contact signatures and shear strength: new insights from simulations, Int. J. Solids Struct. 41 (21) (2004) 5863–5870, https://doi.org/10.1016/j.ijsolstr.2004.05.067.
[24] S. Arasan, E. Yenera, F. Hattatoglu, S. Hinislioglua, S. Akbuluta, Correlation between shape of aggregate and mechanical properties of asphalt concrete: digital image processing approach, Road Mater. Pavement Des. 12 (2) (2011) 239–262, https://doi.org/10.1080/14680629.2011.9695245.
[25] P.W. Cleary, The effect of particle shape on simple shear flows, Powder Technol. 179 (3) (2008) 144–163, https://doi.org/10.1016/j.powtec.2007.06.018.
[26] J.C. Santamarina, G.C. Cho, Soil Behaviour: The Role of Particle Shape, Advances in Geotechnical Engineering: The Skempton Conference, Thomas Telford, London, 2004, pp. 604–617.
[27] H. Shin, J.C. Santamarina, Role of particle angularity on the mechanical behavior of granular mixtures, J. Geotech. Geoenviron. Eng. 139 (2) (2013) 353–355, https://doi.org/10.1061/(ASCE)GT.1943-5606.0000768.
[28] M.J. Vepraskas, D.K. Cassel, Sphericity and roundness of sand in coastal plain soils and relationships with soil physical properties, Soil Sci. Soc. Am. J. 51 (5) (1987) 1108–1112, https://doi.org/10.2136/sssaj1987.03615995005100050003x.
[29] Verena Becker, Oleg Birkholz, Yixiang Gan, Marc Kamlah, Modeling the influence of particle shape on mechanical compression and effective transport properties in granular Lithium-ion battery electrodes, Energ. Technol. 9 (2021), https://doi.org/10.1002/ente.202000886.
[30] S.C. Thakur, H. Ahmadian, J. Sun, J.Y. Ooi, An experimental and numerical study of packing, compression, and caking behaviour of detergent powders, Particuology 12 (2014) 2–12, https://doi.org/10.1016/j.partic.2013.06.009.
[31] F.N. Altuhafi, M.R. Coop, V.N. Georgiannou, Effect of particle shape on the mechanical behavior of natural sands, J. Geotech. Geoenviron. Eng. 142 (12) (2016) 04016071, https://doi.org/10.1061/(ASCE)GT.1943-5606.0001569.
[32] S. Carrasco, D. Cantor, C. Ovalle, Effects of particle size-shape correlations on steady shear strength of granular materials: the case of particle elongation, Int. J. Numer. Anal. Methods 46 (2022) 979–1000, https://doi.org/10.1002/nag.3329.
[33] W. Dai, Dorian Hanaor, Yixiang Gan, The effects of packing structure on the effective thermal conductivity of granular media: A grain scale investigation, Int. J. Therm. Sci. 142 (2019) 266–279, https://doi.org/10.1016/j.ijthermalsci.2019.04.028.
[34] P. Datta, Salah A. Faroughi, Angle of repose for superquadric particles: investigating the effects of shape parameters, Comput. Geotech. 165 (2024) 105918, https://doi.org/10.1016/j.compgeo.2023.105918.
[35] F. De Cola, A. Pellegrino, C. Glößner, et al., Effect of particle morphology, compaction, and confinement on the high strain rate behavior of sand, Exp. Mech. 58 (2018) 223–242, https://doi.org/10.1007/s11340-017-0331-x.
[36] W. Fei, Guillermo A. Narsilio, Joost H. van der Linden, Antoinette Tordesillas, Mahdi M. Disfani, J. Carlos Santamarina, Impact of particle shape on networks in sands, Comput. Geotech. 137 (2021) 104258, https://doi.org/10.1016/j.compgeo.2021.104258.
[37] J. Gan, Zongyan Zhou, Aibing Yu, Effect of particle shape and size on effective thermal conductivity of packed beds, Powder Technol. 311 (2017) 157–166, https://doi.org/10.1016/j.powtec.2017.01.024.
[38] E. Ganju, M. Kılıç, M. Prezzi, et al., Effect of particle characteristics on the evolution of particle size, particle morphology, and fabric of sands loaded under uniaxial compression, Acta Geotech. 16 (2021) 3489–3516, https://doi.org/10.1007/s11440-021-01309-3.
[39] J. Gong, Zhihong Nie, Yangui Zhu, Zhengyu Liang, Xiang Wang, Exploring the effects of particle shape and content of fines on the shear behavior of sand-fines mixtures via the DEM, Comput. Geotech. 106 (2019) 161–176, https://doi.org/10.1016/j.compgeo.2018.10.021.
[40] N. Govender, Paul W. Cleary, Mehran Kiani-Oshtorjani, Daniel N. Wilke, Chuan-Yu Wu, Hermann Kureck, The effect of particle shape on the packed bed effective thermal conductivity based on DEM with polyhedral particles on the GPU, Chem. Eng. Sci. 219 (2020) 115584, https://doi.org/10.1016/j.ces.2020.115584.
[41] Y. He, Y.Y. Li, T.J. Evans, A.B. Yu, R.Y. Yang, Effects of particle characteristics and consolidation pressure on the compaction of non-spherical particles, Miner. Eng. 137 (2019) 241–249, https://doi.org/10.1016/j.mineng.2019.04.007.
[42] M.A. Hosseini, Pejman Tahmasebi, On the influence of the natural shape of particles in multiphase fluid systems: granular collapses, Comput. Geotech. 162 (2023) 105654, https://doi.org/10.1016/j.compgeo.2023.105654.
[43] J. Hu, Hongwei Wu, Gu Xiaoqiang, Qihui Zhou, Particle shape effects on dynamic properties of granular soils: a DEM study, Comput. Geotech. 161 (2023) 105578, https://doi.org/10.1016/j.compgeo.2023.105578.
[44] D. Huck-Jones, Beyond particle size: exploring the influence of particle shape on metal powder performance, Metal AM 3 (4) (2017) 99–103. https://www.metal-am.com/articles/the-influence-of-particle-shape-on-powder-performance-metal-3d-printing/.
[45] Y.X. Huo, Y.F. Leung, C.Y. Kwok, Micro-mechanical perspective on the role of particle shape in shearing of sands, Can. Geotech. J. 60 (10) (2023) 1515–1531, https://doi.org/10.1139/cgj-2022-0270.
[46] J. Landauer, Michael Kuhn, Daniel S. Nasato, Petra Foerst, Heiko Briesen, Particle shape matters – using 3D printed particles to investigate fundamental particle and packing properties, Powder Technol. 361 (2020) 711–718, https://doi.org/10.1016/j.powtec.2019.11.051.
[47] J. Li, Yanli Huang, Shenyang Ouyang, Gang Zhao, Yachao Guo, Huadong Gao, Laiwei Wu, Accurate measurement and quantitative analysis of 3D shape characteristics of irregular gangue blocks, Constr. Build. Mater. 342 (B) (2022) 127880, https://doi.org/10.1016/j.conbuildmat.2022.127880.
[48] T. Li, K. Xie, X. Chen, et al., Computer vision-aided DEM study on the compaction characteristics of graded subgrade filler considering realistic coarse particle shapes, Railw. Eng. Sci. 32 (2024) 194–210, https://doi.org/10.1007/s40534-023-00325-1.
[49] R. Lu, Qiang Luo, Tengfei Wang, David P. Connolly, Kaiwen Liu, Chunfa Zhao, Discrete element modelling of the effect of aspect ratio on compaction and shear behaviour of aggregates, Comput. Geotech. 161 (2023) 105558, https://doi.org/10.1016/j.compgeo.2023.105558.
[50] X. Ma, H. Lei, X. Kang, Effects of particle morphology on the shear response of granular soils by discrete element method and 3D printing technology, Int. J. Numer. Anal. Methods Geomech. 46 (2022) 2191–2208, https://doi.org/10.1002/nag.3384.
[51] M.A. Maroof, A. Mahboubi, E. Vincens, et al., Effects of particle morphology on the minimum and maximum void ratios of granular materials, Granul. Matter 24 (2022) 41, https://doi.org/10.1007/s10035-021-01189-0.
[52] C. Nouguier-Lehon, B. Cambou, E. Vincens, Influence of particle shape and angularity on the behaviour of granular materials: a numerical analysis, Int. J. Numer. Anal. Methods Geomech. 27 (2003) 1207–1226, https://doi.org/10.1002/nag.314.
[53] M. Panchal, Paritosh Chaudhuri, Jon T. Van Lew, Alice Ying, Numerical modelling for the effective thermal conductivity of lithium meta titanate pebble bed with different packing structures, Fusion Eng. Des. 112 (2016) 303–310, https://doi.org/10.1016/j.fusengdes.2016.08.027.
[54] S.J. Rodrigues, Nicole Vorhauer-Huget, Evangelos Tsotsas, Prediction of effective thermal conductivity of packed beds of polyhedral particles, Powder Technol. 430 (2023) 118997, https://doi.org/10.1016/j.powtec.2023.118997.
[55] R. Rorato, M. Arroyo Alvarez de Toledo, E.C.G. Andò, et al., Linking shape and rotation of grains during triaxial compression of sand, Granul. Matter 22 (88) (2020), https://doi.org/10.1007/s10035-020-01058-2.
[56] A.V. Smirnov, S.G. Ponomarev, V.P. Tarasovskii, et al., Hard-sphere close-packing models: possible applications for developing promising ceramic and refractory materials (review), Glas. Ceram. 75 (2019) 345–351, https://doi.org/10.1007/s10717-019-00083-9.
[57] H.S. Suh, K.Y. Kim, J. Lee, T.S. Yun, Quantification of bulk form and angularity of particle with correlation of shear strength and packing density in sands, Eng. Geol. 220 (2017) 256–265, https://doi.org/10.1016/j.enggeo.2017.02.015.
[58] W. Sun, Kai Wu, Songyu Liu, Xiang Zhang, Influence of aspect ratio and arrangement direction on the shear behavior of ellipsoids, Particuology 70 (2022) 82–94, https://doi.org/10.1016/j.partic.2022.01.005.
[59] P. Tahmasebi, A state-of-the-art review of experimental and computational studies of granular materials: properties, advances, challenges, and future directions, Prog. Mater. Sci. 138 (2023) 101157, https://doi.org/10.1016/j.pmatsci.2023.101157.
[60] S.C. Thakur, Hossein Ahmadian, Jin Sun, Jin Y. Ooi, An experimental and numerical study of packing, compression, and caking behaviour of detergent powders, Particuology 12 (2014) 2–12, https://doi.org/10.1016/j.partic.2013.06.009.
[61] X. Tan, Z. Qiu, X. Yin, Y. Hu, X. Liu, L. Zeng, Effects of particle shape and packing density on the mechanical performance of recycled aggregates for construction purposes, Buildings 13 (9) (2023) 2153, https://doi.org/10.3390/buildings13092153.

[62] U. Ulusoy, A review of particle shape effects on material properties for various engineering applications: from macro to nanoscale, Minerals 13 (1) (2023) 91, https://doi.org/10.3390/min13010091.

[63] W. Xu, K. Zhang, Y. Zhang, J. Jiang, Packing fraction, tortuosity, and permeability of granular-porous media with densely packed spheroidal particles: monodisperse and polydisperse systems, Water Resour. Res. 58 (2022) e2021WR031433, https://doi.org/10.1029/2021WR031433.

[64] T. Zhang, Chi Zhang, Quanwei Yang, Fu Ran, Inter-particle friction and particle sphericity effects on isotropic compression behavior in real-shaped sand assemblies, Comput. Geotech. 126 (2020) 103741, https://doi.org/10.1016/j.compgeo.2020.103741.

[65] S. Zhao, T. Matthew Evans, Xiaowen Zhou, Shear-induced anisotropy of granular materials with rolling resistance and particle shape effects, Int. J. Solids Struct. 150 (2018) 268–281, https://doi.org/10.1016/j.ijsolstr.2018.06.024.

[66] Y. Zou, G. Ma, J. Mei, J. Zhao, W. Zhou, Microscopic origin of shape-dependent shear strength of granular materials: a granular dynamics perspective, Acta Geotech. 17 (2022) 2697–2710, https://doi.org/10.1007/s11440-021-01403-6.

[67] H.S. Göktürk, T.J. Fiske, D.M. Kalyon, Effects of particle shape and size distributions on the electrical and magnetic properties of nickel/polyethylene composites, J. Appl. Polym. Sci. 50 (11) (1993) 1891–1901, https://doi.org/10.1002/app.1993.070501105.

[68] X. Fu, Deborah Huck, Lisa Makein, Brian Armstrong, Ulf Willen, Tim Freeman, Effect of particle shape and size on flow properties of lactose powders, Particuology 10 (2) (2012) 203–208, https://doi.org/10.1016/j.partic.2011.11.003.

[69] Y. Guo, Jennifer Sinclair Curtis, Discrete element method simulations for complex granular flows, Annu. Rev. Fluid Mech. 47 (2015) 21–46, https://doi.org/10.1146/annurev-fluid-010814-014644.

[70] L. Haferkamp, L. Haudenschild, A. Spierings, K. Wegener, K. Riener, S. Ziegelmeier, G.J. Leichtfried, The influence of particle shape, powder Flowability, and powder layer density on part density in laser powder bed fusion, Metals 11 (3) (2021) 418, https://doi.org/10.3390/met11030418.

[71] B.H. Kaye, Characterizing the flowability of a powder using the concepts of fractal geometry and Chaos theory, Part. Part. Syst. Charact. 14 (1997) 53–66.

[72] S. Mack, P. Langston, C. Webb, T. York, Experimental validation of polyhedral discrete element model, Powder Technol. 214 (2011) 431–442, https://doi.org/10.1016/j.powtec.2011.08.043.

[73] C.R.K. Windows-Yule, D.R. Tunuguntla, D.J. Parker, Numerical modelling of granular flows: a reality check, Comput. Part. Mech. 3 (2016) 311–332, https://doi.org/10.1007/s40571-015-0083-2.

[74] W. Yu, K. Muteki, L. Zhang, G. Kim, Prediction of bulk powder flow performance using comprehensive particle size and particle shape distributions, J. Pharm. Sci. 100 (1) (2011) 284–293, https://doi.org/10.1002/jps.22254.

[75] Berkinova Zhazira, Yermukhambetova Assiya, Golman Boris, Simulation of flow properties of differently shaped particles using the discrete element method, Comput. Appl. Eng. Educ. 29 (5) (2021) 1061–1070, https://doi.org/10.1002/CAE.22359.

[76] J.T. Clemmer, Joseph M. Monti, Jeremy B. Lechman, A soft departure from jamming: the compaction of deformable granular matter under high pressures, Soft Matter 20 (8) (2024) 1702–1718, https://doi.org/10.1039/D3SM01373A.

[77] G.R. Farrell, Preparation, Mechanics and Structure of Sphere Packings Near the Random Loose Packing Limit, 2018, p. 1338, https://doi.org/10.7275/12634832. Doctoral Dissertations, https://scholarworks.umass.edu/dissertations_2/1338.

[78] A.J. Liu, R. Nagel Sidney, Granular and jammed materials. Themed collection, Soft Matter (6) (2010) 2851–3094 (34 items), https://doi.org/10.1039/C005388K.

[79] E. Somfai, Martin van Hecke, Wouter G. Ellenbroek, Kostya Shundyak, Wim van Saarloos, Critical and noncritical jamming of frictional grains, Phys. Rev. E 75 (2007), https://doi.org/10.1103/PhysRevE.75.020301, 020301(R).

[80] R. Ni, M. Stuart, M. Dijkstra, Pushing the glass transition towards random close packing using self-propelled hard spheres, Nat. Commun. 4 (2013) 2704, https://doi.org/10.1038/ncomms3704.

[81] Z. Duriagina, A. Pankratov, T. Romanova, I. Litvinchev, J. Bennell, I. Lemishka, S. Maximov, Optimized packing titanium alloy powder particles, Computation 11 (2023) 2, https://doi.org/10.3390/computation11020022.

[82] H.C. Kim, Sam Hee Han, Young Jin Lee, Dai Il Kim, Packing placement method using hybrid genetic algorithm for segments of waste components in nuclear reactor decommissioning, Nucl. Eng. Technol. 54 (9) (2022) 3242–3249, https://doi.org/10.1016/j.net.2022.04.004.

[83] C. Lamas-Fernandez, J.A. Bennell, A. Martinez-Sykora, Voxel-based solution approaches to the three-dimensional irregular packing problem, Oper. Res. (2022), https://doi.org/10.1287/opre.2022.2260.

[84] D. Mack, A. Bortfeldt, H. Gehring, A parallel hybrid local search algorithm for the container loading problem, Int. Trans. Oper. Res. 11 (2004) 511–533, https://doi.org/10.1111/j.1475-3995.2004.00474.x.

[85] A.G. Ramos, J.F. Oliveira, M.P. Lopes, A physical packing sequence algorithm for the container loading problem with static mechanical equilibrium conditions, Intl. Trans. Op. Res. 23 (2016) 215–238, https://doi.org/10.1111/itor.12124.

[86] H. Ren, Rui Zhong, An autonomous ore packing system through deep reinforcement learning, Adv. Space Res. (2024), https://doi.org/10.1016/j.asr.2024.01.061 (in press).

[87] Jess Rose Sweley, Devin Jia, Xiaodong Williams, Richard Jackson David, Effect of flake shape on packing characteristics of popped popcorn, J. Food Eng. 127 (2014) 75–79, https://doi.org/10.1016/j.jfoodeng.2013.11.028.

[88] R.A. Williams, Xiaodong Jia, Peter Ikin, David Knight, Use of multiscale particle simulations in the design of nuclear plant decommissioning, Particuology 9 (4) (2011) 358–364, https://doi.org/10.1016/j.partic.2010.10.003.

[89] Feng-Cheng Yang, Huangjau Wu, Packing Optimization for Dismantled Parts of Nuclear Facilities - 18625. WM2018: 44. Annual Waste Management Conference, Phoenix, AZ (United States), 18–22 Mar 2018. https://www.xcdsystem.com/wmsym/2018/pdfs/FinalPaper_18625_0123125235.pdf, 2018.

[90] Y. Zhao, Chris Rausch, Carl Haas, Optimizing 3D irregular object packing from 3D scans using metaheuristics, Adv. Eng. Inform. 47 (2021) 101234, https://doi.org/10.1016/j.aei.2020.101234.

[91] X. Zhao, J.A. Bennell, T. Bektaş, K. Dowsland, A comparative review of 3D container loading algorithms, Intl. Trans. Op. Res. 23 (2016) 287–320, https://doi.org/10.1111/itor.12094.

[92] W. Zhu, Sheng Chen, Min Dai, Jiping Tao, Solving a 3D bin packing problem with stacking constraints, Comput. Ind. Eng. 188 (2024) 109814, https://doi.org/10.1016/j.cie.2023.109814.

[93] F.N. Altuhafi, Matthew R. Coop, Vasiliki N. Georgiannou, Effect of particle shape on the mechanical behavior of Natural Sands, J. Geotech. Geoenviron. Eng. 142 (12) (2016) 04016071, https://doi.org/10.1061/(ASCE)GT.1943-5606.0001569.

[94] G.-C. Cho, Dodds Jake, J. Carlos Santamarina, Particle shape effects on packing density, stiffness, and strength: natural and Crushed Sands, J. Geotech. Geoenviron. Eng. 132 (5) (2006) 591–602, https://doi.org/10.1061/(ASCE)1090-0241(2006)132:5(591).

[95] S. Fennis, Joost Walraven, Using particle packing technology for sustainable concrete mixture design, Heron 57 (2) (2012) 73–101.

[96] M. Payan, Arman Khoshghalb, Kostas Senetakis, Nasser Khalili, Effect of particle shape and validity of Gmax models for sand: a critical review and a new expression, Comput. Geotech. 72 (2016) 28–41, https://doi.org/10.1016/j.compgeo.2015.11.003.

[97] Y. Xiao, Long Leihang, T. Matthew Evans, Hai Zhou, Hanlong Liu, Armin W. Stuedlein, Effect of particle shape on stress-Dilatancy responses of medium-Dense Sands, J. Geotech. Geoenviron. Eng. 145 (2) (2019) 04018105, https://doi.org/10.1061/(ASCE)GT.1943-5606.0001994.

[98] M. Yimam, Osano Simpson Nyambane, Silvester Abuodha, Using particle packing technology and admixtures for sustainable and economical concrete mix design, Int. J. Sci. Res. Publ. (IJSRP) 13 (02) (2023), https://doi.org/10.29322/IJSRP.13.02.2023.p13417 (ISSN: 2250–3153).

[99] Y. Zhao, Yihang Duan, Lingli Zhu, Youkai Wang, Zhenghao Jin, Characterization of coarse aggregate morphology and its effect on rheological and mechanical properties of fresh concrete, Constr. Build. Mater. 286 (2021) 122940, https://doi.org/10.1016/j.conbuildmat.2021.122940.

[100] W. Slusser, 5 Ways Particle Size Impacts Pharmaceutical Product Quality, CPS Customer Processing Services Blog, 2022, in: https://www.customprocessingservices.com/blog/5-ways-particle-size-impacts-pharmaceutical-product-quality.

[101] X. Fu, Dutt Meenakshi, A. Craig Bentham, Bruno C. Hancock, Ruth E. Cameron, James A. Elliott, Investigation of particle packing in model pharmaceutical powders using X-ray microtomography and discrete element method, Powder Technol. 167 (2006) 134–140, https://doi.org/10.1016/j.powtec.2006.06.011.

[102] J. Kassel, Differentiating particle size and shape information in drug products with multiple components, Pharm. Technol. 47 (11) (2023) 28–31. https://www.pharmtech.com/view/differentiating-particle-size-and-shape-information-in-drug-products-with-multiple-components.

[103] K.K. Moravkar, Devanshi S. Shah, Anuja G. Magar, Bhushan A. Bhairav, Sudarshan D. Korde, Ketan M. Ranch, Shailesh S. Chalikwar, Assessment of pharmaceutical powders flowability and comparative evaluation of lubricants on development of gastro retentive tablets: an application of powder flow tester, J. Drug Deliv. Sci. Technol. 71 (2022) 103265, https://doi.org/10.1016/j.jddst.2022.103265.

[104] N. Sandler, David Wilson, Prediction of granule packing and flow behavior based on particle size and shape analysis, J. Pharm. Sci. 99 (2) (2010) 958–968, https://doi.org/10.1002/jps.21884.

[105] W. Yu, Lingzhi Liao, Rahul Bharadwaj, Bruno C. Hancock, What is the “typical” particle shape of active pharmaceutical ingredients? Powder Technol. 313 (2017) 1–8, https://doi.org/10.1016/j.powtec.2017.02.043.

[106] S. Zhang, Paul A. Stroud, Aiden Zhu, Michael J. Johnson, Joshua Lomeo, Christopher L. Burcham, Jeremy Hinds, Kyle Allen-Francis Blakely, Matthew J. Walworth, Characterizing the impact of spray dried particle morphology on tablet dissolution using quantitative X-ray microscopy, Eur. J. Pharm. Sci. 165 (2021) 105921, https://doi.org/10.1016/j.ejps.2021.105921.

[107] V.N. Manoharan, Colloidal matter: packing, geometry, and entropy, Science 349 (2015) 6251, https://doi.org/10.1126/science.1253751.

[108] R. Farhadifar, J.C. Röper, B. Aigouy, S. Eaton, F. Jülicher, The influence of cell mechanics, cell-cell interactions, and proliferation on epithelial packing, Curr. Biol. 17 (24) (2007) 2095–2104, https://doi.org/10.1016/j.cub.2007.11.049.

[109] K.A. Newhall, L.L. Pontani, I. Jorjadze, S. Hilgenfeldt, J. Brujic, Size-topology relations in packings of grains, emulsions, foams, and biological cells, Phys. Rev. Lett. 108 (26) (2012) 268001, https://doi.org/10.1103/PhysRevLett.108.268001.

[110] S. Kriegmana, Douglas Blackiston, Michael Levin, Josh Bongard, A scalable pipeline for designing reconfigurable organisms, Proc. Nation. Academy Sci. (PNAS) 117 (4) (2020) 1853–1859, https://doi.org/10.1073/pnas.1910837117.

[111] J.F.F. Pelletier, L. Sun, K.S. Wise, N. Assad-Garcia, B.J. Karas, T.J. Deerinck, M. H. Ellisman, A. Mershin, N. Gershenfeld, R.-Y. Chuang, J.I. Glass, E.A. Strychalski, Genetic requirements for cell division in a genomically minimal cell, Cell 184 (2021) 2430–2440, https://doi.org/10.1016/j.cell.2021.03.008.

[112] M.E. Allen, James W. Hindley, Nina O'Toole, Yuval Elani, Biomimetic behaviors in hydrogel artificial cells through embedded organelles, PNAS 120 (35) (2023) e2307772120, https://doi.org/10.1073/pnas.2307772120.
[113] M.L. Daly, K. Nishi, S.J. Klawa, et al., Designer peptide–DNA cytoskeletons regulate the function of synthetic cells, Nat. Chem. (2024), https://doi.org/10.1038/s41557-024-01509-w.
[114] S.E. Brika, Morgan Letenneur, Christopher Alex Dion, Vladimir Brailovski, Influence of particle morphology and size distribution on the powder flowability and laser powder bed fusion manufacturability of Ti-6Al-4V alloy, Addit. Manuf. 31 (2020) 100929, https://doi.org/10.1016/j.addma.2019.100929.
[115] X. Chen, Hao Zhang, Jinjie Lin, Ruizhen Hu, Lin Lu, Qixing Huang, Bedrich Benes, Daniel Cohen-Or, Baoquan Chen, Dapper: decompose-and-pack for 3D printing, ACM Trans. Graph. 34 (6) (2015), https://doi.org/10.1145/2816795.2818087. Article 213 (November 2015), 12 pages.
[116] J. Vanek, J.A.G. Galicia, B. Benes, R. Měch, N. Carr, O. Stava, G.S. Miller, PackMerger: A 3D print volume optimizer, Comp. Graph. Forum 33 (2014) 322–332, https://doi.org/10.1111/cgf.12353.
[117] H. Connell, J. Zhu, A. Bassi, Effect of particle shape on crossfow filtration flux, J. Membr. Sci. 153 (1) (1999) 121–139, https://doi.org/10.1016/S0376-7388(98)00250-6.
[118] M. Zielina, Particle shapes in the drinking water filtration process, Clean Soil Air Water 39 (2011) 941–946, https://doi.org/10.1002/clen.201000432.
[119] S. Niazi, M. Habibian, M. Rahimi, A comparative study on the separation of different-shape particles using a mini-hydrocyclone, Chem. Eng. Technol. 40 (2017) 699–708, https://doi.org/10.1002/ceat.201600322.
[120] K. Chen, H. Qin, Z. Ren, Establishment of the microstructure of porous materials and its relationship with effective mechanical properties, Sci. Rep. 13 (2023) 18064, https://doi.org/10.1038/s41598-023-43439-6.
[121] C. Fee, Suhas Nawada, Simone Dimartino, 3D printed porous media columns with fine control of column packing morphology, J. Chromatogr. A 1333 (2014) 18–24, https://doi.org/10.1016/j.chroma.2014.01.043.
[122] W. Fei, G.A. Narsilio, Impact of three-dimensional Sphericity and roundness on coordination number, J. Geotech. Geoenviron. Eng. 146 (12) (2020) 06020025, https://doi.org/10.1061/(ASCE)GT.1943-5606.0002389.
[123] J. Lin, Huisu Chen, Effect of particle morphologies on the percolation of particulate porous media: A study of superballs, Powder Technol. 335 (2018) 388–400, https://doi.org/10.1016/j.powtec.2018.05.015.
[124] J. Lin, Huisu Chen, Lattice Boltzmann simulation of fluid flow through random packing beds of platonic particles: effect of particle characteristics, Particuology 47 (2019) 41–53, https://doi.org/10.1016/j.partic.2018.08.014.
[125] J. Lin, Huisu Chen, Liu Lin, Impact of polydispersity of particle shape and size on percolation threshold of 3D particulate media composed of penetrable superellipsoids, Powder Technol. 360 (2020) 944–955, https://doi.org/10.1016/j.powtec.2019.10.054.
[126] Y.F. Liu, D.-S. Jeng, Pore scale study of the influence of particle geometry on soil permeability, Adv. Water Resour. 129 (2019) 232–249, https://doi.org/10.1016/j.advwatres.2019.05.024.
[127] T.K. Perkins, O.C. Johnston, A review of diffusion and dispersion in porous media, SPE J. 3 (1963) 70–84, https://doi.org/10.2118/480-PA.
[128] L. Riley, P. Cheng, T. Segura, Identification and analysis of 3D pores in packed particulate materials, Nat. Comput. Sci. 3 (2023) 975–992, https://doi.org/10.1038/s43588-023-00551-x.
[129] S. Torquato, Random Heterogeneous Materials: Microstructure and Macroscopic Properties, 2nd Edn, Springer, 2013.
[130] M.R.J. Wyllie, A.R. Gregory, Formation factors of unconsolidated porous media: influence of particle shape and effect of cementation, J. Pet. Technol. 5 (1953) 103–110, https://doi.org/10.2118/223-G.
[131] W. Xu, Bin Zhang, Mingkun Jia, Wei Wang, Gong Zheng, Jinyang Jiang, Discrete element modeling of 3D irregular concave particles: transport properties of particle-reinforced composites considering particles and soft interphase effects, Comput. Methods Appl. Mech. Eng. 394 (2022) 114932, https://doi.org/10.1016/j.cma.2022.114932.
[132] W. Xu, Yufeng Zhang, Jinyang Jiang, Zhiyong Liu, Jiao Yang, Thermal conductivity and elastic modulus of 3D porous/fractured media considering percolation, Int. J. Eng. Sci. 161 (2021) 103456, https://doi.org/10.1016/j.ijengsci.2021.103456.
[133] Y. Yan, L. Zhang, X. Luo, K. Liu, T. Jia, Y. Lu, Influence of the grain shape and packing texture on the primary porosity of sandstone: insights from a numerical simulation, Sedimentology 70 (2023) 1856–1885, https://doi.org/10.1111/sed.13098.
[134] R.Y. Yang, R.P. Zou, A.B. Yu, S.K. Choi, Pore structure of the packing of fine particles, J. Colloid Interface Sci. 299 (2) (2006) 719–725, https://doi.org/10.1016/j.jcis.2006.02.041.
[135] B.J. Ennis, J. Green, R. Davies, The legacy of neglect in the US, Chem. Eng. Prog. 90 (1994) 32–43.
[136] P.V. Danckwerts, The definition and measurement of some characteristics of mixtures, Appl. Sci. Res. Sect. A 3 (1952) 279–296, https://doi.org/10.1007/BF03184936.
[137] N. Harnby, An engineering view of pharmaceutical powder mixing, Pharm. Sci. Technol. Today 3 (9) (2000) 303–309, https://doi.org/10.1016/S1461-5347(00)00283-2.
[138] M. Combarros, H.J. Feise, H. Zetzener, A. Kwade, Segregation of particulate solids: experiments and DEM simulations, Particuology 12 (2014) 25–32, https://doi.org/10.1016/j.partic.2013.04.005.
[139] V. Garzó, Brazil-nut effect versus reverse Brazil-nut effect in a moderately dense granular fluid, Phys. Rev. E 78 (2008), https://doi.org/10.1103/PhysRevE.78.020301, 020301(R).
[140] C.C. Liao, S.S. Hsiau, C.S. Wu, Combined effects of internal friction and bed height on the Brazil-nut problem in a shaker, Powder Technol. 253 (2014) 561–567, https://doi.org/10.1016/j.powtec.2013.12.031.
[141] J.J. McCarthy, Turning the corner in segregation, Powder Technol. 192 (2009) 137–142.
[142] A. Rosato, K.J. Strandburg, F. Prinz, R.H. Swendsen, Why the Brazil nuts are on top: size segregation of particulate matter by shaking, Phys. Rev. Lett. 58 (10) (1987) 1038, https://doi.org/10.1103/PhysRevLett.58.1038.
[143] T. Shinbrot, The Brazil nut effect — in reverse, Nature 429 (2004) 352–353, https://doi.org/10.1038/429352b.
[144] F. Wang, Yrjö Jun Huang, Investigation of local process in granular segregation based on discrete element method, Adv. Powder Technol. 33 (10) (2022) 103753, https://doi.org/10.1016/j.apt.2022.103753.
[145] R. Caulkin, X. Jia, M. Fairweather, R.A. Williams, Geometric aspects of particle segregation. Physical review, E Stat. Nonlinear Soft Matt. Phys. 81 (2010) 051302, https://doi.org/10.1103/PhysRevE.81.051302.
[146] M. Ramaioli, et al., Brazil nut's effect beyond spherical grains: elongation matters! WCPT5, paper #205f, 2006, 2006.
[147] W.M. Ambrós, C.H. Sampaio, B.G. Cazacliu, G.L. Miltzarek, L.R. Miranda, Usage of air jigging for multi-component separation of construction and demolition waste, Waste Manag. 60 (2017 Feb) 75–83, https://doi.org/10.1016/j.wasman.2016.11.029.
[148] Y. Chen, J. Tang, H. Li, Y. Yan, Z. Xu, F. Cai, Research on the particle movement in a flexible air chamber jig, Adv. Powder Technol. 34 (1) (2023) 103922, https://doi.org/10.1016/j.apt.2022.103922.
[149] J. Conway-Baker, R.W. Barley, Richard A. Williams, Xiaodong Jia, J. Kostuch, B. McLoughlin, D.J. Parker, Measurement of the motion of grinding media in a vertically stirred mill using positron emission particle tracking (PEPT), Miner. Eng. 15 (1–2) (2002) 53–59, https://doi.org/10.1016/S0892-6875(01)00199-6.
[150] A. Laplante, S. Gray, Advances in gravity gold technology, Developm. Miner. Proc. 15 (2005) 280–307, https://doi.org/10.1016/S0167-4528(05)15013-3.
[151] M.C. Garcia, H.J. Feise, S. Strege, A. Kwade, Segregation in heaps and silos: comparison between experiment, simulation and continuum model, Powder Technol. 293 (2016) 26–36, https://doi.org/10.1016/j.powtec.2015.09.036.
[152] Ramasamy B. Narendran, Fuji Jian, Digvir S. Jayas, Paul G. Fields, Noel D. G. White, Segregation of canola, kidney bean, and soybean in wheat bulks during bin loading, Powder Technol. 344 (2019) 307–313, https://doi.org/10.1016/j.powtec.2018.12.042.
[153] R.L. Brown, The fundamental principles of segregation, J. Inst. Fuel 13 (1939) 15–19.
[154] S.Y. He, J.Q. Gan, D. Pinson, Z.Y. Zhou, Particle shape-induced radial segregation of binary mixtures in a rotating drum, Powder Technol. ISSN 0032-5910 341 (2019) 157–166. 10.1016/j.powtec.2018.06.005.
[155] R. Hogg, Mixing and segregation in powders: evaluation, mechanisms and processes, KONA Powder Part. J. 27 (2009) 3–17, https://doi.org/10.14356/kona.2009005.
[156] R. Maione, Sébastien Kiesgen De Richter, Guillain Mauviel, Gabriel Wild, DEM investigation of granular flow and binary mixture segregation in a rotating tumbler: influence of particle shape and internal baffles, Powder Technol. 286 (2015) 732–739, https://doi.org/10.1016/j.powtec.2015.09.011.
[157] M.J. Metzger, Brenda Remy, Benjamin J. Glasser, All the Brazil nuts are not on top: vibration induced granular size segregation of binary, ternary and multi-sized mixtures, Powder Technol. 205 (1–3) (2011) 42–51, https://doi.org/10.1016/j.powtec.2010.08.062.
[158] G.F. Smith, L.V. Hardy, E.L. Gard, The segregation of analyzed samples, Ind. Eng. Chem. Anal. Ed. 1 (1929) 228–230.
[159] M. Alizadeh, Ali Hassanpour, Mehrdad Pasha, Mojtaba Ghadiri, Andrew Bayly, The effect of particle shape on predicted segregation in binary powder mixtures, Powder Technol. 319 (2017) 313–322, https://doi.org/10.1016/j.powtec.2017.06.059.
[160] M. Asachi, Ali Hassanpour, Mojtaba Ghadiri, Andrew Bayly, Experimental evaluation of the effect of particle properties on the segregation of ternary powder mixtures, Powder Technol. 336 (2018) 240–254, https://doi.org/10.1016/j.powtec.2018.05.017.
[161] P. Gajjar, C.G. Johnson, J. Carr, et al., Size segregation of irregular granular materials captured by time-resolved 3D imaging, Sci. Rep. 11 (2021) 8352, https://doi.org/10.1038/s41598-021-87280-1.
[162] S. Kumar, Salma Khatoon, Praveen Dubey, Jeetram Yogi, Anshu Anand, Shape-dependent radial segregation in rotating drum: insights from DEM simulations, Powder Technol. 432 (2024) 119134, https://doi.org/10.1016/j.powtec.2023.119134.
[163] S. Kumar, S. Khatoon, J. Yogi, S.K. Verma, A. Anand, Experimental investigation of segregation in a rotating drum with non-spherical particles, Powder Technol. 411 (2022) 117918, https://doi.org/10.1016/j.powtec.2022.117918.
[164] A. Rosato, Kit Windows-Yule (Eds.), Segregation in Vibrated Granular Systems, Academic Press, 2020, https://doi.org/10.1016/B978-0-12-814199-1.00002-0. ISBN 9780128141991.
[165] J.T. Carstensen, M.R. Patel, Blending of irregularly shaped particles, Powder Technol. 17 (3) (1977) 273–282, https://doi.org/10.1016/0032-5910(77)80031-4.
[166] M.H. Cooke, D.J. Stephens, J. Bridgwater, Powder mixing—a literature survey, Powder Technol. 15 (1) (1976) 1–20, https://doi.org/10.1016/0032-5910(76)80025-3.

[167] P.V. Danckwerts, Theory of mixtures and mixing, Research 6 (7) (1953) 355–361.
[168] Y.L. Ding, J.P.K. Seville, R. Forster, D.J. Parker, Solids motion in rolling mode rotating drums operated at low to medium rotational speeds, Chem. Eng. Sci. 56 (5) (2001) 1769–1780, https://doi.org/10.1016/S0009-2509(00)00468-1. ISSN 0009-2509.
[169] P. Dubey, Jeetram Yogi, Sunil Kumar, Salma Khatoon, Kiran Kumari, Anshu Anand, Shape-dependent size polydispersity: DEM investigation of mixing behavior in a vibrating packed bed system, Powder Technol. 441 (2024) 119804, https://doi.org/10.1016/j.powtec.2024.119804.
[170] R. Escudié, N. Epstein, J.R. Grace, H.T. Bi, Effect of particle shape on liquid-fluidized beds of binary (and ternary) solids mixtures: segregation vs. mixing, Chem. Eng. Sci. 61 (5) (2006) 1528–1539, https://doi.org/10.1016/j.ces.2005.08.028.
[171] N. Govender, Daniel N. Wilke, Chuan-Yu Wu, Raj Rajamani, Johannes Khinast, Benjamin J. Glasser, Large-scale GPU based DEM modeling of mixing using irregularly shaped particles, Adv. Powder Technol. 29 (10) (2018) 2476–2490, https://doi.org/10.1016/j.apt.2018.06.028.
[172] B. Jadidi, Mohammadreza Ebrahimi, Farhad Ein-Mozaffari, Ali Lohi, Investigation of impacts of particle shape on mixing in a twin paddle blender using GPU-based DEM and experiments, Powder Technol. 417 (2023) 118259, https://doi.org/10.1016/j.powtec.2023.118259.
[173] S. Ji, Siqiang Wang, Zongyan Zhou, Influence of particle shape on mixing rate in rotating drums based on super-quadric DEM simulations, Adv. Powder Technol. 31 (8) (2020) 3540–3550, https://doi.org/10.1016/j.apt.2020.06.040.
[174] S. Kumar, Anshu Anand, Effect of different categories of nonsphericity on mixing in a rotating drum using the Discrete Element Method (DEM), DEM9 (2023) 170. https://www.dem9.fau.de/.
[175] P.M.C. Lacey, Developments in the theory of particle mixing, J. Appl. Chem. 4 (1954) 257–268, https://doi.org/10.1002/jctb.5010040504.
[176] Y. Mori, Mikio Sakai, Advanced DEM simulation on powder mixing for ellipsoidal particles in an industrial mixer, Chem. Eng. J. 429 (2022) 132415, https://doi.org/10.1016/j.cej.2021.132415.
[177] A.W. Nienow, M.F. Edwards, N. Harnby, Mixing in the Process Industries, 2nd edition, Butterworth-Heinemann, 1997. ISBN 0750637609.
[178] C.D. Rielly, Mixing theory, in: P.J. Cullen, R.J. Romañach, N. Abatzoglou, C. D. Rielly (Eds.), Pharmaceutical Blending and Mixing, 2015, https://doi.org/10.1002/9781118682692.ch1.
[179] M.K. Saeed, Muhammad Shafiq Siraj, Mixing study of non-spherical particles using DEM, Powder Technol. 344 (2019) 617–627, https://doi.org/10.1016/j.powtec.2018.12.057.
[180] M.D. Sinnott, P.W. Cleary, The effect of particle shape on mixing in a high shear mixer, Comput. Part. Mech. 3 (2016) 477–504, https://doi.org/10.1007/s40571-015-0065-4.
[181] V. Swaminathan, D.O. Kildsig, Polydisperse powder mixtures: effect of particle size and shape on mixture stability, Drug Dev. Ind. Pharm. 28 (1) (2002) 41–48, https://doi.org/10.1081/DDC-120001484.
[182] H.J. Venables, J.I. Wells, Powder mixing, Drug Dev. Ind. Pharm. 27 (7) (2001) 599–612, https://doi.org/10.1081/DDC-100107316.
[183] L.W. Wong, N. Pilpel, Effect of particle shape on the mixing of powders, J. Pharm. Pharmacol. 42 (1) (January 1990) 1–6, https://doi.org/10.1111/j.2042-7158.1990.tb05339.x.
[184] J. Zhang, Josh Tuohey, Negin Amini, David A.V. Morton, Karen P. Hapgood, 3D printing of customised particles for powder rheology, mixing and segregation study, Powder Technol. 425 (2023) 118576, https://doi.org/10.1016/j.powtec.2023.118576.
[185] G.H. Bagheri, C. Bonadonna, I. Manzella, P. Vonlanthen, On the characterization of size and shape of irregular particles, Powder Technol. 270 (A) (2015) 141–153, https://doi.org/10.1016/j.powtec.2014.10.015.
[186] A. Boschetto, Veronica Giordano, Powder sampling and characterization by digital image analysis, Measurement 45 (5) (2012) 1023–1038, https://doi.org/10.1016/j.measurement.2012.01.041.
[187] D. Cardenas del Rio, Dorte Juul Jensen, Niels Skat Tiedje, Søren Fæster, Tianbo Yu, Factors affecting particle characterization of powders used in additive manufacturing, Powder Technol. 434 (2024) 119324, https://doi.org/10.1016/j.powtec.2023.119324.
[188] S.T. Erdoğan, E.J. Garboczi, D.W. Fowler, Shape and size of microfine aggregates: X-ray microcomputed tomography vs. laser diffraction, Powder Technol. 177 (2) (2007) 53–63, https://doi.org/10.1016/j.powtec.2007.02.016.
[189] J.M.R. Fernlund, Robert Zimmerman, Danica Kragic, Influence of volume/mass on grain-size curves and conversion of image-analysis size to sieve size, Eng. Geol. 90 (3–4) (2007) 124–137.
[190] K. Grubbs, C. Tsaknopoulos, B. Massar, A. Young, C. O'Connell, A. Walde, M. Birt, D. Cote Siopis, Comparison of laser diffraction and image analysis techniques for particle size-shape characterization in additive manufacturing applications, Powder Technol. 391 (2021) (2021) 20–33, https://doi.org/10.1016/j.powtec.2021.06.003.
[191] J.E. Houghton, J. Behnsen, R.A. Duller, T.E. Nichols, R.H. Worden, Particle size analysis: a comparison of laboratory-based techniques and their application to geoscience (2024), Sediment. Geol. 464 (2024) 106607, https://doi.org/10.1016/j.sedgeo.2024.106607.
[192] O.J. Karlsson, B.E.H. Schade, Particle analysis: particle size, particle shape and structure and surface characterisation, in: Chemistry and Technology of Emulsion Polymerisation, A. van Herk (Ed.), 2005, https://doi.org/10.1002/9780470988466.ch9.
[193] M. Poston, Luminita Dudu, Tony Thornton, Peter Bouza, Greg Thiele, Rich Brown, Effects of Particle Shape on Measured Particle Size. Technical Notes, Micromeritics Instrument Corporation, 2014. https://www.pharmaceutica lonline.com/doc/effects-of-particle-shape-on-measured-0001.
[194] J.P.K. Seville, J.R. Coury, M. Ghadiri, R. Clift, Comparison of techniques for measuring the size of fine non-spherical particles, Part. Part. Syst. Charact. 1 (1984) 45–52, https://doi.org/10.1002/ppsc.19840010108.
[195] A.R. Steinherz, The shape of particles in finely ground powders, J. Chem. Technol. Biotechnol. 65 (1946) 314–320, https://doi.org/10.1002/jctb.5000651008.
[196] A. Timoumi, Tien Cuong Nguyen, Tuan Le, Hazar Kraiem, Julien Cescut, Dominique Anne-Archard, Nathalie Gorret, Carole Molina-Jouve, T.O. Kim Anh, Luc Fillaudeau, Comparison of methods to explore the morphology and granulometry of biological particles with complex shapes: interpretation and limitations, Powder Technol. 415 (2023) 118067, https://doi.org/10.1016/j.powtec.2022.118067.
[197] A.P. Tinke, R. Govoreanu, K. Vanhoutte, Particle size and shape characterization of nano and submicron liquid dispersions, Am. Pharm. Rev. 9 (6) (2006) 33–37, https://www.researchgate.net/profile/Arij-Tinke/publication/289090063_Particle_size_and_shape_characterization_of_nano_and_submicron_liquid_dispersions/links/5eaa7f73299bf18b9587e0a9/Particle-size-and-shape-characterization-of-nano-and-submicron-liquid-dispersions.pdf.
[198] R. Xu, Light scattering: A review of particle characterization applications, Particuology 18 (2015) 11–21, https://doi.org/10.1016/j.partic.2014.05.002.
[199] N. Gabas, N. Hiquily, C. Laguérie, Response of laser diffraction particle sizer to anisometric particles, Part. Part. Syst. Charact. 11 (1994) 121–126, https://doi.org/10.1002/ppsc.19940110203.
[200] R.N. Kelly, Jacqueline Kazanjian, Commercial reference shape standards use in the study of particle shape effect on laser diffraction particle size analysis, AAPS PharmSciTech 7 (2) (2006) E49, https://doi.org/10.1208/pt070249.
[201] R.E. Cavicchi, Michael J. Carrier, Joshua B. Cohen, Shir Boger, Christopher B. Montgomery, Zhishang Hu, Dean C. Ripple, Particle shape effects on subvisible particle sizing measurements, J. Pharm. Sci. 104 (3) (2015) 971–987, https://doi.org/10.1002/jps.24263.
[202] I. de Albuquerque, M. Mazzotti, D.R. Ochsenbein, M. Morari, Effect of needle-like crystal shape on measured particle size distributions, AICHE J. 62 (2016) 2974–2985, https://doi.org/10.1002/aic.15270.
[203] N.A. Krotkov, D.E. Flittner, A.J. Krueger, A. Kostinski, C. Riley, W. Rose, O. Torres, Effect of particle non-sphericity on satellite monitoring of drifting volcanic ash clouds, J. Quant. Spectrosc. Radiat. Transf. 63 (2–6) (1999) 613–630, https://doi.org/10.1016/S0022-4073(99)00041-2.
[204] J.G. Whiting, Edward J. Garboczi, Vipin N. Tondare, John Henry J. Scott, M. Alkan Donmez, Shawn P. Moylan, A comparison of particle size distribution and morphology data acquired using lab-based and commercially available techniques: application to stainless steel powder, Powder Technol. 396 (B) (2022) 648–662, https://doi.org/10.1016/j.powtec.2021.10.063.
[205] J.M.R. Fernlund, The effect of particle form on sieve analysis: a test by image analysis, Eng. Geol. 50 (1–2) (1998) 111–124.
[206] G. Lees, The measurement of particle shape and its influence in engineering materials, British Granite Whinstone Federat. 4 (2) (1964) 17–38.
[207] J. Gebhart, Response of single-particle optical counters to particles of irregular shape, Part. Part. Syst. Charact. 8 (1991) 40–47, https://doi.org/10.1002/ppsc.19910080109.
[208] L. Feltner, Ethan Korte, David F. Bahr, Paul Mort, Particle size and shape analyses for powder bed additive manufacturing, Particu (2023) 2023, https://doi.org/10.1016/j.partic.2023.09.001.
[209] G. Domokos, D.J. Jerolmack, A.A. Sipos, A. Torok, How river rocks round: resolving the shape-size paradox, PLoS One 9 (2) (2014) e88657, https://doi.org/10.1371/journal.pone.0088657.
[210] D. Wei, Zhai Chongpu, Hanaor Dorian, Gan Yixiang, Contact behaviour of simulated rough spheres generated with spherical harmonics, Int. J. Solids Struct. 193–194 (2020) 54–68, https://doi.org/10.1016/j.ijsolstr.2020.02.009.
[211] B. Asgharian, T.P. Owen, E.D. Kuempel, A.M. Jarabek, Dosimetry of inhaled elongate mineral particles in the respiratory tract: the impact of shape factor, Toxicol. Appl. Pharmacol. 361 (2018 Dec 15) 27–35, https://doi.org/10.1016/j.taap.2018.05.001. Epub 2018 May 5. PMID: 29738812; PMCID: PMC6329593.
[212] W.-S. Ryu, Chapter 2 - Virus Structure, Editor(S): Wang-Shick Ryu, Molecular Virology of Human Pathogenic Viruses, Academic Press, 2017, pp. 21–29. ISBN 9780128008386, https://doi.org/10.1016/B978-0-12-800838-6.00002-3.
[213] A. Sukhanova, S. Bozrova, P. Sokolov, et al., Dependence of nanoparticle toxicity on their physical and chemical properties, Nanoscale Res. Lett. 13 (2018) 44, https://doi.org/10.1186/s11671-018-2457-x.
[214] R. Abbasi, G. Shineh, M. Mobaraki, et al., Structural parameters of nanoparticles affecting their toxicity for biomedical applications: a review, J. Nanopart. Res. 25 (2023) 43, https://doi.org/10.1007/s11051-023-05690-w.
[215] S.T. Beckett, The Science of Chocolate, Royal Society of Chemistry, York, 2008. ISBN: 978-0-85404-970-7.
[216] F. Lenfant, Christoph Hartmann, Brigitte Watzke, Olivier Breton, Chrystel Loret, Nathalie Martin, Impact of the shape on sensory properties of individual dark chocolate pieces, LWT Food Sci. Technol. 51 (2) (2013) 545–552, https://doi.org/10.1016/j.lwt.2012.11.001.
[217] Q. Liu, V. Lazouskaya, Q. He, Y. Jin, Effect of particle shape on colloid retention and release in saturated porous media, J. Environ. Qual. 39 (2010) 500–508, https://doi.org/10.2134/jeq2009.0100.
[218] M.B. Seymour, Gexin Chen, Su Chunming, Yusong Li, Transport and retention of colloids in porous media: does shape really matter? Environ. Sci. Technol. 47 (15) (2013) 8391–8398, https://doi.org/10.1021/es4016124.

[219] M.K. Shave, Aiste Balciunaite, Zhou Xu, Maria M. Santore, Rapid electrostatic capture of rod-shaped particles on planar surfaces: standing up to shear, Langmuir 35 (40) (2019) 13070–13077, https://doi.org/10.1021/acs.langmuir.9b01871.
[220] W. Xia, Role of particle shape in the floatability of mineral particle: An overview of recent advances, Powder Technol. 317 (2017) 104–116, https://doi.org/10.1016/j.powtec.2017.04.050.
[221] K. Li, Huilian Ma, High fluid velocity and narrow channels enhance the influences of particle shape on colloid retention in saturated groundwater systems under favorable deposition conditions, Front. Water (2021) 3, https://doi.org/10.3389/frwa.2021.604204.
[222] H.Z. Ting, Pavel Bedrikovetsky, Zhao Feng Tian, Themis Carageorgos, Impact of shape on particle detachment in linear shear flows, Chem. Eng. Sci. 241 (2021) 116658, https://doi.org/10.1016/j.ces.2021.116658.
[223] G. Ma, Bu Xiangning, Ugur Ulusoy, Guangyuan Xie, Effect of particle shape on bubble-particle attachment behavior: roles of surfaces, edges, and vertexes, J. Clean. Prod. 429 (2023) 139606, https://doi.org/10.1016/j.jclepro.2023.139606.
[224] M. Sadowska, Małgorzata Nattich-Rak, Maria Morga, Zbigniew Adamczyk, Teresa Basinska, Damian Mickiewicz, Mariusz Gadzinowski, Anisotropic particle deposition kinetics from quartz crystal microbalance measurements: beyond the sphere paradigm, Langmuir 40 (15) (2024) 7907–7919, https://doi.org/10.1021/acs.langmuir.3c03676.
[225] S.W. Churchill, Viscous Flows – The Practical Use of Theory, Butterworth, London, 1988. ISBN: 0409951854.
[226] E.E. Michaelides, Z. Feng, Review—drag coefficients of non-spherical and irregularly shaped particles, ASME. J. Fluids Eng. 145 (6) (March 20, 2023) 060801, https://doi.org/10.1115/1.4057019.
[227] J.S. McNown, J. Malaika, Effects of particle shape on settling velocity at low Reynolds numbers, Eos Trans. AGU 31 (1) (1950) 74–82, https://doi.org/10.1029/TR031i001p00074.
[228] W.E. Dietrich, Settling velocity of natural particles, Water Resour. Res. 18 (6) (1982) 1615–1626, https://doi.org/10.1029/WR018i006p01615.
[229] N. Hawley, Settling velocity distribution of natural aggregates, J. Geophys. Res. 87 (C12) (1982) 9489–9498, https://doi.org/10.1029/JC087iC12p09489.
[230] X. Hu, Xianzhi Song, Gensheng Li, Zhonghou Shen, Zehao Lyu, Shi Yu, Shape factor of the flake-like particle in thermal spallation and its effects on settling and transport behavior in drilling annulus, Powder Technol. 335 (2018) 211–221, https://doi.org/10.1016/j.powtec.2018.05.014.
[231] L. Li, K. Osada, Preferential settling of elongated mineral dust particles in the atmosphere, Geophys. Res. Lett. 34 (2007) L17807, https://doi.org/10.1029/2007GL030262.
[232] F. Maggi, The settling velocity of mineral, biomineral, and biological particles and aggregates in water, J. Geophys. Res. Oceans 118 (2013) 2118–2132, https://doi.org/10.1002/jgrc.20086.
[233] L. Mao, J. Li, T. Shimozono, Y. Tajima, Impacts of particle shape, skeletal porosity and density on the settling velocity of gravel-size coral debris, J. Geophys. Res. Earth Surf. 128 (2023) e2022JF006996, https://doi.org/10.1029/2022JF006996.
[234] E.A. Variano, H.I. Andersson, L. Zhao, M. Byron, Tumbling in turbulence: How much does particle shape effect particle motion? American Geophysical Union, Fall Meeting 2014 (2014) abstract id. H31N-05, https://ui.adsabs.harvard.edu/abs/2014AGUFM.H31N..05V/abstract.
[235] D.O. Cooney, Effect of geometry on the dissolution of pharmaceutical tablets and other solids: surface detachment kinetics controlling, AICHE J. 18 (1972) 446–449, https://doi.org/10.1002/aic.690180234.
[236] X. Jia, R.A. Williams, A hybrid mesoscale modelling approach to dissolution of granules and tablets, Chem. Eng. Res. Des. 85 (7) (2007) 1027–1038, https://doi.org/10.1205/cherd06218.
[237] H. Cao, Xiaodong Jia, Yongliang Li, Carlos Amador, Yulong Ding, CFD-DNS simulation of irregular-shaped particle dissolution, Particuology 50 (2020) 144–155, https://doi.org/10.1016/j.partic.2019.08.003.
[238] N. Prajapati, Michael Späth, Linus Knecht, Michael Selzer, Britta Nestler, Quantitative phase-field modeling of faceted crystal dissolution processes, Cryst. Growth Des. 21 (2021) 3266–3279, https://doi.org/10.1021/acs.cgd.0c01715.
[239] J. Chen, Nicholas E. Clay, No-hyung Park, Hyunjoon Kong, Non-spherical particles for targeted drug delivery, Chem. Eng. Sci. 125 (2015) 20–24, https://doi.org/10.1016/j.ces.2014.10.022.
[240] J. Mougin, Claudie Bourgaux, Patrick Couvreur, Elongated self-assembled nanocarriers: from molecular organization to therapeutic applications, Adv. Drug Deliv. Rev. 172 (2021) 127–147, https://doi.org/10.1016/j.addr.2021.02.018.
[241] Y. Lu, Zhang Lu, Maarten A.I. Schutyser, Linking particle morphology and functionality of colloid-milled dietary fibre concentrates from various plant sources, LWT 186 (2023) 115206, https://doi.org/10.1016/j.lwt.2023.115206.
[242] A.T. Asifa, P. Kumam, Z. Shah, K. Sitthithakerngkiet, Significance of shape factor in heat transfer performance of molybdenum-disulfide nanofluid in multiple flow situations; A comparative fractional study, Molecules 26 (12) (2021 Jun 18) 3711, https://doi.org/10.3390/molecules26123711. PMID: 34207000; PMCID: PMC8235011.
[243] A. Subray, B.N. Hanumagowda, S.V.K. Varma, et al., The impacts of shape factor and heat transfer on two-phase flow of nano and hybrid nanofluid in a saturated porous medium, Sci. Rep. 12 (2022) 21864, https://doi.org/10.1038/s41598-022-26169-z.
[244] A. Dwyer, D.S. Dandy, Some influences of particle shape on drag and heat transfer, Phys. Fluids 2 (12) (1 December 1990) 2110–2118, https://doi.org/10.1063/1.857797.
[245] Y.A. Cengel, Afshin Jahanshahi Ghajar, Heat and Mass Transfer: Fundamentals and Applications. Chapter 3, 6th edition, McGraw Hill / Asia, 2020. ISBN: 9813158964.
[246] J.P.K. Seville, C.-Y. Wu, Particle Technology and Engineering, Butterworth-Heinemann, 2016. ISBN: 0080983375.
[247] S. Szerakowska, Parametry kształtu ziaren gruntowych oraz analityczne sposoby ich wyznaczania, Prz. Geol. 62 (10/2) (2014).
[248] L. Bates, Glossary of Terms in Powder and Bulk Technology, The British Materials Handling Board, 2012. ISBN 978-0-946637-12-6.
[249] Y. Wanibe, T. Itoh, New Quantitative Approach to Powder Technology, Wiley, 1999. ISBN: 0471981540.
[250] H.G. Brittain, Representations of particle, shape, size, and distribution, Pharm. Technol. N. Am. 25 (12) (2001) 38–45. https://cdn.sanity.io/files/0vv8moc6/pharmtech/d8b4c7d6b859d6ffee1bc6ebe410434f0023b71e.pdf/article-3391.pdf.
[251] L.R. Feret, La Grosseur des Grains des Matières Pulvérulentes. Eidgen. Materialprüfungsanstalt ad Eidgen. Technischen Hochschule, Premières Communications de la Nouvelle Association Internationale pour l'Essai des Matériaux, Groupe D (1930).
[252] M.R. Walter. Stromatolites, Elsevier, 1976, p. 47. ISBN 978-0-444-41376-5.
[253] B.H. Kaye, The use of Feret's diameter signature waveform as a shape characterization parameter in Fineparticle science, J. Powder Bulk Solids Technol. 2 (1978) 24–33.
[254] H.G. Merkus, Particle Size Measurements: Fundamentals, Practice, Quality, Springer Science & Business Media B.V, 2009. ISBN: 978-1-4020-9015-8.
[255] H. Wadell, Volume, shape and roundness of rock particles, J. Geol. 40 (5) (1932) 443–451, https://doi.org/10.1086/623964.
[256] H. Wadell, Sphericity and roundness of rock particles, J. Geol. 41 (3) (1933) 310–331, https://doi.org/10.1086/624040.
[257] H. Wadell, Volume, shape, and roundness of quartz particles, J. Geol. 41 (3) (1935) 250–280, https://doi.org/10.1086/624298.
[258] G. Lees, A new method for determining the angularity of particles, Sedimentology 3 (1964) 2–21, https://doi.org/10.1111/j.1365-3091.1964.tb00271.x.
[259] F. Podzceck, A shape factor to assess the shape of particles using image analysis, Powder Technol. 93 (1) (1997) 47–53, https://doi.org/10.1016/S0032-5910(97)03257-9.
[260] R.L. Folk, Student operator error in determination of roundness, sphericity and grain size, J. Sediment. Res. 25 (4) (1955) 297–301.
[261] M.R. Muszynski, S.J. Vitton, Particle shape estimates of uniform sands: visual and automated methods comparison, J. Mater. Civ. Eng. (2012) 194–206.
[262] R.D. Hryciw, J. Zheng, K. Shetler, Particle roundness and Sphericity from images of assemblies by chart estimates and computer methods, J. Geotech. Geoenviron. Eng. 142 (9) (2016) 04016038, https://doi.org/10.1061/(ASCE)GT.1943-5606.0001485.
[263] Yudhbir, R. Abedinzadeh, Quantification of particle shape and angularity using the image analyzer, ASTM International. Geotech. Test. J. 14 (3) (1991) 296–308, https://doi.org/10.1520/GTJ10574J.
[264] S. Endoh, Y. Kuga, H. Ohya, C. Ikeda, H. Iwata, Shape estimation of anisometric particles using size measurement techniques, Part. Part. Syst. Charact. 15 (1998) 145–149, https://doi.org/10.1002/(SICI)1521-4117(199817)15:3<145::AID-PPSC145>3.0.CO;2-B.
[265] E.F. Kruis, J. van Denderen, H. Buurman, B. Scarlett, Characterization of agglomerated and aggregated aerosol particles using image analysis, Part. Part. Syst. Charact. 11 (1994) 426–435, https://doi.org/10.1002/ppsc.19940110605.
[266] A.T. Williams, R.J. Wiltshire, M.C. Thomas, Sand grain analysis—image processing, textural algorithms and neural nets, Comput. Geosci. 24 (1998) 111–118, https://doi.org/10.1016/S0098-3004(98)00004-1.
[267] M. Bloom, J. Corriveau, P. Giordano, G.D. Lecakes, S. Mandayam, B. Sukumaran, Imaging systems and algorithms for the numerical characterization of three-dimensional shapes of granular particles, IEEE Trans. Instrum. Meas. 59 (9) (Sept. 2010) 2365–2375, https://doi.org/10.1109/TIM.2009.2034579.
[268] E.T. Bowman, K. Soga, W. Drummond, Particle shape characterisation using Fourier descriptor analysis, Geotechnique 51 (6) (2001) 545–554, https://doi.org/10.1680/geot.2001.51.6.545.
[269] M.N. Pons, H. Vivier, K. Belaroui, B. Bernard-Michel, F. Cordier, et al., Particle morphology: from visualisation to measurement, Powder Technol. 103 (1999) 44–57.
[270] K.A. Alshibli, Mustafa I. Alsaleh, Characterizing surface roughness and shape of sands using digital microscopy, J. Comput. Civ. Eng. 18 (1) (2004) 36–45, https://doi.org/10.1061/(ASCE)0887-3801(2004)18:1(36).
[271] J.A. Calderon De Anda, X.Z. Wang, K.J. Roberts, Multi-scale segmentation image analysis for the in-process monitoring of particle shape with batch crystallisers, Chem. Eng. Sci. 60 (4) (2005) 1053–1065, https://doi.org/10.1016/j.ces.2004.09.068.
[272] N. Faria, M.N. Pons, S. Feyo de Azevedo, F.A. Rocha, H. Vivier, Quantification of the morphology of sucrose crystals by image analysis, Powder Technol. 133 (2003) 54–67.
[273] G.H. Schmid, M. Dvorak, J. Müller, J. Müssig, Characterizing flock Fibres using quantitative image analysis, Flock 30 (2004) 6–12.
[274] L. Wang, X. Wang, L. Mohammad, C. Abadie, Unified method to quantify aggregate shape angularity and texture using Fourier analysis, J. Mater. Civ. Eng. 17 (5) (2005) 498–504, https://doi.org/10.1061/(ASCE)0899-1561(2005)17:5(498).
[275] J.M.R. Fernlund, Image analysis method for determining 3-D shape of coarse aggregate, Cem. Concr. Res. 35 (8) (2005) 1629–1637, https://doi.org/10.1016/j.cemconres.2004.11.017.

[276] T. Roussillon, H. Piegay, I. Sivignon, L. Tougne, F. Lavigne, Automatic computation of pebble roundness using digital imagery and discrete geometry, Comput. Geosci. 10 (35) (2009) 1992–2000, https://doi.org/10.1016/j.cageo.2009.01.013.
[277] D.R. Barclay, M.J. Buckingham, On the shapes of natural sand grains, J. Geophys. Res. 114 (2009) B02209, https://doi.org/10.1029/2008JB005993.
[278] S. Szerakowska, M.J. Sulewska, J. Trzciński, B. Woronko, Comparison of methods determining particle sphericity, in: Applied Mechanics and Materials Vol. 797, Trans Tech Publications, Ltd, 2015, pp. 231–237, https://doi.org/10.4028/www.scientific.net/amm.797.231.
[279] S. Tafesse, J.M. Robison Fernlund, W. Sun, F. Bergholm, Evaluation of image analysis methods used for quantification of particle angularity, Sedimentology 60 (2013) 1100–1110, https://doi.org/10.1111/j.1365-3091.2012.01367.x.
[280] J. Zheng, R.D. Hryciw, Traditional soil particle sphericity, roundness and surface roughness by computational geometry, Géotechnique 65 (6) (2015) 494–506, https://doi.org/10.1680/geot.14.p.192.
[281] Z. Nie, Z. Liang, X. Wang, A three-dimensional particle roundness evaluation method, Granul. Matter 20 (2018) 32, https://doi.org/10.1007/s10035-018-0802-5.
[282] Budi Zhao, J. Wang, 3D quantitative shape analysis on form, roundness, and compactness with μCT, Powder Technol. 291 (2015), https://doi.org/10.1016/j.powtec.2015.12.029.
[283] T. Dürig, P.S. Ross, P. Dellino, et al., A review of statistical tools for morphometric analysis of juvenile pyroclasts, Bull. Volcanol. 83 (2021) 79, https://doi.org/10.1007/s00445-021-01500-0.
[284] J. Huyan, W. Li, S. Tighe, Y. Zhang, B. Yue, Image-based coarse-aggregate angularity analysis and evaluation, J. Mater. Civ. Eng. 32 (6) (2020) 04020140.
[285] N.S.S.P. Kalyan, Ramesh Kannan Kandasami, Computationally efficient approach to quantify 2D particle morphological descriptors, in: EPJ Web Conf. 249, 2021, p. 05002, https://doi.org/10.1051/epjconf/202124905002.
[286] L. Li, M. Iskander, Evaluation of roundness parameters in use for sand, J. Geotech. Geoenviron. Eng. 147 (9) (2021) 04021081, https://doi.org/10.1061/(ASCE)GT.1943-5606.0002585.
[287] M. Tunwal, Kieran F. Mulchrone, Patrick A. Meere, A new approach to particle shape quantification using the curvature plot, Powder Technol. 374 (2020) 377–388, https://doi.org/10.1016/j.powtec.2020.07.045.
[288] M. Tunwal, Kieran F. Mulchrone, Patrick A. Meere, Image based particle shape analysis toolbox (IPSAT), Comput. Geosci. 135 (2020) 104391, https://doi.org/10.1016/j.cageo.2019.104391.
[289] J. Chen, Z. Zhang, D. Lin, et al., An improved corner dealiasing and recognition algorithm for 2D Wadell roundness computation, Sci. Rep. 14 (2024) 9439, https://doi.org/10.1038/s41598-024-60240-1.
[290] H. Isik, A.F. Cabalar, A shape parameter for soil particles using a computational method, Arab. J. Geosci. 15 (2022) 581, https://doi.org/10.1007/s12517-022-09777-x.
[291] N. Arora, A. Kumar, S.K. Singal, Quantifying sediment size and shape using SEM and ImageJ-Based approach for sediment management in hydropower plants, in: B.M. Hodge, S.K. Prajapati (Eds.), Proceedings from the International Conference on Hydro and Renewable Energy. ICHRE 2022. Lecture Notes in Civil Engineering vol 391, Springer, Singapore, 2024, https://doi.org/10.1007/978-981-99-6616-5_30.
[292] N. Bouvet, M. Kim, Firebrands generated during WUI fires: a novel framework for 3D morphology characterization, Fire. Technol 60 (2024) 1503–1542, https://doi.org/10.1007/s10694-023-01530-4.
[293] S. Kwunjai, P. Jitsangiam, T. Somsri, Morphological analysis of ballast particles: Characterization and simplified analysis of particle morphology using imaging data, IOP Conf. Ser.: Earth Environ. Sci. 1332 (2024) 012016, https://doi.org/10.1088/1755-1315/1332/1/012016.
[294] J. Zheng, H. He, H. Alimohammadi, Three-dimensional Wadell roundness for particle angularity characterization of granular soils, Acta Geotech. 16 (2021) 133–149, https://doi.org/10.1007/s11440-020-01004-9.
[295] D.J. Graham, R.J. Gadsden, New statistical methods for the comparison and characterization of particle shape, Earth Surf. Process. Landf. 44 (2019) 2396–2407, https://doi.org/10.1002/esp.4669.
[296] W.C. Krumbein, Size frequency distribution of sediments, J. Sediment. Petrol. 4 (1934) 65–77, https://doi.org/10.1306/D4268EB9-2B26-11D7-8648000102C1865D.
[297] W.C. Krumbein, Measurement and geological significance of shape and roundness of sedimentary particles, J. Sediment. Petrol. 11 (1941) 64–72, https://doi.org/10.1306/D42690F3-2B26-11D7-8648000102C1865D.
[298] H. Heywood, Proc. Symp. PSA, London, 1947, Supplement to Trans. Inst. Chem. Eng. 25 (1947) 19–24.
[299] R.F. Mclean, Zingg shape, in: Beaches and Coastal Geology. Encyclopedia of Earth Sciences Series, Springer, New York, NY, 1984, https://doi.org/10.1007/0-387-30843-1_510.
[300] Th. Zingg, Beitrage zur Schotteranalyse, Schweizer. Mineralog. Petrog. Mitt. 15 (1935) 39–140.
[301] H.H. Hausner, Characterization of the powder particle shape, Planseeber Pulvermetall. 14 (2) (1966) 74–84.
[302] M. Sugimoto, Y. Muguruma, M. Hirota, T. Oshima, J. Soc. Powder Technol. Jpn. 25 (1988) 287.
[303] J. Tsubaki, G. Jimbo, The identification of particles using diagrams and distributions of shape indices, Powder Technol. 22 (2) (1979) 171–178, https://doi.org/10.1016/0032-5910(79)80023-6.
[304] J. Tsubaki, G. Jimbo, A proposed new characterization of particle shape and its application, Powder Technol. 22 (2) (1979) 161–169, https://doi.org/10.1016/0032-5910(79)80022-4.
[305] V. Mikli, H. Kaerdi, P. Kulu, M. Besterci, Chracterisation of powder particle morphology, Proc. Estonian Acad. Sci. Eng. 7 (2001) 22–34.
[306] J.C. Russ, The Image Processing Handbook 2nd Ed, 1995, CRC, 1995. ISBN: 0849325161.
[307] E.D. Sneed, R.L. Folk, Pebbles in the lower Colorado River, Texas, a study in particle morphogenesis, J. Geol. 66 (1958) 114–150.
[308] D.I. Benn, Colin K. Ballantyne, The description and representation of particle shape, Earth Surf. Process. Landf. 18 (7) (1993) 665–672, https://doi.org/10.1002/esp.3290180709.
[309] D.J. Graham, N.G. Midgley, Graphical representation of particle shape using triangular diagrams: an excel spreadsheet method, Earth Surf. Process. Landf. 25 (2000) 1473–1477, https://doi.org/10.1002/1096-9837(200012)25:13<1473::AID-ESP158>3.0.CO;2-C.
[310] B.H. Kaye, Jerry Junkala, Garry G. Clark, Domain plotting as a technique for summarizing fineparticle shape, texture and size information, Part. Part. Syst. Charact. 15 (1998) 180–190.
[311] R. Khan, G.M. Latha, Statistical interdependence of multi-scale 3D morphological descriptors of sand grains, Granul. Matter 26 (2024) 19, https://doi.org/10.1007/s10035-023-01390-3.
[312] T. Szabo, G. Domokos, A new classification system for pebble and crystal shapes based on static equilibrium points, Central Europ. Geol. 53/1 (2010) 1–19, https://doi.org/10.1556/CEuGeol.53.2010.1.1.
[313] K. Gotoh, H. Masuda, K. Higashitani, Powder Technology Handbook, 2nd Ed, Marcel Dekker Inc., 1997. ISBN: xxx.
[314] J.C. Earnshaw, D.J. Robinson, Aggregation in interfacial colloidal systems, Progr. Colloid Polym. Sci. 79 (1989) 162–166.
[315] B.H. Kaye, Characterization of powders and aerosols, Wiley-VCH 1999 (1999). ISBN: 3-527-28853-8.
[316] Gulam Rabbani, Y.H. Shaikh, Temporal Evolution of Viscous Fingering in Hele Shaw Cell: A Fractal Approach, 2015.
[317] J.M. García-Ruiz, F. Otálora, A. Sanchez-Navas, F.J. Higes-Rolando, The formation of manganese dendrites as the mineral record of flow structures, in: J. H. Kruhl (Ed.), Fractals and Dynamic Systems in Geoscience, Springer, Berlin, Heidelberg, 1994, https://doi.org/10.1007/978-3-662-07304-9_23.
[318] R. Ehrlich, Bernhard Weinberg, An exact method for characterization of grain shape, J. Sediment. Res. 40 (1970) 205–212, https://doi.org/10.1306/74D71F1E-2B21-11D7-8648000102C1865D.
[319] H.P. Schwarcz, K.C. Shane, Measurement of particle shape by Fourier analysis, Sedimentology 13 (3–4) (1969) 213–231, https://doi.org/10.1111/j.1365-3091.1969.tb00170.x.
[320] M. Diepenbroek, A. Bartholomä, H. Ibbeken, How round is round? A new approach to the topic 'roundness'by Fourier grain shape analysis, Sedimentology 39 (1992) 411–422, https://doi.org/10.1111/j.1365-3091.1992.tb02125.x.
[321] T. Réti, I. Czinege, Shape characterization of particles via generalized Fourier analysis, J. Microsc. 156 (1989) 15–32, https://doi.org/10.1111/j.1365-2818.1989.tb02903.x.
[322] E.J. Garboczi, Three-dimensional mathematical analysis of particle shape using X-ray tomography and spherical harmonics: application to aggregates used in concrete, Cem. Concr. Res. 32 (2002) 1621–1638, https://doi.org/10.1016/S0008-8846(02)00836-0.
[323] P.M. Raj, W.R. Cannon, 2-D particle shape averaging and comparison using Fourier descriptors, Powder Technol. 104 (1999) 180–189.
[324] M.C. Thomas, R.J. Wiltshire, A.T. Williams, The use of Fourier descriptors in the classification of particle shape, Sedimentology 4 (42) (1995) 635–645, https://doi.org/10.1111/j.1365-3091.1995.tb00397.x.
[325] R. Wettimuny, D. Penumadu, Application of Fourier analysis to digital imaging for particle shape analysis, J. Comput. Civ. Eng. 18 (1) (2004) 2–9, https://doi.org/10.1061/(asce)0887-3801(2004)18:1(2).
[326] H. Zhu, B.G. Goodyear, M.L. Lauzon, R.A. Brown, G.S. Mayer, A.G. Law, L. Mansinha, J.R. Mitchell, A new local multiscale Fourier analysis for medical imaging, Med. Phys. 30 (2003) 1134–1141, https://doi.org/10.1118/1.1576931.
[327] R.A. Brown, R. Frayne, A comparison of texture quantification techniques based on the Fourier and S transforms, Med. Phys. 35 (2008) 4998–5008, https://doi.org/10.1118/1.2992051.
[328] P. Stroeven, Huan He, Shape assessment in concrete technology by Fourier analysis, in: A.M. Brandt, J. Olek, M.A. Glinicki, C.K.Y. Leung (Eds.), Brittle Matrix Composites 10 2012, Woodhead Publishing, 2012, pp. 233–242. ISBN 9780857099884, https://doi.org/10.1533/9780857099891.233.
[329] M.A. Taylor, E.J. Garboczi, S.T. Erdogan, D.W. Fowler, Some properties of irregular 3-D particles, Powder Technol. 162 (1) (2006) 1–15, https://doi.org/10.1016/j.powtec.2005.10.013.
[330] D. Zhang, G. Lu, Study and evaluation of different Fourier methods for image retrieval, Image Vis. Comput. 23 (1) (2005) 33–49, https://doi.org/10.1016/j.imavis.2004.09.001.
[331] U. Radvilaitė, Álvaro Ramírez-Gómez, Rimantas Kačianauskas, Determining the shape of agricultural materials using spherical harmonics, Comput. Electron. Agric. 128 (2016) 160–171, https://doi.org/10.1016/j.compag.2016.09.003.
[332] G. Bhattarai, V. Bonhomme, P. Conner, Image-based morphometric analysis reveals moderate to highly heritable nut shape traits in pecan, Euphytica 218 (2022) 102, https://doi.org/10.1007/s10681-022-03049-1.
[333] G.M. Chávez, F. Castillo-Rivera, J.A. Montenegro-Ríos, L. Borselli, A. Rodríguez-Sedano, D. Sarocchi, Fourier shape analysis, FSA: Freeware for quantitative study

of particle morphology, J. Volcanol. Geotherm. Res. 404 (2020) 107008, https://doi.org/10.1016/j.jvolgeores.2020.107008.
[334] B. Demir, B. Sayinci, N. Çetin, et al., Shape discrimination of almond cultivars by elliptic Fourier descriptors, Erwerbs-Obstbau 61 (2019) 245–256, https://doi.org/10.1007/s10341-019-00423-7.
[335] T. Yan, Y. Liu, D. Wei, et al., Shape analysis of sand particles based on Fourier descriptors, Environ. Sci. Pollut. Res. 30 (2023) 62803–62814, https://doi.org/10.1007/s11356-023-26388-5.
[336] T.T. Le, H.B.K. Nguyen, M.M. Rahman, M.R. Karim, Computational geometric and discrete fourier series approaches for particle shape analysis, in: J.N. Reddy, C. M. Wang, V.H. Luong, A.T. Le (Eds.), Proceedings of the Third International Conference on Sustainable Civil Engineering and Architecture. ICSCEA 2023. Lecture Notes in Civil Engineering, Singapore vol 442, Springer, 2024, https://doi.org/10.1007/978-981-99-7434-4_112.
[337] M. Wu, Shengli Jin, Morphology characterization for refractory aggregates, Open Ceramics 15 (2023) 100408, https://doi.org/10.1016/j.oceram.2023.100408.
[338] M.W. Clark, Quantitative shape analysis: A review, Math. Geol. 13 (1981) 303–320, https://doi.org/10.1007/BF01031516.
[339] E.J. Garboczi, Quantifying Particle Shape in 3D. In Advances in Computed Tomography for Geomaterials (eds K.A. Alshibli and A.H. Reed), 2010, https://doi.org/10.1002/9781118557723.ch11.
[340] E.J. Garboczi, J.W. Bullard, 3D analytical mathematical models of random star-shape particles via a combination of X-ray computed microtomography and spherical harmonic analysis, Adv. Powder Technol. 28 (2) (2017) 325–339, https://doi.org/10.1016/j.apt.2016.10.014.
[341] Y. Liu, D.S. Jeng, H. Xie, et al., On the particle morphology characterization of granular geomaterials, Acta Geotech. 18 (2023) 2321–2347, https://doi.org/10.1007/s11440-022-01733-z.
[342] M. Sonka, V. Hlavac, R. Boyle, Image Processing Analysis and Machine Vision, Chapman & Hall, London, 1993. ISBN: 978-0-412-45570-4.
[343] D. Su, Xiang Wang, Hong-Wei Yang, Chengyu Hong, Roughness analysis of general-shape particles, from 2D closed outlines to 3D closed surfaces, Powder Technol. 356 (2019) 423–438, https://doi.org/10.1016/j.powtec.2019.08.042.
[344] D. Su, Xiang Wang, Xuetao Wang, An in-depth comparative study of three-dimensional angularity indices of general-shape particles based on spherical harmonic reconstruction, Powder Technol. 364 (2020) 1009–1024, https://doi.org/10.1016/j.powtec.2019.10.019.
[345] J.C. Pena, Manuel Alejandro Castro, Marcio Muniz de Farias, Eugenio Oñate, Luis A. Moreno, Carlos A. Recarey, Development of an individual 3D particle reconstruction method for discrete mechanical modeling: interpolation by Fourier composition, Comput. Methods Appl. Mech. Eng. 420 (2024) 116705, https://doi.org/10.1016/j.cma.2023.116705.
[346] N.N. Clark, H. Diamond, G. Gelles, B. Bocoum, T.P. Meloy, Polygonal harmonics of silhouettes: shape analysis, Part. Part. Syst. Charact. 4 (1987) 38–43, https://doi.org/10.1002/ppsc.19870040108.
[347] P. Hurter, N.N. Clark, Persistence of polygonal harmonics as shape descriptors, Part. Part. Syst. Charact. 4 (1987) 101–105, https://doi.org/10.1002/ppsc.19870040121.
[348] D. Young, A.W. Bryson, B.M. Van Vliet, An evaluation of the technique of polygonal harmonics for the characterisation of particle shape, Powder Technol. 63 (1990) 157–168.
[349] M.-N. Pons, H. Vivier, J. Dodds, Particle shape characterization using morphological descriptors, Part. Part. Syst. Charact. 14 (1997) 272–277, https://doi.org/10.1002/ppsc.19970140603.
[350] H. Vivier, B. Marcant, M.-N. Pons, Morphological shape characterization: application to oxalate crystals, Part. Part. Syst. Charact. 11 (1994) 150–155, https://doi.org/10.1002/ppsc.19940110207.
[351] M.N. Pons, H. Vivier, T. Rolland, Pseudo-3D shape description for facetted materials, Part. Part. Syst. Charact. 15 (1998) 100–107.
[352] A. Reinhold, H. Briesen, Convex geometry for the morphological modeling and characterization of crystal shapes, Part. Part. Syst. Charact. 28 (2011) 37–56, https://doi.org/10.1002/ppsc.201100021.
[353] C.N. Davies, Particle-fluid interaction, J. Aerosol Sci. 10 (5) (1979) 477–513, https://doi.org/10.1016/0021-8502(79)90006-5.
[354] M. Furuuchi, A. Ikeuchi, T. Fukagawa, K. Gotoh, J. Chem. Sci. Jpn. 21 (1988) 528.
[355] A.I. Medalia, Dynamic shape factors of particles, Powder Technol. 4 (3) (1971) 117–138, https://doi.org/10.1016/0032-5910(71)80021-9.
[356] M.D. Allen, O.R. Moss, J.K. Briant, Dynamic shape factors for LMFBR mixed-oxide fuel aggregates, J. Aerosol Sci. 10 (1) (1979) 43–48, https://doi.org/10.1016/0021-8502(79)90134-4.
[357] I. Colbeck, Dynamic shape factors of fractal clusters of carbonaceous smoke, J. Aerosol Sci. 21 (S1) (1990) S43–S46, https://doi.org/10.1016/0021-8502(90)90185-Z.
[358] R. Sturm, Theoretical models for dynamic shape factors and lung deposition of small particle aggregates originating from combustion processes, Z. Med. Phys. 20 (3) (2010) 226–234, https://doi.org/10.1016/j.zemedi.2010.04.001.
[359] J. van Brakel, P.M. Heertjes, Analysis of diffusion in macroporous media in terms of a porosity, a tortuosity and a constrictivity factor, Int. J. Heat Mass Transf. 17 (1974) 1093–1103, https://doi.org/10.1016/0017-9310(74)90190-2.
[360] L. Shen, Zhangxin Chen, Critical review of the impact of tortuosity on diffusion, Chem. Eng. Sci. 62 (2007) 3748–3755, https://doi.org/10.1016/j.ces.2007.03.041.
[361] M. Lawrence, Y. Jiang, Porosity, pore size distribution, micro-structure, in: S. Amziane, F. Collet (Eds.), Bio-aggregates Based Building Materials. RILEM State-of-the-Art Reports vol 23, Springer, Dordrecht, 2017, https://doi.org/10.1007/978-94-024-1031-0_2.
[362] Y. Zhang, Bin Hu, Yanguo Teng, Tu Kevin, Chen Zhu, A library of BASIC scripts of reaction rates for geochemical modeling using phreeqc, Comput. Geosci. 133 (2019) 104316, https://doi.org/10.1016/j.cageo.2019.104316.
[363] A. Rabbani, Masoud Babaei, Hybrid pore-network and lattice-Boltzmann permeability modelling accelerated by machine learning, Adv. Water Resour. 126 (2019) 116–128, https://doi.org/10.1016/j.advwatres.2019.02.012.
[364] J. Ávila, J. Pagalo, M. Espinoza-Andaluz, Evaluation of geometric tortuosity for 3D digitally generated porous media considering the pore size distribution and the A-star algorithm, Sci. Rep. 12 (2022) 19463, https://doi.org/10.1038/s41598-022-23643-6.
[365] P.A. Webb, Clyde Orr, Analytical Methods in Fine Particle Technology, Micromeritics Instrument Corporation, 1997. ISBN 0965678318.
[366] A. Rodríguez de Castro, Mehrez Agnaou, Azita Ahmadi-Sénichault, Abdelaziz Omari, Numerical porosimetry: evaluation and comparison of yield stress fluids method, mercury intrusion porosimetry and pore network modelling approaches, Comput. Chem. Eng. 133 (2020) 106662, https://doi.org/10.1016/j.compchemeng.2019.106662.
[367] T. Bultreys, Wesley De Boever, Veerle Cnudde, Imaging and image-based fluid transport modeling at the pore scale in geological materials: A practical introduction to the current state-of-the-art, Earth Sci. Rev. 155 (2016) 93–128, https://doi.org/10.1016/j.earscirev.2016.02.001.
[368] R. Caulkin, Mishal S. Islam, Xiaodong Jia, Michael Fairweather, Studies for the development of a virtual permeameter, Comput. Chem. Eng. 68 (2014) 190–202, https://doi.org/10.1016/j.compchemeng.2014.05.027.
[369] M. Johnson, J. Peakall, X. Jia, M. Fairweather, D. Harbottle, S. Biggs, T.N. Hunter, Enhanced gas migration through permeable bubble networks within consolidated soft sediments, AICHE J. 64 (2018) 4131–4147, https://doi.org/10.1002/aic.16223.
[370] S. Weis, Philipp W.A. Schönhöfer, Fabian M. Schaller, Matthias Schröter, Gerd E. Schröder-Turk, Pomelo, a tool for computing Generic Set Voronoi diagrams of aspherical particles of arbitrary shape, EPJ Web Conf. 140 (2017) 06007, https://doi.org/10.1051/epjconf/201714006007.
[371] P.J. Barrett, The shape of rock particles, a critical review, Sedimentology 27 (3) (1980) 291–303, https://doi.org/10.1111/j.1365-3091.1980.tb01179.x.
[372] S.J. Blott, K. Pye, Particle shape: a review and new methods of characterization and classification, Sedimentology 55 (2008) 31–63, https://doi.org/10.1111/j.1365-3091.2007.00892.x.
[373] I.L. Dryden, Kanti V. Mardia, Statistical Shape Analysis, with Applications in R, John Wiley & Sons, 2016, https://doi.org/10.1002/9781119072492. ISBN: 9780470699621.
[374] P.K. Ghosh, Koichiro Deguchi, Mathematics of Shape Description: A Morphological Approach to Image Processing and Computer Graphics, John Wiley & Sons (Asia) Pte Ltd, 2008. ISBN: 978-0-470-82307-1.
[375] A.E. Hawkins, The Shape of Powder-Particle Outlines, Wiley, New York, 1993. ISBN: 0471938785.
[376] N.C. Janke, The shape of rock particles, a critical review, Sedimentology 28 (1981) 737–738, https://doi.org/10.1111/j.1365-3091.1981.tb01934.x.
[377] X. Jia, E.J. Garboczi, Advances in shape measurement in the digital world, Particuology 26 (2016) 19–31, https://doi.org/10.1016/j.partic.2015.12.005.
[378] Norman MacLeod, Geometric morphometrics and geological shape-classification systems, Earth Sci. Rev. 59 (2002) 27–47, https://doi.org/10.1016/S0012-8252(02)00068-5.
[379] B. Sukumaran, A.K. Ashmawy, Quantitative characterization of the geometry of discrete particles, Géotechnique 51 (7) (2001) 171–179, https://doi.org/10.1680/geot.2001.51.7.619.
[380] K.V. Anusree, G.M. Gali, Characterization of sand particle morphology: state-of-the-art, Bull. Eng. Geol. Environ. 82 (2023) 269, https://doi.org/10.1007/s10064-023-03309-x.
[381] G. Korvin, The shape of pebbles, grains and pores, in: Statistical Rock Physics. Earth and Environmental Sciences Library, Springer, Cham, 2024, https://doi.org/10.1007/978-3-031-46700-4_7.
[382] J.M. Rodriguez, Tommy Edeskär, Sven Knutsson, Particle shape quantities and measurement techniques–A review, Electron. J. Geotech. Eng. 18 (2013) 169–198.
[383] J.K. Mitchell, K. Soga. Fundamentals of Soil Behaviour, 3rd ed., John Wiley & Sons, Hoboken, NJ, USA, 2005, ISBN 978-0-471-46302-3.
[384] R. Cepuritis, Edward J. Garboczi, Stefan Jacobsen, Kenneth A. Snyder, Comparison of 2-D and 3-D shape analysis of concrete aggregate fines from VSI crushing, Powder Technol. 309 (2017) 110–125, https://doi.org/10.1016/j.powtec.2016.12.037.
[385] M. Iskander, L. Li, Comparison of 2D and 3D DIA, in: Dynamic Image Analysis of Granular Materials. Springer Series in Geomechanics and Geoengineering, Springer, Cham, 2024, https://doi.org/10.1007/978-3-031-47534-4_6.
[386] F. Kaviani-Hamedani, M. Esmailzade, K. Adineh, et al., Quantifying three-dimensional sphericity indices of irregular fine particles from 2D images through sequential sieving tests, Granul. Matter 26 (2024) 13, https://doi.org/10.1007/s10035-023-01376-1.
[387] D. Su, W.M. Yan, Prediction of 3D size and shape descriptors of irregular granular particles from projected 2D images, Acta Geotech 15 (2020) 1533–1555, https://doi.org/10.1007/s11440-019-00845-3.
[388] T. Ueda, Tatsuya Oki, Shigeki Koyanaka, 2D-3D conversion method for assessment of multiple characteristics of particle shape and size, Powder Technol. 343 (2019) 287–295, https://doi.org/10.1016/j.powtec.2018.11.019.
[389] R. Ehrlich, P.J. Brown, J.M. Yarus, R.S. Przygocki, The origin of shape frequency distributions and the relationship between size and shape, J. Sediment. Res. 50

(2) (1980) 475–483, https://doi.org/10.1306/212F7A2C-2B24-11D7-8648000102C1865D.
[390] B.V. Elsevier, J. Patrick Laceby, Olivier Evrard, Hugh G. Smith, Will H. Blake, Jon M. Olley, Jean Paolo Gomes Minella, Philip N. Owens, The challenges and opportunities of addressing particle size effects in sediment source fingerprinting: a review, Earth Sci. Rev. 169 (2017) 85–103, https://doi.org/10.1016/J.EARSCIREV.2017.04.009.
[391] L. Holzer, R.J. Flatt, S.T. Erdoğan, J.W. Bullard, E.J. Garboczi, Shape comparison between 0.4–2.0 and 20–60 μm cement particles, J. Am. Ceram. Soc. 93 (2010) 1626–1633, https://doi.org/10.1111/j.1551-2916.2010.03654.x.
[392] T. Miyajima, Ken-Ichi Yamamoto, Masunori Sugimoto, The effect of particle orientation and/or position on two-dimensional shape measurements, Adv. Powder Technol. 12 (3) (2001) 413–426, https://doi.org/10.1163/156855201750537938.
[393] E. Pirard, G. Dislaire, Robustness of Planar Shape Descriptors of Particles, Paper Presented at Meeting of the International Association for Mathematical Geology in Liège, 3–8, Sept. 2006.
[394] M. Schäfer, Digital optics: some remarks on the accuracy of particle image analysis, Part. Part. Syst. Charact. 19 (2002) 158–168, https://doi.org/10.1002/1521-4117(200207)19:3<158::AID-PPSC158>3.0.CO;2-8.
[395] Q. Sun, Junxing Zheng, Matthew R. Coop, Fatin N. Altuhafi, Minimum image quality for reliable optical characterizations of soil particle shapes, Comput. Geotech. 114 (2019) 103110, https://doi.org/10.1016/j.compgeo.2019.103110.
[396] M. Tunwal, A. Lim, A low-cost, repeatable method for 3D particle analysis with SfM photogrammetry, Geosciences 13 (7) (2023) 190, https://doi.org/10.3390/geosciences13070190.
[397] Y. Yang, X.-M. Fu, L. Liu, Computing surface PolyCube-maps by constrained Voxelization, Comp. Graph. Forum 38 (2019) 299–309, https://doi.org/10.1111/cgf.13838.
[398] M. Zeidan, X. Jia, R.A. Williams, Errors implicit in digital particle characterisation, Chem. Eng. Sci. 62 (7) (2007) 1905–1914, https://doi.org/10.1016/j.ces.2006.12.011.
[399] M. Đuriš, Zorana Arsenijević, Darko Jaćimovski, Tatjana Kaluđerović Radoičić, Optimal pixel resolution for sand particles size and shape analysis, Powder Technol. 302 (2016) 177–186, https://doi.org/10.1016/j.powtec.2016.08.045.
[400] S. Kröner, María Teresa Doménech Carbó, Determination of minimum pixel resolution for shape analysis: proposal of a new data validation method for computerized images, Powder Technol. 245 (2013) 297–313, https://doi.org/10.1016/j.powtec.2013.04.048.
[401] M.L. Hentschel, Neil W. Page, Selection of descriptors for particle shape characterization, Part. Part. Syst. Charact. 20 (1) (2003) 25–38, https://doi.org/10.1002/ppsc.200390002.
[402] J.P. Mitchell, Particle standards: their development and application, in: KONA Powder and Particle No. 18, 2000.
[403] R.M. Haralick, S.R. Sternberg, X. Zhuang, Image analysis using mathematical morphology, IEEE Trans. Pattern Anal. Mach. Intell. PAMI-9 (4) (1987) 532–550, https://doi.org/10.1109/TPAMI.1987.4767941.
[404] B.K. Jang, Shape analysis using mathematical morphology, PhD Thesis, The University of Wisconsin, Madison, 1990. Order number 9108276.
[405] Y. Kimori, Morphological image processing for quantitative shape analysis of biomedical structures: effective contrast enhancement, J. Synchrotron Radiat. 20 (2013) 848–853, https://doi.org/10.1107/S0909049513020761.
[406] S. Velasco-Forero, Samy Blusseau, Mateus Sangalli, Mathematical morphology meets Deep Learning, in: 13th European Congress for Stereology and Image Analysis (ECSIA), Jun 2021. Saint-Étienne, France. hal-03355356.
[407] L. Yu, R. Wang, Shape representation based on mathematical morphology, Pattern Recogn. Lett. 26 (9) (2005) 1354–1362.
[408] M.A. Lopez-Sanchez, Which average, how many grains, and how to estimate robust confidence intervals in unimodal grain size populations, J. Struct. Geol. 135 (2020) 104042, https://doi.org/10.1016/j.jsg.2020.104042.
[409] M. Pasha, Nurul Lukman Hekiem, Xiaodong Jia, Mojtaba Ghadiri, Prediction of flowability of cohesive powder mixtures at high strain rate conditions by discrete element method, Powder Technol. 372 (2020) 59–67, https://doi.org/10.1016/j.powtec.2020.05.110.
[410] M.-N. Pons, Hervé Vivier, Vincent Delcour, Jean-René Authelin, Laurence Paillères-Hubert, Morphological analysis of pharmaceutical powders, Powder Technol. 128 (2–3) (2002) 276–286, https://doi.org/10.1016/S0032-5910(02)00177-8.
[411] U. Ulusoy, M. Yekeler, Dynamic image analysis of calcite particles created by different mills, Int. J. Miner. Process. 133 (2014) 83–90, https://doi.org/10.1016/j.minpro.2014.10.006.
[412] J. Chen, R. Li, P.Q. Mo, et al., A unified 2D and 3D morphology quantification and geometric parameters-driven reconstruction method for irregular particles, Granul. Matter 26 (2024) 31, https://doi.org/10.1007/s10035-024-01402-w.
[413] E. Garboczi, X-Ray computed microtomography and spherical harmonic analysis were used to create 3D analytical mathematical models of random star-shaped particles, J. General. Lie Theory App. 16 (7) (2022) 352, https://doi.org/10.37421/1736-4337.2022.16.352.
[414] K.V. Kostas, A. Amiralin, S. Sagimbayev, T. Massalov, Y. Kalel, C.G. Politis, Parametric model for the reconstruction and representation of hydrofoils and airfoils, Ocean Eng. 199 (2020) 107020.
[415] Z. Liang, X. Wang, J. Gong, et al., Random generation of 2D geometry-controlled particles via the epicycle series, Granul. Matter 22 (2020) 84, https://doi.org/10.1007/s10035-020-01031-z.
[416] J. Lu, Mingyang Gong, Generation of 3D realistic geological particles using conditional generative adversarial network aided spherical harmonic analysis, Powder Technol. 436 (2024) 119488, https://doi.org/10.1016/j.powtec.2024.119488.
[417] Z. Tan, Fu-qiang Guo, Zhen Leng, Zhen-Jun Yang, Peng Cao, A novel strategy for generating mesoscale asphalt concrete model with controllable aggregate morphology and packing structure, Comput. Struct. 296 (2024) (2024) 107315, https://doi.org/10.1016/j.compstruc.2024.107315.
[418] G. Mollon, J. Zhao, 3D generation of realistic granular samples based on random fields theory and Fourier shape descriptors, Comput. Methods Appl. Mech. Eng. 279 (2014) 46–65, https://doi.org/10.1016/j.cma.2014.06.022.
[419] Y. Zhou, Wei Guan, Changming Zhao, Hengshan Hu, Zhennan He, Xiaojing Zou, Xiaowei Gong, A computational workflow to study CO2 transport in porous media with irregular grains: coupling a Fourier series-based approach and CFD, J. Clean. Prod. 418 (2023) 138037, https://doi.org/10.1016/j.jclepro.2023.138037.
[420] S. Zhang, Lianheng Zhao, Xiang Wang, Dongliang Huang, Quantifying the effects of elongation and flatness on the shear behavior of realistic 3D rock aggregates based on DEM modelling, Adv. Powder Technol. 32 (5) (2021) 1318–1332.
[421] Z. Nie, C. Fang, J. Gong, Z. Liang, DEM study on the effect of roundness on the shear behaviour of granular materials, Comput. Geotech. 121 (2020) (2020) 1–11.
[422] T. Ueda, Estimation of three-dimensional particle size and shape characteristics using a modified 2D–3D conversion method employing spherical harmonic-based principal component analysis, Powder Technol. 404 (2022) 117461, https://doi.org/10.1016/j.powtec.2022.117461.
[423] T. Ueda, Reproducibility of the repose angle, porosity, and coordination number of particles generated by spherical harmonic-based principal component analysis using discrete element simulation, Powder Technol. 415 (2022) 118143, https://doi.org/10.1016/j.powtec.2022.118143.
[424] Xiang Wang, Nie Zhihong, Zhengyu Liang, Random generation of convex aggregates for DEM study of particle shape effect, Constr. Build. Mater. 268 (2021) 121468, https://doi.org/10.1016/j.conbuildmat.2020.121468.
[425] R. Ge, Mojtaba Ghadiri, Tina Bonakdar, Qijun Zheng, Zongyan Zhou, Ian Larson, Karen Hapgood, Deformation of 3D printed agglomerates: multiscale experimental tests and DEM simulation, Chem. Eng. Sci. 217 (2020) 115526, https://doi.org/10.1016/j.ces.2020.115526.
[426] A. Sanchez-Barra, Gonzalo Zambrano-Narvaez, Rick Chalaturnyk, An In-depth Analysis of Strength and Stiffness Variability in 3D-Printed Sandstones: Implications for Geomechanics, 2023, https://doi.org/10.20944/preprints202306.1832.v1.
[427] R. Song, Mingyang Wu, Yao Wang, Jianjun Liu, Chunhe Yang, In-situ X-CT scanning and numerical modeling on the mechanical behavior of the 3D printing rock, Powder Technol. 416 (2023) 118240, https://doi.org/10.1016/j.powtec.2023.118240.
[428] C. Cao, M. Preda, T. Zaharia, 3D Point Cloud Compression: A Survey, 2019, pp. 1–9, https://doi.org/10.1145/3329714.3338130.
[429] P. Gajjar, T.T.H. Nguyen, J. Sun, I.D. Styliari, H. Bale, S.A. McDonald, T. L. Burnett, B. Tordoff, E. Lauridsen, R.B. Hammond, D. Murnane, P.J. Withers, K. J. Roberts, Crystallographic tomography and molecular modelling of structured organic polycrystalline powders, Cryst. Eng. Comm. 23 (13) (2021) 2483–2624, https://doi.org/10.1039/D0CE01712D.
[430] Y. Liu, S. Ruan Wu, G. Chirikjian, Robust and accurate superquadric recovery: a probabilistic approach, in: 2022 IEEE/CVF Conference on Computer Vision and Pattern Recognition (CVPR), New Orleans, LA, USA, 2022, pp. 2666–2675, https://doi.org/10.1109/CVPR52688.2022.00270.
[431] Anshuman Razdan, Jeremy Rowe, Matt Tocheri, Wilson Sweitzer, Adding Semantics to 3D Digital Libraries, 2002, pp. 419–420, https://doi.org/10.1007/3-540-36227-4_47.
[432] L. Shen, Hany Farid, Mark A. McPeek, Modeling three-dimensional morphological structures using spherical harmonics, Evolution 63 (2009) 1003–1016, https://doi.org/10.1111/j.1558-5646.2008.00557.x.
[433] S. Wang, S. Ji, Poly-superquadric model for DEM simulations of asymmetrically shaped particles, Comput. Part. Mech. 9 (2022) 299–313, https://doi.org/10.1007/s40571-021-00410-4.
[434] R.A. Williams, X. Jia, Tomographic imaging of particulate systems, Adv. Powder Technol. 14 (1) (2003) 1–16.
[435] Robin Green, Spherical Harmonic Lighting: The Gritty Details. https://3dvar.com/Green2003Spherical.pdf.
[436] https://www.liverpool.ac.uk/science-and-engineering/our-research/shared-research-facilities/micro-x-ray-ct/xct-research/xct-sediment-core/.
[437] Simon Giraudot, Surface Reconstruction from Point Clouds, CGAL 5.6.1 – Manual. https://doc.cgal.org/latest/Manual/tuto_reconstruction.html.
[438] M. Asachi, Miller Alonso Camargo-Valero, Multi-sensors data fusion for monitoring of powdered and granule products: current status and future perspectives, Adv. Powder Technol. 34 (7) (2023) 104055, https://doi.org/10.1016/j.apt.2023.104055.
[439] H. Eisenschmidt, Naim Bajcinca, Kai Sundmacher, Optimal control of crystal shapes in batch crystallization experiments by growth-dissolution cycles, Cryst. Growth Des. 16 (6) (2016) 3297–3306, https://doi.org/10.1021/acs.cgd.6b00288.
[440] J.R. Hart, Yingdan Zhu, Eric Pirard, Particle size and shape characterization: current technology and practice, in advances in the characterization of industrial minerals, in: G.E. Christidis (Ed.), European Mineralogical Union and the Mineralogical Society of Great Britain & Ireland, 2010, https://doi.org/10.1180/EMU-notes.9.4. ISBN: 9780903056281.
[441] S. Leroy, Eric Pirard, Mineral recognition of single particles in ore slurry samples by means of multispectral image processing, Miner. Eng. 132 (2019) 228–237, https://doi.org/10.1016/j.mineng.2018.12.009.

[442] S.B. Lindström, R. Amjad, E. Gåhlin, L. Andersson, M. Kaarto, K. Liubytska, J. Persson, J.-E. Berg, B.A. Engberg, F. Nilsson, Pulp particle classification based on optical Fiber analysis and machine learning techniques, Fibers 12 (1) (2024) 2, https://doi.org/10.3390/fib12010002.
[443] H.H. Murray, Jessica Elzea Kogel, Engineered clay products for the paper industry, Appl. Clay Sci. 29 (3–4) (2005) 199–206, https://doi.org/10.1016/j.clay.2004.12.005.
[444] D.B. Patience, J.B. Rawlings, Particle-shape monitoring and control in crystallization processes, AICHE J. 47 (9) (2001) 2125–2130, https://doi.org/10.1002/aic.690470922.
[445] P. Schirg, Online image analysis of particulate materials, in: J. Irudayaraj, C. Reh (Eds.), Nondestructive Testing of Food Quality, 2007, https://doi.org/10.1002/9780470388310.ch8.
[446] H.G. Schmid, Image analysis for quality control of diamonds, Diamante Applicatione & Technologia 18 (1999) 112.
[447] M.F. Ashby, Materials Selection in Mechanical Design, 4th edition, Elsvier, 2011, https://doi.org/10.1016/C2009-0-25539-5. ISBN: 978-1-85617-663-7.
[448] Y. Ding, Guangtao Zhang, Hao Wu, Bin Hai, Liangbin Wang, Yitai Qian, Nanoscale magnesium hydroxide and magnesium oxide powders: control over size, shape, and structure via hydrothermal synthesis, Chem. Mater. 13 (2) (2001) 435–440, https://doi.org/10.1021/cm000607e.
[449] F. Hrdlicka, Martin Kratochvil, Ivana Mazinova, Pavel Florian, Use of material-shape factors in mechanical design, Manufact. Technol. 19 (3) (2019) 397–403, https://doi.org/10.21062/ujep/303.2019/a/1213–2489/MT/19/3/397.
[450] J. Panetta, Haleh Mohammadian, Emiliano Luci, Vahid Babaei, Shape from release: inverse design and fabrication of controlled release structures, ACM Trans. Graph. 41 (6) (2022) 1–14, https://doi.org/10.1145/3550454.3555518.
[451] D.A. Canelas, K.P. Herlihy, J.M. DeSimone, Top-down particle fabrication: control of size and shape for diagnostic imaging and drug delivery, Wiley Interdiscip Rev Nanomed Nanobiotechnol 1 (4) (2009 Jul-Aug) 391–404, https://doi.org/10.1002/wnan.40. PMID: 20049805; PMCID: PMC2804992.
[452] K. Lebow, Take topography up a notch, Rev. Optom. 139 (2002) 08. https://www.reviewofoptometry.com/article/take-topography-up-a-notch.
[453] D. Tralic, J. Bozek, S. Grgic, Shape analysis and classification of masses in mammographic images using neural networks, in: Systems, Signals and Image Processing (IWSSIP), 18th International Conference, 2011.
[454] S. Zimmermann, K. Landes, J. Schein, Particle shape imaging-a method for analyzing particles-in-flight, in: 2008 IEEE 35th International Conference on Plasma Science, Karlsruhe, Germany, 2008, p. 1, https://doi.org/10.1109/PLASMA.2008.4591013.
[455] C. Turchiuli, E. Castillo-Castaneda, Agglomerates structure characterization using 3D-image reconstruction, Part. Part. Syst. Charact. 26 (2009) 25–33, https://doi.org/10.1002/ppsc.200700028.
[456] W. Choi, C. Fang-Yen, K. Badizadegan, et al., Tomographic phase microscopy, Nat. Methods 4 (2007) 717–719, https://doi.org/10.1038/nmeth1078.
[457] M.R. Cox, Muniram Budhu, A practical approach to grain shape quantification, Eng. Geol. 96 (1–2) (2008) 1–16, https://doi.org/10.1016/j.enggeo.2007.05.005.
[458] Umesh Tiwari, Why particle shape matters too… Friday, 8th December 2023. https://www.malvernpanalytical.com/en/learn/knowledge-center/insights/why-particle-shape-matters-too.
[459] Z. Ren, Jianhao Zeng, Yang Zheng, Huiyue Tang, Jingnan Wang, Lepeng Jiang, Wei Feng, Digital image analysis for contact and shape recognition of coffee particles in grinding, Powder Technol. (2024) 119717, https://doi.org/10.1016/j.powtec.2024.119717.
[460] Quan Sun, Yi Zheng, Beiwen Li, Junxing Zheng, Ziwei Wang, Three-dimensional particle size and shape characterization using structural light, Géotechn. Lett. (2019), https://doi.org/10.1680/jgele.18.00207.
[461] Z. Ma, Henk G. Merkus, Jan G.A.E. de Smet, Camiel Heffels, Brian Scarlett, New developments in particle characterization by laser diffraction: size and shape, Powder Technol. 111 (1–2) (2000) 66–78, https://doi.org/10.1016/S0032-5910(00)00242-4.
[462] M. Weirich, D. Misiulia, S. Antonyuk, Characterization of particle shape with an improved 3D light scattering sensor (3D-LSS) for aerosols, Sensors 24 (2024) 955, https://doi.org/10.3390/s24030955.
[463] A. Ali, N. Zhang, R.M. Santos, Mineral characterization using scanning electron microscopy (SEM): A review of the fundamentals, advancements, and research directions, Appl. Sci. 13 (23) (2023) 12600, https://doi.org/10.3390/app132312600.
[464] M. Olbert, Vilem Nedela, Josef Jirak, Jiri Hudec, Size and shape analysis of micro- to nano-particles of quartz powders using advanced electron microscopy and laser diffraction methods, Powder Technol. 433 (2024) 119250, https://doi.org/10.1016/j.powtec.2023.119250.
[465] O. Ersoy, Surface area and volume measurements of volcanic ash particles by SEM stereoscopic imaging, J. Volcanol. Geotherm. Res. 190 (3–4) (2010) 290–296, https://doi.org/10.1016/j.jvolgeores.2009.12.006.
[466] O.P. Mills, I. Rose William, Shape and surface area measurements using scanning electron microscope stereo-pair images of volcanic ash particles, Geosphere 6 (6) (2010) 805–811, https://doi.org/10.1130/GES00558.1.
[467] E. Binaghi, Ignazio Gallo, Giuseppe Marino, Mario Raspanti, Neural adaptive stereo matching, Pattern Recogn. Lett. 25 (15) (2004) 1743–1758, https://doi.org/10.1016/j.patrec.2004.07.001.
[468] A. Takase, CT vs. SEM: Which Is Better? Blog, article at, imaging.rigaku.com, 2022, https://imaging.rigaku.com/blog/ct-vs-sem-which-is-better. Accessed 16May2024.
[469] M.A. Groeber, B. Haley, M.D. Uchic, D.M. Dimiduk, S. Ghosh, 3d reconstruction and characterization of polycrystalline microstructures using a fib-sem system, Mater. Charact. 57 (4–5) (2006) 259–273.
[470] Y. Fan, K. Liu, Large-volume FIB-SEM 3D reconstruction: An effective method for characterizing pore space of lacustrine shales, Front. Earth Sci. 10 (2023) 2022, https://doi.org/10.3389/feart.2022.1046927.
[471] S. Liu, Shuxun Sang, Geoff Wang, Jingsheng Ma, Xin Wang, Wenfeng Wang, Du Yi, Tian Wang, FIB-SEM and X-ray CT characterization of interconnected pores in high-rank coal formed from regional metamorphism, J. Pet. Sci. Eng. 148 (2017) 21–31, https://doi.org/10.1016/j.petrol.2016.10.006.
[472] A. Jacob, M. Peltz, S. Hale, F. Enzmann, O. Moravcova, L.N. Warr, G. Grathoff, P. Blum, M. Kersten, Simulating permeability reduction by clay mineral nanopores in a tight sandstone by combining computer X-ray microtomography and focussed ion beam scanning electron microscopy imaging, Solid Earth 12 (2021) 1–14, https://doi.org/10.5194/se-12-1-2021.
[473] O. Ersoy, Erkan Aydar, Alain Gourgaud, Hasan Bayhan, Quantitative analysis on volcanic ash surfaces: application of extended depth-of-field (focus) algorithm for light and scanning electron microscopy and 3D reconstruction, Micron 39 (2) (2008) 128–136, https://doi.org/10.1016/j.micron.2006.11.010.
[474] J.E. Cryer, P.S. Tsai, M. Shah, Integration of shape from shading and stereo, Pattern Recogn. 28 (7) (1995) 1033–1043, https://doi.org/10.1016/0031-3203(94)00183-M.
[475] P. Gao, Jie Zhou, Weibin Rong, Jian Gao, Lefeng Wang, Lining Sun, Vertical distance from shading in the SEM, Micron 141 (2021) 102978, https://doi.org/10.1016/j.micron.2020.102978.
[476] D. Samak, A. Fischer, D. Rittel, 3D reconstruction and visualization of microstructure surfaces from 2D images, CIRP Ann. 56 (1) (2007) 149–152, https://doi.org/10.1016/j.cirp.2007.05.036.
[477] Q. Shi, Stéphane Roux, Félix Latourte, François Hild, Dominique Loisnard, Nicolas Brynaert, Measuring topographies from conventional SEM acquisitions, Ultramicroscopy 191 (2018) 18–33, https://doi.org/10.1016/j.ultramic.2018.04.006.
[478] J. Paluszyński, W. Słówko, Surface reconstruction with the photometric method in SEM, Vacuum 78 (2–4) (2005) 533–537, https://doi.org/10.1016/j.vacuum.2005.01.081.
[479] A.P. Tafti, Andrew B. Kirkpatrick, Zahrasadat Alavi, Heather A. Owen, Zeyun Yu, Recent advances in 3D SEM surface reconstruction, Micron 78 (2015) 54–66, https://doi.org/10.1016/j.micron.2015.07.005.
[480] S. Yan, Aderonke Adegbule, Tohren C.G. Kibbey, A hybrid 3D SEM reconstruction method optimized for complex geologic material surfaces, Micron 99 (2017) 26–31, https://doi.org/10.1016/j.micron.2017.03.018.
[481] O. Altingövde, Anastasiia Mishchuk, Gulnaz Ganeeva, Emad Oveisi, Cecile Hebert, Pascal Fua, 3D reconstruction of curvilinear structures with stereo matching deep convolutional neural networks, Ultramicroscopy 234 (2022) 113460, https://doi.org/10.1016/j.ultramic.2021.113460.
[482] E. Oveisi, Antoine Letouzey, Sandro De Zanet, Guillaume Lucas, Marco Cantoni, Pascal Fua, Cécile Hébert, Stereo-vision three-dimensional reconstruction of curvilinear structures imaged with a TEM, Ultramicroscopy 184 (A) (2018) 116–124, https://doi.org/10.1016/j.ultramic.2017.08.010.
[483] Z. Barkay, Ilia Rivkin, Rimona Margalit, Three-dimensional characterization of drug-encapsulating particles using STEM detector in FEG-SEM, Micron 40 (4) (2009) 480–485, https://doi.org/10.1016/j.micron.2008.12.003.
[484] W. Dachraoui, Maryna I. Bodnarchuk, Rolf Erni, Direct imaging of the atomic mechanisms governing the growth and shape of bimetallic Pt–Pd nanocrystals by in situ liquid cell STEM, ACS Nano 16 (9) (2022) 14198–14209, https://doi.org/10.1021/acsnano.2c04291.
[485] A. Jácome, G. Eggeler, A. Dlouhý, Advanced scanning transmission stereo electron microscopy of structural and functional engineering materials, Ultramicroscopy 122 (2012) 48–59, https://doi.org/10.1016/j.ultramic.2012.06.017.
[486] E. Oveisi, A. Letouzey, D.T.L. Alexander, Q. Jeangros, R. Schäublin, G. Lucas, P. Fua, C. Hébert, Tilt-less 3-D electron imaging and reconstruction of complex curvilinear structures, Sci. Rep. 7 (1) (2017 Sep 6) 10630, https://doi.org/10.1038/s41598-017-07537-6.
[487] P. Ercius, O. Alaidi, M.J. Rames, G. Ren, Electron tomography: A three-dimensional analytic tool for hard and soft materials research, Adv. Mater. 27 (38) (2015 Oct 14) 5638–5663, https://doi.org/10.1002/adma.201501015.
[488] J. Schwartz, C. Harris, J. Pietryga, et al., Real-time 3D analysis during electron tomography using tomviz, Nat. Commun. 13 (2022) 4458, https://doi.org/10.1038/s41467-022-32046-0.
[489] J.G. Behnsen, K. Black, J.E. Houghton, R.H. Worden, A, review of particle size analysis with X-ray CT, Materials 16 (2023) 1259, https://doi.org/10.3390/ma16031259.
[490] T.A. Kramer, M.M. Clark, The measurement of particles suspended in a stirred vessel using microphotography and digital image analysis, Part. Part. Syst. Charact. 13 (1996) 3–9, https://doi.org/10.1002/ppsc.19960130103.
[491] C. Redenbach, R. Ohser-Wiedemann, R. Löffler, T. Bernthaler, A. Nagel, Characterization of powders using Micro computed tomography, Part. Part. Syst. Charact. 28 (2011) 3–12, https://doi.org/10.1002/ppsc.200900088.
[492] M. Kampschulte, et al., Nano-computed tomography: technique and applications 188 (2) (2016) 146–154 (Georg Thieme Verlag KG, 2016).
[493] F. Beckmann, U. Bonse, F. Busch, O. Günnewig, X-ray microtomography (microCT) using phase contrast for the investigation of organic matter, J. Comput. Assist. Tomogr. 21 (4) (1997) 539–553, https://doi.org/10.1097/00004728-199707000-00006.

[494] C. Karunakaran, R. Lahlali, N. Zhu, et al., Factors influencing real time internal structural visualization and dynamic process monitoring in plants using synchrotron-based phase contrast X-ray imaging, Sci. Rep. 5 (2015) 12119, https://doi.org/10.1038/srep12119.
[495] Z.H. Levine, A.P. Peskin, E.J. Garboczi, A.D. Holmgren, Multi-energy X-ray tomography of an optical Fiber: the role of spatial averaging, Microsc. Microanal. 25 (1) (2019 Feb) 70–76, https://doi.org/10.1017/S1431927618016136.
[496] A. Korolkovas, Alexander Katsevich, Michael Frenkel, et al., Fast X-Ray Diffraction (XRD) Tomography for Enhanced Identification of Materials. TechRxiv. December 10, 2021.
[497] T.M. Ajayi, N. Shirato, T. Rojas, et al., Characterization of just one atom using synchrotron X-rays, Nature 618 (2023) 69–73, https://doi.org/10.1038/s41586-023-06011-w.
[498] I. Arganda-Carreras, V. Kaynig, C. Rueden, K.W. Eliceiri, J. Schindelin, A. Cardona, H. Sebastian Seung, Trainable Weka segmentation: a machine learning tool for microscopy pixel classification, Bioinformatics 33 (2017) 2424–2426.
[499] D. Puzyrev, K. Harth, T. Trittel, et al., Machine learning for 3D particle tracking in granular gases, Microgravity Sci. Technol. 32 (2020) 897–906, https://doi.org/10.1007/s12217-020-09800-4.
[500] H. Chan, M. Cherukara, T.D. Loeffler, et al., Machine learning enabled autonomous microstructural characterization in 3D samples, NPJ Comput. Mater. 6 (1) (2020), https://doi.org/10.1038/s41524-019-0267-z.
[501] C.F. Berg, Olivier Lopez, Håvard Berland, Industrial applications of digital rock technology, J. Pet. Sci. Eng. 157 (2017) 131–147, https://doi.org/10.1016/j.petrol.2017.06.074.
[502] S. Budhathoki, J. Lamba, P. Srivastava, et al., Temporal and spatial variability in 3D soil macropore characteristics determined using X-ray computed tomography, J. Soils Sediments 22 (2022) 1263–1277, https://doi.org/10.1007/s11368-022-03150-x.
[503] N. Dal Ferro, P. Charrier, F. Morari, Dual-scale micro-CT assessment of soil structure in a long-term fertilization experiment, Geoderma 204–205 (2013) 84–93, https://doi.org/10.1016/j.geoderma.2013.04.012.
[504] B. Ghanbarian, Qingyang Lin, Luiz F. Pires, Scale dependence of tortuosity in soils under contrasting cultivation conditions, Soil Tillage Res. 233 (2023) 105788, https://doi.org/10.1016/j.still.2023.105788.
[505] Gostick, et al., PoreSpy: A python toolkit for quantitative analysis of porous media images, J. Open Source Softw. 4 (37) (2019) 1296, https://doi.org/10.21105/joss.01296.
[506] P. Kaur, J. Lamba, T.R. Way, et al., Cover crop effects on X-ray computed tomography–derived soil pore characteristics, J. Soils Sediments 24 (2024) 111–125, https://doi.org/10.1007/s11368-023-03596-7.
[507] A.O. Sangotayo, P. Chakraborty, S. Xu, et al., Author correction: cattle manure application for 12 and 17 years enhanced depth distribution of soil organic carbon and X-ray computed tomography-derived pore characteristics, Sci. Rep. 14 (2024) 4992, https://doi.org/10.1038/s41598-024-55738-7.
[508] L.F. Pires, Behzad Ghanbarian, Qingyang Lin, Physical, topological and hydraulic properties of an Oxisol under conservation practices: X-ray tomography imaging and pore-network simulation, Soil Tillage Res. 239 (2024) 106055, https://doi.org/10.1016/j.still.2024.106055.
[509] R. Ditscherlein, Thomas Leißner, Urs A. Peuker, Preparation strategy for statistically significant micrometer-sized particle systems suitable for correlative 3D imaging workflows on the example of X-ray microtomography, Powder Technol. 395 (2022) 235–242, https://doi.org/10.1016/j.powtec.2021.09.038.
[510] Q. Sun, Junxing Zheng, Li Cheng, Improved watershed analysis for segmenting contacting particles of coarse granular soils in volumetric images, Powder Technol. 356 (2019) 295–303, https://doi.org/10.1016/j.powtec.2019.08.028.
[511] A. Videla, C.-L. Lin, J.D. Miller, Watershed functions applied to a 3D image segmentation problem for the analysis of packed particle beds, Part. Part. Syst. Charact. 23 (2006) 237–245.
[512] E.J. Garboczi, N. Hrabe, Three-dimensional particle shape analysis using X-ray computed tomography: experimental procedure and analysis algorithms for metal powders, J. Vis. Exp. 166 (2020 Dec 4), https://doi.org/10.3791/61636.
[513] M. Li, Huisu Chen, Jianjun Lin, Rongling Zhang, Liu Lin, Effects of the pore shape polydispersity on the percolation threshold and diffusivity of porous composites: theoretical and numerical studies, Powder Technol. 386 (2021) 382–393, https://doi.org/10.1016/j.powtec.2021.03.055.
[514] O. Stamati, Edward Andò, Emmanuel Roubin, Rémi Cailletaud, Max Wiebicke, Gustavo Pinzón, Cyrille Couture, Ryan Hurley, Robert Caulk, Denis Caillerie, Takashi Matsushima, Pierre Bésuelle, Félix Bertoni, Tom Arnaud, Ortega Laborin Alejandro, Riccardo Rorato, Sun Yue, Alessandro Tengattini, Olumide Okubadejo, Georgios Birmpilis, Spam: software for practical analysis of materials, Journal of Open Source Software 5 (2020) 2286, https://doi.org/10.21105/joss.02286.
[515] P. Tan, Hasitha Sithadara Wijesuriya, Nicholas Sitar, XRCT image processing for sand fabric reconstruction, Granul. Matter 26 (2024) 15, https://doi.org/10.1007/s10035-023-01368-1.
[516] P. Zhang, Zhen-Yu Yin, Qiushi Chen, Image-based 3D reconstruction of granular grains via hybrid algorithm and level set with convolution kernel, J. Geotech. Geoenviron. Eng. 148 (2022) 5, https://doi.org/10.1061/(ASCE)GT.1943-5606.0002790.
[517] L. Zhuang, H.S. Shin, S. Yeom, et al., A novel method for estimating subresolution porosity from CT images and its application to homogeneity evaluation of porous media, Sci. Rep. 12 (2022) 16229, https://doi.org/10.1038/s41598-022-20086-x.
[518] X. Bao, H. Jia, C. Lang, Dragonfly algorithm with opposition-based learning for multilevel thresholding color image segmentation, Symmetry 11 (5) (2019) 716, https://doi.org/10.3390/sym11050716.
[519] R. Wieland, Chinatsu Ukawa, Monika Joschko, Adrian Krolczyk, Guido Fritsch, Thomas B. Hildebrandt, Olaf Schmidt, Juliane Filser, Juan J. Jimenez, Use of deep learning for structural analysis of computer tomography images of soil samples, R. Soc. Open Sci. 8 (3) (2021) 201275, https://doi.org/10.1098/rsos.201275.
[520] Höving Stefan, Maria Laura, Timo Neuendorf, Norbert Betting, Kockmann, Determination of particle size distributions of bulk samples using Micro-computed tomography and artificial intelligence, Materials 16 (3) (2023) 1002, https://doi.org/10.3390/ma16031002.
[521] H. Li, X. Yang, H. Zhai, Y. Liu, H. Bao, G. Zhang, Vox-Surf: Voxel-based implicit surface representation, IEEE Trans. Vis. Comput. Graph. 30 (3) (2024) 1743–1755. March 2024, https://doi.org/10.1109/TVCG.2022.3225844.
[522] J. Xi, Junxing Zheng, Gao Lin, Wang Dong, Jin Jiang, Shuangping Li, Jinsong Song, Hyperbolic regularization-PointNet++: automated three-dimensional soil particle roundness classification, Powder Technol. 434 (2024) 119326, https://doi.org/10.1016/j.powtec.2023.119326.
[523] Z.-Y. Zhang, Y.-F. Jin Yin, Three-dimensional quantitative analysis on granular particle shape using convolutional neural network, Num. Anal. Meth. Geomech. 46 (2022) 187–204.
[524] K.J. Dobson, S.B. Coban, S.A. McDonald, J.N. Walsh, R.C. Atwood, P.J. Withers, 4-D imaging of sub-second dynamics in pore-scale processes using real-time synchrotron X-ray tomography, Solid Earth 7 (2016) 1059–1073. 10.5194/se-7-1059-2016.
[525] T. Afshar, Mahdi M. Disfani, Guillermo A. Narsilio, Arul Arulrajah, Post-breakage changes in particle properties using synchrotron tomography, Powder Technol. 325 (2018) 530–544, https://doi.org/10.1016/j.powtec.2017.11.039.
[526] Y. Ouyang, Sheng Luo, Pengyuan Ren, Hongze Wang, Yi Wu, Fu Yanan, Haowei Wang, Synchrotron X-ray computed tomography analysis of the morphological characterization of aluminum alloy powders produced by gas atomization, Powder Technol. 429 (2023) 118904, https://doi.org/10.1016/j.powtec.2023.118904.
[527] C. Sivakumar, Jarvis A. Stobbs, Tu Kaiyang, Chithra Karunakaran, Jitendra Paliwal, Unravelling particle morphology and flour porosity of roller-milled green lentil flour using scanning electron microscopy and synchrotron X-ray micro-computed tomography, Powder Technol. 436 (2024) 119470, https://doi.org/10.1016/j.powtec.2024.119470.
[528] F. Xu, Klaus Mueller, Real-time 3D computed tomographic reconstruction using commodity graphics hardware, Phys. Med. Biol. 52 (2007) 3405, https://doi.org/10.1088/0031-9155/52/12/006.
[529] J.W. Buurlage, F. Marone, D.M. Pelt, et al., Real-time reconstruction and visualisation towards dynamic feedback control during time-resolved tomography experiments at TOMCAT, Sci. Rep. 9 (2019) 18379, https://doi.org/10.1038/s41598-019-54647-4.
[530] V.V. Nikitin, Real-time micro-CT reconstruction with zooming to features of interest (Conference Presentation), in: Proc. SPIE 12242, Developments in X-Ray Tomography XIV, 122420C (3 October 2022), 2022, https://doi.org/10.1117/12.2636637.
[531] A. Graas, S.B. Coban, K.J. Batenburg, et al., Just-in-time deep learning for real-time X-ray computed tomography, Sci. Rep. 13 (2023) 20070, https://doi.org/10.1038/s41598-023-46028-9.
[532] L.F. Gladden, Andrew J. Sederman, Recent advances in flow MRI, J. Magn. Reson. 229 (2013) 2–11, https://doi.org/10.1016/j.jmr.2012.11.022.
[533] R.T. Lewis, John Georg Seland, Characterization of pore geometry using correlations between magnetic field and internal gradient, Microporous Mesoporous Mater. 269 (2018) 31–34, https://doi.org/10.1016/j.micromeso.2017.05.041.
[534] R. Oliveira, Branko Bijeljic, Martin J. Blunt, Adam Colbourne, Andrew J. Sederman, Mick D. Mantle, Lynn F. Gladden, A continuous time random walk method to predict dissolution in porous media based on validation of experimental NMR data, Adv. Water Resour. 149 (2021) 103847, https://doi.org/10.1016/j.advwatres.2021.103847.
[535] N. Romijn, Y.E.I. Bergmans, V. de Haas, M.W. Hoogendoorn, M. Miloshevska, W. Baltussen, K.A. Buist, E.A.J.F. Peters, J.A.M. Kuipers, Reconstruction of particle positions and orientations from 3D MRI images of non-spherical particle packings, PARTICU 2023 (2023), https://doi.org/10.1016/j.partic.2023.10.003.
[536] M.A. Browne, O. Akinyemi, A. Boyde, Confocal surface profiling utilizing chromatic aberration, Scanning 14 (1992) 145–153, https://doi.org/10.1002/sca.4950140304.
[537] P. Neoptolemou, Thomas Vetter, Aurora J. Cruz-Cabeza, Ashwin Kumar Rajagopalan, Combined imaging and chromatic confocal microscopy technique to characterize size and shape of ensembles of cuboidal particles, Powder Technol. 430 (2023) 119032, https://doi.org/10.1016/j.powtec.2023.119032.
[538] M.R. Singh, J. Chakraborty, N. Nere, H.-H. Tung, S. Bordawekar, D. Ramkrishna, Image-analysis-based method for 3D crystal morphology measurement and polymorph identification using confocal microscopy, Cryst. Growth Des. 12 (2012) 3735–3748, https://doi.org/10.1021/cg300547w.
[539] D. Wertheim, Gavin Gillmore, Ian Gill, Nick Petford, High resolution 3D confocal microscope imaging of volcanic ash particles, Sci. Total Environ. 590–591 (2017) 838–842, https://doi.org/10.1016/j.scitotenv.2017.02.230.
[540] J. Zheng, Quan Sun, Hang Zheng, Deheng Wei, Zhaochao Li, Gao Lin, Three-dimensional particle shape characterizations from half particle geometries, Powder Technol. 367 (2020) 122–132, https://doi.org/10.1016/j.powtec.2020.03.046.

[541] B. Bujak, Michael Bottlinger, Three-dimensional measurement of particle shape, Part. Part. Syst. Charact. 25 (4) (2008) 293–297, https://doi.org/10.1002/ppsc.200800027.
[542] J.F. Ziegel, J.R. Nyengaard, E.B. Vedel Jensen, Estimating particle shape and orientation using volume tensors, Scand. J. Stat. 42 (2015) 813–831, https://doi.org/10.1111/sjos.12138.
[543] Y. Sung, Carl A. Anderson, Size and shape measurement of microscopic powder particles using digital holographic tomography and 2.5D reconstruction, Powder Technol. 436 (2024) 119496, https://doi.org/10.1016/j.powtec.2024.119496.
[544] E. Wolf, Three-dimensional structure determination of semi-transparent objects from holographic data, Opt. Commun. 1 (4) (1969) 153–156, https://doi.org/10.1016/0030-4018(69)90052-2.
[545] P. An, Huiming Tang, Changdong Li, Kun Fang, Sha Lu, Jiefei Zhang, A fast and practical method for determining particle size and shape by using smartphone photogrammetry, Measurement 193 (2022) 110943, https://doi.org/10.1016/j.measurement.2022.110943.
[546] K. Fang, Jiefei Zhang, Huiming Tang, Xiaolong Hu, Honghui Yuan, Xiaotao Wang, Pengju An, Bingdong Ding, A quick and low-cost smartphone photogrammetry method for obtaining 3D particle size and shape, Eng. Geol. 322 (2023) 107170, https://doi.org/10.1016/j.enggeo.2023.107170.
[547] R.A.A.R. Adnan, Mohd Ashraf Mohamad Ismail, Intan Norsheira Yusoff, Hayato Tobe, Takako Miyoshi, Kensuke Date, Yasuhiro Yokota, Preliminary assessment of joint roughness coefficient of rock slope using close-range photogrammetry technique, Phys. Chem. Earth Parts A/B/C 130 (2023) 103347, https://doi.org/10.1016/j.pce.2022.103347.
[548] P. An, Rui Yong, Jiamin Song, Du Shigui, Changshuo Wang, Hanhua Xu, Kun Fang, Shuochao Tong, Exploring the potential of smartphone photogrammetry for field measurement of joint roughness, Measurement 225 (2024) 114055, https://doi.org/10.1016/j.measurement.2023.114055.
[549] S. Zhang, X. Liu, H. Xie, et al., Learning geometric transformation for point cloud completion, Int. J. Comput. Vis. 131 (2023) 2425–2445, https://doi.org/10.1007/s11263-023-01820-y.
[550] Chuan-Yu Wu, Alan C.F. Cocks, Olivier T. Gillia, David A. Thompson, Experimental and numerical investigations of powder transfer, Powder Technol. 138 (2–3) (2003) 216–228, https://doi.org/10.1016/j.powtec.2003.09.011. ISSN 0032-5910.
[551] P.A. Cundall, O.D.L. Strack, A discrete numerical model for granular assemblies, Geotechnique 29 (1979) 47–65, https://doi.org/10.1680/geot.1979.29.1.47.
[552] M. Furuichi, D. Nishiura, M. Asai, T. Hori, The first real-scale DEM simulation of a sand-box experiment using 2.4 billion particles, in: The International Conference for High Performance Computing, Networking, Storage and Analysis, 2017.
[553] J. Xu, Huabiao Qi, Xiaojian Fang, Liqiang Lu, Wei Ge, Xiaowei Wang, Ming Xu, Feiguo Chen, Xianfeng He, Jinghai Li, Quasi-real-time simulation of rotating drum using discrete element method with parallel GPU computing, Particuology 9 (4) (2011) 446–450, https://doi.org/10.1016/j.partic.2011.01.003.
[554] R. Yasuda, T. Harada, Y. Kawaguchi, Real-time simulation of granular materials using graphics hardware, in: 2008 Fifth International Conference on Computer Graphics, Imaging and Visualisation, Penang, Malaysia, 2008, pp. 28–31, https://doi.org/10.1109/CGIV.2008.45.
[555] J. Ye, Jing-Xiong Chen, Xiao-Qing Chen, He-Ping Tao, Modeling and rendering of real-time large-scale granular flow scene on GPU, Procedia Environ. Sci. 10 (B) (2011) 1035–1045, https://doi.org/10.1016/j.proenv.2011.09.166.
[556] Y. Shigeto, Mikio Sakai, Parallel computing of discrete element method on multi-core processors, Particuology 9 (4) (2011) 398–405, https://doi.org/10.1016/j.partic.2011.04.002.
[557] J.Q. Gan, Z.Y. Zhou, A.B. Yu, A GPU-based DEM approach for modelling of particulate systems, Powder Technol. 301 (2016) 1172–1182, https://doi.org/10.1016/j.powtec.2016.07.072.
[558] N. Govender, Daniel N. Wilke, Schalk Kok, Blaze-DEMGPU: modular high performance DEM framework for the GPU architecture, SoftwareX 5 (2016) 62–66, https://doi.org/10.1016/j.softx.2016.04.004.
[559] L. Lu, GPU accelerated MFiX-DEM simulations of granular and multiphase flows, Particuology 62 (2022) 14–24, https://doi.org/10.1016/j.partic.2021.08.001.
[560] E.L. Chan, Kimiaki Washino, Coarse grain model for DEM simulation of dense and dynamic particle flow with liquid bridge forces, Chem. Eng. Res. Des. 132 (2018) 1060–1069, https://doi.org/10.1016/j.cherd.2017.12.033.
[561] H. Che, Dominik Werner, Jonathan Seville, Tzany Kokalova Wheldon, Kit Windows-Yule, Evaluation of coarse-grained CFD-DEM models with the validation of PEPT measurements, Particuology 82 (2023) 48–63, https://doi.org/10.1016/j.partic.2022.12.018.
[562] Y. Mori, Chuan-Yu Wu, Mikio Sakai, Validation study on a scaling law model of the DEM in industrial gas-solid flows, Powder Technol. 343 (2019) 101–112, https://doi.org/10.1016/j.powtec.2018.11.015.
[563] D.S. Nasato, Rodrigo Queiroz Albuquerque, Heiko Briesen, Predicting the behavior of granules of complex shapes using coarse-grained particles and artificial neural networks, Powder Technol. 383 (2021) 328–335, https://doi.org/10.1016/j.powtec.2021.01.029.
[564] J. Pachón-Morales, Patrick Perré, Joel Casalinho, Huy Do, Dingena Schott, François Puel, Julien Colin, Potential of DEM for investigation of non-consolidated flow of cohesive and elongated biomass particles, Adv. Powder Technol. 31 (4) (2020) 1500–1515, https://doi.org/10.1016/j.apt.2020.01.023.
[565] P.M. Widartiningsih, Yuki Mori, Kazuya Takabatake, Chuan-Yu Wu, Kensuke Yokoi, Akira Yamaguchi, Mikio Sakai, Coarse graining DEM simulations of a powder die-filling system, Powder Technol. 371 (2020) 83–95, https://doi.org/10.1016/j.powtec.2020.05.063.
[566] K. Chu, Jiang Chen, Aibing Yu, Applicability of a coarse-grained CFD–DEM model on dense medium cyclone, Miner. Eng. 90 (2016) 43–54, https://doi.org/10.1016/j.mineng.2016.01.020.
[567] Y. Kosaku, Yuki Tsunazawa, Chiharu Tokoro, Investigating the upper limit for applying the coarse grain model in a discrete element method examining mixing processes in a rolling drum, Adv. Powder Technol. 32 (11) (2021) 3980–3989, https://doi.org/10.1016/j.apt.2021.08.039.
[568] F. Müller, R. Polke, M. Schäfer, N. Scholz, Particle system characterization and modelling, Part. Part. Syst. Charact. 18 (2001) 248–253, https://doi.org/10.1002/1521-4117(200112)18:5/6<248::AID-PPSC248>3.0.CO;2-L.
[569] S.C. Thakur, Jin Y. Ooi, Hossein Ahmadian, Scaling of discrete element model parameters for cohesionless and cohesive solid, Powder Technol. 293 (2016) 130–137, https://doi.org/10.1016/j.powtec.2015.05.051.
[570] T. Weinhart, Carlos Labra, Stefan Luding, Jin Y. Ooi, Influence of coarse-graining parameters on the analysis of DEM simulations of silo flow, Powder Technol. 293 (2016) 138–148, https://doi.org/10.1016/j.powtec.2015.11.052.
[571] H. Haiyang Zeng, Wei Xu, Mengyan Zang, Peng Yang, Xiaobing Guo, Calibration and validation of DEM-FEM model parameters using upscaled particles based on physical experiments and simulations, Adv. Powder Technol. 31 (9) (2020) 3947–3959, https://doi.org/10.1016/j.apt.2020.06.044.
[572] R. Cabiscol, Jan Henrik Finke, Arno Kwade, Calibration and interpretation of DEM parameters for simulations of cylindrical tablets with multi-sphere approach, Powder Technol. 327 (2018) 232–245, https://doi.org/10.1016/j.powtec.2017.12.041.
[573] R. Caulkin, W. Tian, M. Pasha, A. Hassanpour, X. Jia, Impact of shape representation schemes used in discrete element modelling of particle packing, Comput. Chem. Eng. (2015) 76, https://doi.org/10.1016/j.compchemeng.2015.02.015.
[574] Y.T. Feng, Thirty years of developments in contact modelling of non-spherical particles in DEM: a selective review, Acta Mech. Sinica 39 (2023) 1, https://doi.org/10.1007/s10409-022-22343-x.
[575] A. Khazeni, Zahra Mansourpour, Influence of non-spherical shape approximation on DEM simulation accuracy by multi-sphere method, Powder Technol. 332 (2018) 265–278, https://doi.org/10.1016/j.powtec.2018.03.030.
[576] J.E. Lane, T. Metzger Philip, R. Allen Wilkinson, A Review of Discrete Element Method (DEM) Particle Shapes and Size Distributions for Lunar Soil. NASA/TM—2010–216257. https://ntrs.nasa.gov/api/citations/20110004246/downloads/20110004246.pdf, 2010.
[577] J.R. Lu, C.R. Müller Third, Discrete element models for non-spherical particle systems: from theoretical developments to applications, Chem. Eng. Sci. 127 (2015) 425–465, https://doi.org/10.1016/j.ces.2014.11.050.
[578] O.C. Scheffler, Corné Coetzee, DEM calibration for simulating bulk cohesive materials, Comput. Geotech. 161 (2023) 105476, https://doi.org/10.1016/j.compgeo.2023.105476.
[579] B. Soltanbeigi, A. Podlozhnyuk, C. Kloss, et al., Influence of various DEM shape representation methods on packing and shearing of granular assemblies, Granul. Matter 23 (2021) 26, https://doi.org/10.1007/s10035-020-01078-y.
[580] M. Tolomeo, Glenn R. McDowell, Modelling real particle shape in DEM: a comparison of two methods with application to railway ballast, Int. J. Rock Mech. Min. Sci. 159 (2022) 105221, https://doi.org/10.1016/j.ijrmms.2022.105221.
[581] W. Hong, Bihui Wang, Jianxiang Zheng, Numerical study on the influence of fine particle deposition characteristics on wall roughness, Powder Technol. 360 (2020) 120–128, https://doi.org/10.1016/j.powtec.2019.09.079.
[582] D. Liu, X. Liu, X. Fu, LES-DEM simulations of sediment saltation in a rough-wall turbulent boundary layer, J. Hydraul. Res. 57 (6) (2019) 786–797, https://doi.org/10.1080/00221686.2018.1509384.
[583] B. Mikulich, M. Nassauer, C. Brücker Kuna, Experimental and numerical study of interaction between particle loaded fluid and a rough wall with micropillars, Tribol. Int. 83 (2015) 42–50, https://doi.org/10.1016/j.triboint.2014.10.009.
[584] M. Fan, Su Dong, Xiangsheng Chen, Framework for incorporating multi-level morphology of particles in DEM simulations: independent control of polydisperse distributions of roundness and roughness while preserving form distributions in granular materials, Acta Geotech. (2024), https://doi.org/10.1007/s11440-023-02177-9.
[585] J.-Y. Nie, Yifei Cui, Guodong Wang, Rui Wang, Ningning Zhang, Lei Zhang, Zhijun Wu, A comprehensive numerical investigation of multi-scale particle shape effects on small-strain stiffness of sands, Géotechnique (2024) 1–14, https://doi.org/10.1680/jgeot.23.00118.
[586] N. Zhang, M. Arroyo, M. Ciantia, A. Gens, Incorporating surface roughness into DEM models of crushable soils, in: D. Billaux, J. Hazzard, M. Nelson, M. Schöpfer (Eds.), Proceedings of the 5th Itasca Symposium on Applied Numerical Modeling - 2020 [13-07], Itasca International, 2020.
[587] J. Gan, Zongyan Zhou, Aibing Yu, Particle scale study of heat transfer in packed and fluidized beds of ellipsoidal particles, Chem. Eng. Sci. 144 (2016) 201–215, https://doi.org/10.1016/j.ces.2016.01.041.
[588] Z. Peng, Elham Doroodchi, Behdad Moghtaderi, Heat transfer modelling in discrete element method (DEM)-based simulations of thermal processes: theory and model development, Prog. Energy Combust. Sci. 79 (2020) 100847, https://doi.org/10.1016/j.pecs.2020.100847.
[589] H. Ma, X. Xia, L. Zhou, C. Xu, Z. Liu, T. Song, G. Zou, Y. Liu, Z. Huang, X. Liao, et al., A comparative study of the performance of different particle models in simulating particle charging and burden distribution in a blast furnace within the DEM framework, Energies 16 (9) (2023) 3890, https://doi.org/10.3390/en16093890.
[590] C. Pei, Chuan-Yu Wu, Michael Adams, David England, Stephen Byard, Harald Berchtold, Contact electrification and charge distribution on elongated

particles in a vibrating container, Chem. Eng. Sci. 125 (2015) 238–247, https://doi.org/10.1016/j.ces.2014.03.014.
[591] E. Šupuk, Ali Hassanpour, Hossein Ahmadian, Mojtaba Ghadiri, Tatsushi Matsuyama, Tribo-electrification and associated segregation of pharmaceutical bulk powders, KONA Powder Part. J. 29 (2011) 208–223, https://doi.org/10.14356/kona.2011022.
[592] M. Dosta, D. Andre, V. Angelidakis, R.A. Caulk, M.A. Celigueta, B. Chareyre, J.-F. Dietiker, J. Girardot, N. Govender, C. Hubert, R. Kobyłka, A.F. Moura, V. Skorych, D.K. Weatherley, T. Weinhart, Comparing open-source DEM frameworks for simulations of common bulk processes, Comput. Phys. Commun. 296 (2024) 109066, https://doi.org/10.1016/j.cpc.2023.109066.
[593] John Steuben, Athanasios Iliopoulos, John Michopoulos, Recent Developments of the Multiphysics Discrete Element Method for Additive Manufacturing Modeling and Simulation, 2017, https://doi.org/10.1115/DETC2017-67597.
[594] H.P. Zhu, Z.Y. Zhou, R.Y. Yang, A.B. Yu, Discrete particle simulation of particulate systems: theoretical developments, Chem. Eng. Sci. 62 (13) (2007) 3378–3396, https://doi.org/10.1016/j.ces.2006.12.089.
[595] H. Ma, Lei Xu, Yongzhi Zhao, CFD-DEM simulation of fluidization of rod-like particles in a fluidized bed, Powder Technol. 314 (2017) 355–366, https://doi.org/10.1016/j.powtec.2016.12.008.
[596] W. Zhong, Aibing Yu, Xuejiao Liu, Zhenbo Tong, Hao Zhang, DEM/CFD-DEM modelling of non-spherical particulate Systems: theoretical developments and applications, Powder Technol. 302 (2016) 108–152, https://doi.org/10.1016/j.powtec.2016.07.010.
[597] A. Atxutegi, P. Kieckhefen, S. Pietsch, R. Aguado, M. Olazar, S. Heinrich, Unresolved CFD-DEM simulation of spherical and ellipsoidal particles in conical and prismatic spouted beds, Powder Technol 389 (2021) 493–506, https://doi.org/10.1016/j.powtec.2021.05.012.
[598] Fei Jiang, Haihu Liu, Xian Chen, Takeshi Tsuji, A coupled LBM-DEM method for simulating the multiphase fluid-solid interaction problem, J. Comput. Phys. 454 (2022) 110963, https://doi.org/10.1016/j.jcp.2022.110963.
[599] L.-C. Qiu, A coupling model of DEM and LBM for fluid flow through porous media, Procedia Eng. 102 (2015) 1520–1525, https://doi.org/10.1016/j.proeng.2015.01.286.
[600] G.C. Yang, L. Jing, C.Y. Kwok, Y.D. Sobral, A comprehensive parametric study of LBM-DEM for immersed granular flows, Comput. Geotech. 114 (2019) 103100, https://doi.org/10.1016/j.compgeo.2019.103100.
[601] Q.J. Zheng, R.Y. Yang, Q.H. Zeng, H.P. Zhu, K.J. Dong, A.B. Yu, Interparticle forces and their effects in particulate systems, Powder Technol. 436 (2024) 119445, https://doi.org/10.1016/j.powtec.2024.119445.
[602] K. Cui, Wei Ci, Shangchuan Yang, Dem Simulations of Particle Dissolution Effects on the Passive Earth Pressure of Retaining Walls, 2024, https://doi.org/10.2139/ssrn.4704798.
[603] James A. Kimber, Sergei G. Kazarian, František Štěpánek, Modelling of pharmaceutical tablet swelling and dissolution using discrete element method, Chem. Eng. Sci. 69 (1) (2012) 394–403, https://doi.org/10.1016/j.ces.2011.10.066.
[604] P. Sadrish, Soltanpour Yasser, Bo Hu Liang, Multi-scale modeling of enhanced dissolution and deformation of Geomaterials: A discrete element approach, in: Proceedings in Soil Behavior and Geomechanics, Geo-Shanghai 2014, Shanghai, China, May 26-28, 2014, 2014, https://doi.org/10.1061/9780784413388.052.
[605] C.D. Cho, D.C. Sego Martin, A clumped particle model for rock, Int. J. Rock Mech. Min. Sci. 44 (7) (2007) 997–1010.
[606] J.F. Ferellec, G.R. McDowell, A method to model realistic particle shape and inertia in DEM, Granul. Matter 12 (2010) 459–467, https://doi.org/10.1007/s10035-010-0205-8.
[607] R. Fu, Xinli Hu, Bo Zhou, Discrete element modeling of crushable sands considering realistic particle shape effect, Comput. Geotech. 91 (2017) 179–191, https://doi.org/10.1016/j.compgeo.2017.07.016.
[608] John de Bono, Glenn McDowell, Simulating multifaceted interactions between kaolinite platelets, Powder Technol. 413 (2023) 118062, https://doi.org/10.1016/j.powtec.2022.118062.
[609] J. Li, Yanli Huang, Wei Li, Hong Yu, Shenyang Ouyang, Yachao Guo, Huadong Gao, Yibing Shi, Lei Zhu, The 3D reconstruction of a digital model for irregular gangue blocks and its application in PFC numerical simulation, Eng. Comput. 38 (2021), https://doi.org/10.1007/s00366-021-01500-w.
[610] M.R. Tamadondar, L. de Martín, A. Rasmuson, Agglomerate breakage and adhesion upon impact with complex-shaped particles, AICHE J. 65 (2019) e16581, https://doi.org/10.1002/aic.16581.
[611] M.R. Tamadondar, A. Rasmuson, The effect of carrier surface roughness on wall collision-induced detachment of micronized pharmaceutical particles, AICHE J. 66 (2020) e16771, https://doi.org/10.1002/aic.16771.
[612] Y. Xu, Wenying Yu, Luchao Qie, Hong Wang, Na Ning, Analysis of influence of ballast shape on abrasion resistance using discrete element method, Constr. Build. Mater. 273 (2021) 121708, https://doi.org/10.1016/j.conbuildmat.2020.121708.
[613] Z. Bibak, S. Banisi, A combined physical and DEM modelling approach to investigate particle shape effects on load movement in tumbling mills, Adv. Powder Technol. 32 (3) (2021) 916–930, https://doi.org/10.1016/j.apt.2021.01.034.
[614] J.C. Lopera Perez, C.Y. Kwok, K. Senetakis, Effect of rubber size on the behaviour of sand-rubber mixtures: A numerical investigation, Comput. Geotech. 80 (2016) 199–214, https://doi.org/10.1016/j.compgeo.2016.07.005.
[615] J. Zhang, Xiaobin Chen, Jiasheng Zhang, Peerapong Jitsangiam, Xiang Wang, DEM investigation of macro- and micro-mechanical properties of rigid-grain and soft-chip mixtures, Particuology 55 (2020) 128–139, https://doi.org/10.1016/j.partic.2020.06.002.
[616] Y. Guo, Jiawei Han, Discrete Element Modelling of Flexible and Shape Memory Fibres. DEM9, 2023, p. 129. https://www.dem9.fau.de/.
[617] D. Peng, LiGe Wang, Yuquan Lin, Chongqiang Zhu, Xizhong Chen, Zhihui Liu, Ruihuan Ge, Oblique impact breakage unification of nonspherical particles using discrete element method, Particuology 90 (2024) 61–71, https://doi.org/10.1016/j.partic.2023.11.012.
[618] P. Grohn, D. Weis, U. Bröckel, S. Heinrich, S. Antonyuk, Contact models and DEM simulation of micrometer-sized particles and agglomerates at static loading based on experimental characterization, in: S. Antonyuk (Ed.), Particles in Contact, Springer, Cham, 2019, https://doi.org/10.1007/978-3-030-15899-6_5.
[619] S.W. Höhner, H. Kruggel-Emden, V. Scherer, Comparison of the multi-sphere and polyhedral approach to simulate non-spherical particles within the discrete elementmethod: influence on temporal force evolution for multiple contacts, Powder Technol. 208 (2011) 643–656.
[620] S.W. Höhner, V. Scherer, A study on the influence of particle shape and shape approximation on particle mechanics in a rotating drum using the discrete element method, Powder Technol. 253 (2014) 256–265.
[621] H. Kruggel-Emden, S. Rickelt, V. Scherer Wirtz, A study on the validity of the multi-sphere discrete element method, Powder Technol. 188 (2008) 153–165.
[622] R. Markauskas, A. Kačianauskas, R. Navakas Džiugys, Investigation of adequacy of multi-sphere approximation of elliptical particles for DEM simulations, Granul. Matter 12 (2009) 107–123.
[623] Y. You, Y. Zhao, Discrete element modelling of ellipsoidal particles using superellipsoids and multi-spheres: a comparative study, Powder Technol. 331 (2018) 179–191.
[624] L. Benvenuti, C. Kloss, S. Pirker, Identification of DEM simulation parameters by artificial neural networks and bulk experiments, Powder Technol. 291 (2016) 456–465, https://doi.org/10.1016/j.powtec.2016.01.003.
[625] C.J. Coetzee, Calibration of the discrete element method and the effect of particle shape, Powder Technol. 297 (2016) 50–70, https://doi.org/10.1016/j.powtec.2016.04.003.
[626] C.J. Coetzee, Review: calibration of the discrete element method, Powder Technol. 310 (2017) 104–142, https://doi.org/10.1016/j.powtec.2017.01.015.
[627] Huy Q. Do, Alejandro M. Aragón, Dingena L. Schott, A calibration framework for discrete element model parameters using genetic algorithms, Adv. Powder Technol. 29 (6) (2018) 1393–1403, https://doi.org/10.1016/j.apt.2018.03.001. ISSN 0921-8831.
[628] Luca Orefice, Johannes G. Khinast, A novel framework for a rational, fully-automatised calibration routine for DEM models of cohesive powders, Powder Technol. 361 (2020) 687–703, https://doi.org/10.1016/j.powtec.2019.11.054. ISSN 0032-5910.
[629] T. Falke, K.M. de Payrebrune, S. Kirchhof, L. Kühnel, R. Kühnel, T. Mütze, M. Kröger, An alternative DEM parameter identification procedure based on experimental investigation: a case study of a ring shear cell, Powder Technol. 328 (2018) 227–234, https://doi.org/10.1016/j.powtec.2017.12.072.
[630] H. Zhou, Zhanqi Hu, Jigang Chen, Xuan Lv, Nan Xie, Calibration of DEM models for irregular particles based on experimental design method and bulk experiments, Powder Technol. 332 (2018) 210–223, https://doi.org/10.1016/j.powtec.2018.03.064.
[631] S. Kirsch, Avoiding ambiguity in DEM in-situ calibration for dry bulk materials, Miner. Eng. 145 (2020) 106094, https://doi.org/10.1016/j.mineng.2019.106094.
[632] J.R. Williams, A.P. Pentland, Superquadrics and modal dynamics for discrete elements in interactive design, Eng. Comput. 9 (1992) 115–127, https://doi.org/10.1108/eb023852.
[633] P.W. Cleary, N. Stokes, J. Hurley, "Efficient collision detection for three dimensional super-ellipsoidal particles", Proceedings of8th International Computational Techniques and Applications Conference CTAC97, Adelaide. pp. 1–7. http://citeseerx.ist.psu.edu/viewdoc/download?.
[634] P.W. Cleary, Large scale industrial DEM modelling, Eng. Comput. 21 (2004) 169–204.
[635] A.H. Barr, Superquadrics and angle-preserving transformations, IEEE Comput. Graph. Appl. 1 (1981) 11–23.
[636] J. Kozicki, Frederic Victor Donze, YADE-OPEN DEM: An opensource software using a discrete element method to simulate granular material, Eng. Comput. 26 (7) (2008) 786–805, https://doi.org/10.1108/02644400910985170.
[637] S. Zhao, Jidong Zhao, SudoDEM: unleashing the predictive power of the discrete element method on simulation for non-spherical granular particles, Comput. Phys. Commun. 259 (2021) 107670, https://doi.org/10.1016/j.cpc.2020.107670.
[638] S. Wang, Shunying Ji, Computational Mechanics of Arbitrarily Shaped Granular Materials, Springer, Singapore, 2024, https://doi.org/10.1007/978-981-99-9927-9.
[639] H. Chen, Shiwei Zhao, Xiaowen Zhou, DEM investigation of angle of repose for super-ellipsoidal particles, Particuology 50 (2020) 53–66, https://doi.org/10.1016/j.partic.2019.05.005.
[640] P. Datta, Salah A. Faroughi, Angle of repose for superquadric particles: investigating the effects of shape parameters, Comput. Geotech. 165 (2024) 105918, https://doi.org/10.1016/j.compgeo.2023.105918.
[641] X. Wang, Z.Y. Yin, H. Xiong, D. Su, Y.T. Feng, A spherical-harmonic-based approach to discrete element modeling of 3D irregular particles, Int. J. Numer. Methods Eng. 122 (20) (2021) 5626–5655, https://doi.org/10.1002/nme.6766.

[642] R. Capozza, K.J. Hanley, A hierarchical, spherical harmonic-based approach to simulate abradable, irregularly shaped particles in DEM, Powder Technol. 378 (2021) 528–537, https://doi.org/10.1016/j.powtec.2020.10.015.
[643] S. Wang, Zhijun Wei, Shunying Ji, Investigation of the flow characteristics of spherical harmonic particles using the level set method, Powder Technol. 413 (2023) 118069, https://doi.org/10.1016/j.powtec.2022.118069.
[644] J. Gao, Tu Fubin, Chengbao Hu, Daosheng Ling, Zhijiao Zeng, Rockfall simulation via spherical harmonic based discrete element method, Comput. Geosci. 186 (2024) 105573, https://doi.org/10.1016/j.cageo.2024.105573.
[645] Dingeman L.H. van der Haven, Ioannis S. Fragkopoulos, James A. Elliott, A physically consistent discrete element method for arbitrary shapes using volume-interacting level sets, Comput. Methods Appl. Mech. Eng. 414 (2023) 116165, https://doi.org/10.1016/j.cma.2023.116165.
[646] Y.T. Feng, An effective energy-conserving contact modelling strategy for spherical harmonic particles represented by surface triangular meshes with automatic simplification, Comput. Methods Appl. Mech. Eng. 379 (2021) 113750, https://doi.org/10.1016/j.cma.2021.113750.
[647] J. Gan, Aibing Yu, DEM study on the packing density and randomness for packing of ellipsoids, Powder Technol. 361 (2020) 424–434, https://doi.org/10.1016/j.powtec.2019.07.012.
[648] X. Gao, Jia Yu, Ricardo J.F. Portal, Jean-François Dietiker, Mehrdad Shahnam, William A. Rogers, Development and validation of SuperDEM for non-spherical particulate systems using a superquadric particle method, Particuology 61 (2022) 74–90, https://doi.org/10.1016/j.partic.2020.11.007.
[649] Z. Liu, Yongzhi Zhao, Multi-super-ellipsoid model for non-spherical particles in DEM simulation, Powder Technol. 361 (2020) 190–202, https://doi.org/10.1016/j.powtec.2019.09.042.
[650] G. Lu, J.R. Third, C.R. Müller, Critical assessment of two approaches for evaluating contacts between super-quadric shaped particles in DEM simulations, Chem. Eng. Sci. 78 (2012) 226–235, https://doi.org/10.1016/j.ces.2012.05.041. ISSN 0009-2509.
[651] C.E. Torrence, Zachary Grasley, William B. Lawrimore, Edward J. Garboczi, Using surface asperities for efficient random particle overlap detection in the generation of randomly oriented and located particle arrangements, Powder Technol. 399 (2022) 116979, https://doi.org/10.1016/j.powtec.2021.11.023.
[652] S. Wang, Qingwei Xu, Shunying Ji, A novel Minkowski sum contact algorithm for arbitrarily shaped particles constructed by multiple dilated DEM models, Int. J. Solids Struct. 280 (2023) 112409, https://doi.org/10.1016/j.ijsolstr.2023.112409.
[653] S. Wang, Yinuo Fan, Shunying Ji, Interaction between super-quadric particles and triangular elements andits application to hopper discharge, Powder Technol. 339 (2018) 534–549, https://doi.org/10.1016/j.powtec.2018.08.026.
[654] C. Zhao, Xinyu Cheng, Yixue Peng, Chengbo Li, Discrete element simulations of heart-shaped particle systems, Powder Technol. 375 (2020) 369–383, https://doi.org/10.1016/j.powtec.2020.07.108.
[655] Y. Zhao, Lei Xu, Paul B. Umbanhowar, Richard M. Lueptow, Discrete element simulation of cylindrical particles using super-ellipsoids, Particuology 46 (2019) 55–66, https://doi.org/10.1016/j.partic.2018.04.007.
[656] C. Coetzee, Otto Carl Scheffler, Comparing particle shape representations and contact models for DEM simulation of bulk cohesive behaviour, Comput. Geotech. 159 (2023) 105449, https://doi.org/10.1016/j.compgeo.2023.105449.
[657] Christian Wellmann, Claudia Lillie, Peter Wriggers, A contact detection algorithm for superellipsoids based on the common-normal concept, Eng. Comput. 25 (5) (2008) 432–442, https://doi.org/10.1108/02644400810881374.
[658] A. Podlozhnyuk, S. Pirker, C. Kloss, Efficient implementation of superquadric particles in Discrete Element Method within an open-source framework, Comp. Part. Mech. 4 (2017) 101–118, https://doi.org/10.1007/s40571-016-0131-6.
[659] L. Liu, Shunying Ji, Comparison of sphere-based and dilated-polyhedron-based discrete element methods for the analysis of ship–ice interactions in level ice, Ocean Eng. 244 (12) (2022) 110364, https://doi.org/10.1016/j.oceaneng.2021.110364.
[660] S. Alaniz, M. Mancini, Z. Akata, Iterative superquadric recomposition of 3D objects from multiple views, in: 2023 IEEE/CVF International Conference on Computer Vision (ICCV), Paris, France, 2023, pp. 17967–17977, https://doi.org/10.1109/ICCV51070.2023.01651.
[661] B. Soltanbeigi, Alexander Podlozhnyuk, Stefanos-Aldo Papanicolopulos, Christoph Kloss, Stefan Pirker, Jin Y. Ooi, DEM study of mechanical characteristics of multi-spherical and superquadric particles at micro and macro scales, Powder Technol. 329 (2018) 288–303, https://doi.org/10.1016/j.powtec.2018.01.082.
[662] C. Xu, X. Jia, R.A. Williams, E.H. Stitt, M. Nijemeisland, S. El-Bachir, L. F. Gladden, Property predictions for packed columns using Monte Carlo and discrete element digital packing algorithms, Comput. Model. Eng. Sci. 23 (2) (2008) 117–125.
[663] R. Caulkin, X. Jia, C. Xu, M. Fairweather, R.A. Williams, H. Stitt, M. Nijemeisland, S. Aferka, M. Crine, A. Léonard, D. Toye, P. Marchot, Simulations of structures in packed columns and validation by X-ray tomography, Ind. Eng. Chem. Res. 48 (1) (2009) 202–213, https://doi.org/10.1021/ie800033a.
[664] X. Zhang, Pejman Tahmasebi, Investigation of particle shape and ambient fluid on sandpiles using a coupled micro-geomechanical model, Powder Technol. 409 (2022) 117711, https://doi.org/10.1016/j.powtec.2022.117711.
[665] Ruaidhr'i M. O'Connor, John R. Torczynski, Dale S. Preece, Justin T. Klosek, John R. Williams, Discrete element modeling of sand production, Int. J. Rock Mech. Min. Sci. 34 (3–4) (1997) 231.e1–231.e15, https://doi.org/10.1016/S1365-1609(97)00198-6. ISSN 1365-1609.
[666] E.G. Nezami, Y.M. Hashash, D. Zhao, J. Ghaboussi, A fast contact detection algorithm for 3-D discrete element method, Comput. Geotech. 31 (7) (2004) 575–587.
[667] S. Amir Reza Beyabanaki, Roozbeh Geraili Mikola, Kianoosh Hatami, Three-dimensional discontinuous deformation analysis (3-D DDA) using a new contact resolution algorithm, Comput. Geotech. 35 (3) (2008) 346–356, https://doi.org/10.1016/j.compgeo.2007.08.006.
[668] A.G. Neto, Framework for automatic contact detection in a multibody system, Comput. Methods Appl. Mech. Eng. 403 (A) (2023) 115703, https://doi.org/10.1016/j.cma.2022.115703.
[669] B. Smeets, Tim Odenthal, Simon Vanmaercke, Herman Ramon, Polygon-based contact description for modeling arbitrary polyhedra in the discrete element method, Comput. Methods Appl. Mech. Eng. 290 (2015) 277–289, https://doi.org/10.1016/j.cma.2015.03.004.
[670] E. Illana, Klidi Qyteti, Maik Scharnowski, Maximilian Brommer, Siegmar Wirtz, Viktor Scherer, Shape-changing particles for locally resolved particle geometry in DEM simulations, Particuology 89 (2024) 185–190, https://doi.org/10.1016/j.partic.2023.11.003.
[671] S. Zhao, Jidong Zhao, Revolutionizing granular matter simulations by high-performance ray tracing discrete element method for arbitrarily-shaped particles, Comput. Methods Appl. Mech. Eng. 416 (2023) 116370, https://doi.org/10.1016/j.cma.2023.116370.
[672] J.E. Andrade, K.-W. Lim, C.F. Avila, I. Vlahini'c, Granular element method for computational particle mechanics, Comput. Methods Appl. Mech. Eng. 241 (2012) 262–274, https://doi.org/10.1016/j.cma.2012.06.012.
[673] K.-W. Lim, J.E. Andrade, Granular element method for three-dimensional discrete element calculations, Int. J. Numer. Anal. Methods Geomech. 38 (2014) 167–188, https://doi.org/10.1002/nag.2203.
[674] M.V. Craveiro, Alfredo Gay Neto, Peter Wriggers, Contact between rigid convex NURBS particles based on computer graphics concepts, Comput. Methods Appl. Mech. Eng. 386 (2021) 114097, https://doi.org/10.1016/j.cma.2021.114097.
[675] Shiwen Liu, Feiguo Chen, Wei Ge, Philippe Ricoux, NURBS-based DEM for non-spherical particles, Particuology 49 (2020) 65–76, https://doi.org/10.1016/j.partic.2019.04.005. ISSN 1674-2001.
[676] M.V. Craveiro, A. Gay Neto, P. Wriggers, DEM simulations using convex NURBS particles, Comp. Part. Mech. 11 (2024) 1087–1118, https://doi.org/10.1007/s40571-023-00675-x.
[677] R.D. Morrison, P.W. Cleary, Using DEM to model ore breakage within a pilot scale SAG mill, Miner. Eng. 17 (2004) 1117–1124, https://doi.org/10.1016/j.mineng.2004.06.016.
[678] Jens Lichter, King Lim, Alex Potapov, Dean Kaja, New developments in cone crusher performance optimization, Miner. Eng. 22 (7–8) (2009) 613–617, https://doi.org/10.1016/j.mineng.2009.04.003. ISSN 0892-6875.
[679] L.M. Tavares, F.P. André, A. Potapov, C. Maliska, Adapting a breakage model to discrete elements using polyhedral particles, Powder Technol. 362 (2020) 208–220, https://doi.org/10.1016/j.powtec.2019.12.007.
[680] A.V. Potapov, C.S. Campbell, Parametric dependence of particle breakage mechanisms, Powder Technol. 120 (2001) 164–174, https://doi.org/10.1016/S0032-5910(01)00272-8.
[681] M.A. Hosseini, Pejman Tahmasebi, A novel graph-based 3D breakage method for angular particles with an image-based DEM, Int. J. Rock Mech. Min. Sci. 174 (2024) 105640, https://doi.org/10.1016/j.ijrmms.2024.105640.
[682] R. Kawamoto, Edward Andò, Gioacchino Viggiani, José E. Andrade, Level set discrete element method for three-dimensional computations with triaxial case study, J. Mech. Phys. Solids 91 (2016) 1–13, https://doi.org/10.1016/j.jmps.2016.02.021.
[683] R. Reid Kawamoto, Edward Andò, Gioacchino Viggiani, José E. Andrade, All you need is shape: predicting shear banding in sand with LS-DEM, J. Mech. Phys. Solids 111 (2018) 375–392, https://doi.org/10.1016/j.jmps.2017.10.003.
[684] P. Tan, N. Sitar, Parallel level-set DEM (LS-DEM) development and application to the study of deformation and flow of granular media, PEER Report 2022/06, in: Pacific Earthquake Engineering Research Center, University of California, Berkeley, CA, 2022, https://doi.org/10.55461/KMIZ5819.
[685] S. Feldfogel, Konstantinos Karapiperis, Jose Andrade, David S. Kammer, A Discretization-convergent Level-set-discrete-element-method using a continuum-based contact formulation, Int. J. Numer. Methods Eng. November (2023) e7400, https://doi.org/10.1002/nme.7400.
[686] S. Wang, Dongfang Liang, Shunying Ji, DEM study on mixing behaviors of concave-shaped particles in rotating drum based on level-set method, Powder Technol. 430 (2023) 118961, https://doi.org/10.1016/j.powtec.2023.118961.
[687] Z. Zhou, Rigoberto Moncada, Nathan Jones, Jacinto Ulloa, Fu Xiaojing, José E. Andrade, Simplified level set discrete element modeling of particle suspension flows in microfluidics: clogging statistics controlled by particle friction and shape, Granul. Matter 26 (2024) 2, https://doi.org/10.1007/s10035-024-01405-7.
[688] Dingeman L.H. van der Haven, Ioannis S. Fragkopoulos, James A. Elliott, Volume-interacting level set discrete element method: the porosity and angle of repose of aspherical, angular, and concave particles, Powder Technol. 433 (2024) 119295, https://doi.org/10.1016/j.powtec.2023.119295.
[689] Y. Zhao, Pei Zhang, Lei Liang, Lingwei Kong, S.A. Galindo-Torres, Stan Z. Li, Metaball-imaging discrete element lattice Boltzmann method for fluid–particle system of complex morphologies with case studies, Phys. Fluids 35 (2023) 2, https://doi.org/10.1063/5.0135834.
[690] O.R. Walton, Application of molecular dynamics to macroscopic particles, Int. J. Eng. Sci. 22 (8–10) (1984) 1097–1107, https://doi.org/10.1016/0020-7225(84)90110-1.

[691] P. Thompson, H.M. Aktulga, R. Berger, D.S. Bolintineanu, W.M. Brown, P. S. Crozier, P.J. Int Veld, A. Kohlmeyer, S.G. Moore, T.D. Nguyen, R. Shan, M. J. Stevens, J. Tranchida, C. Trott, S.J. Plimpton, LAMMPS - A flexible simulation tool for particle-based materials modeling at the atomic, meso, and continuum scales, Comput. Phys. Commun. 271 (2022) 108171, https://doi.org/10.1016/j.cpc.2021.108171.
[692] D. Braile, Colin Hare, Chuan-Yu Wu, DEM analysis of swelling behaviour in granular media, Adv. Powder Technol. 33 (11) (2022) 103806, https://doi.org/10.1016/j.apt.2022.103806.
[693] D. Sulsky, Z. Chen, H.L. Schreyer, A particle method for history-dependent materials, Comput. Meths. Appl. Mech. Engrg. 118 (1994) 179–196.
[694] D. Sulsky, S.-J. Zhou, H.L. Schreyer, Application of a particle-in-cell method to solid mechanics, Comput. Phys. Commun. 87 (1995) 236–252.
[695] L. Beuth, T. Benz, P. Vermeer, Z. Wickowski, Large deformation analysis using a quasi-static material point method, J. Theor. Appl. Mech. 38 (2008) 45–60. http://hdl.handle.net/11652/869.
[696] Y. Jiang, Tao Yang, Jian Chang, Solid deformation by material point method, Commun. Inf. Syst. 16 (2016) 127–146, https://doi.org/10.4310/CIS.2016.v16.n3.a1.
[697] X. Zhang, Zhen Chen, Yan Liu, The Material Point Method: A Continuum-Based Particle Method for Extreme Loading Cases, Academic Press, 2017. ISBN 978-0-12-407716-4.
[698] W.T. Sołowski, Martin Berzins, William M. Coombs, James E. Guilkey, Matthias Möller, Quoc Anh Tran, Tito Adibaskoro, Seyedmohammadjavad Seyedan, Roel Tielen, Kenichi Soga, Chapter Two - Material point method: Overview and challenges ahead, in: Stéphane P.A. Bordas, Daniel S. Balint (Eds.), Advances in Applied Mechanics 54, Elsevier, 2021, pp. 113–204. ISBN 9780323885195, https://doi.org/10.1016/bs.aams.2020.12.002.
[699] S. Nezamabadi, M. Ghadiri, J.Y. Delenne, et al., Modelling the compaction of plastic particle packings, Comput. Part. Mech. 9 (2022) 45–52, https://doi.org/10.1007/s40571-021-00391-4.
[700] V.P. Nguyen, Alban de Vaucorbeil, Stephane Bordas, The Material Point Method: Theory, Implementations and Applications, Springer, Cham, 2023, https://doi.org/10.1007/978-3-031-24070-6. ISBN 978-3-031-24069-0.
[701] M. Dorduncu, Huilong Ren, Xiaoying Zhuang, Stewart Silling, Erdogan Madenci, Timon Rabczuk, A review of peridynamic theory and nonlocal operators along with their computer implementations, Comput. Struct. 299 (2024) 107395, https://doi.org/10.1016/j.compstruc.2024.107395.
[702] E. Madenci, Erkan Oterkus, Peridynamic Theory and its Applications, Springer, New York, NY, 2014, https://doi.org/10.1007/978-1-4614-8465-3. ISBN 978-1-4614-8464-6.
[703] E. Oterkus, Selda Oterkus, Erdogan Madenci, Peridynamic Modeling, Numerical Techniques, and Applications, Elsevier, 2021. ISBN 0128204419.
[704] S.A. Silling, Reformulation of elasticity theory for discontinuities and long-range forces, J. Mech. Phys. Solids 48 (1) (2000) 175–209, https://doi.org/10.1016/S0022-5096(99)00029-0.
[705] S.A. Silling, M. Epton, O. Weckner, et al., Peridynamic states and constitutive modeling, J. Elast. 88 (2007) 151–184, https://doi.org/10.1007/s10659-007-9125-1.
[706] C. Willberg, Jan-Timo Hesse, Anna Pernatii, PeriLab — Peridynamic laboratory, SoftwareX 26 (2024) 101700, https://doi.org/10.1016/j.softx.2024.101700.
[707] F. Zhu, Jidong Zhao, Interplays between particle shape and particle breakage in confined continuous crushing of granular media, Powder Technol. 378 (A) (2021) 455–467, https://doi.org/10.1016/j.powtec.2020.10.020.
[708] H. Bagherzadeh, O.R. Barani, Coupling the material point method and Peridynamics via the force partitioning and concurrent coupling schemes, Comput. Part. Mech. 11 (2024) 55–71, https://doi.org/10.1007/s40571-023-00608-8.
[709] Y. Lyu, J. Zhang, A. Sarafopoulos, J. Chang, S. Guo, J.J. Zhang, Integral-based material point method and peridynamics model for animating elastoplastic material, in: M. Gavrilova, C. Tan, J. Chang, N. Thalmann (Eds.), Transactions on Computational Science XXXVII. Lecture Notes in Computer Science vol 12230, Springer, Berlin, Heidelberg, 2020, https://doi.org/10.1007/978-3-662-61983-4_6.
[710] Z. Zeng, Heng Zhang, Xiong Zhang, Yan Liu, Zhen Chen, An adaptive peridynamics material point method for dynamic fracture problem, Comput. Methods Appl. Mech. Eng. 393 (2022) 114786, https://doi.org/10.1016/j.cma.2022.114786.
[711] S. Saifoori, S. Nezamabadi, M. Ghadiri, Analysis of impact deformation of elastic-perfectly plastic particles, Comput. Part. Mech. (2024), https://doi.org/10.1007/s40571-024-00742-x.
[712] J. Li, Bin Wang, Di Wang, Pei Zhang, Philip J. Vardon, A coupled MPM-DEM method for modelling soil-rock mixtures, Comput. Geotech. 160 (2023) 105508, https://doi.org/10.1016/j.compgeo.2023.105508.
[713] L. Liu, Zhiyuan Yu, Weiwei Jin, Ye Yuan, Shuixiang Li, Uniform and decoupled shape effects on the maximally dense random packings of hard superellipsoids, Powder Technol. 338 (2018) 67–78, https://doi.org/10.1016/j.powtec.2018.06.033.
[714] Z. Qian, A novel coupling algorithm for MPM-DEM, in: DEM9 Abstract Book, 2023, p. 52. https://www.dem9.fau.de/.
[715] V. Singer, K.B. Sautter, A. Larese, et al., A partitioned material point method and discrete element method coupling scheme, Adv. Model. Simul. Eng. Sci. 9 (16) (2022), https://doi.org/10.1186/s40323-022-00229-5.
[716] P.K. Jha, Prathamesh S. Desai, Debdeep Bhattacharya, Robert Lipton, Peridynamics-based discrete element method (PeriDEM) model of granular systems involving breakage of arbitrarily shaped particles, J. Mech. Phys. Solids 151 (2021) 104376, https://doi.org/10.1016/j.jmps.2021.104376.
[717] H.G. Matuttis, S. Luding, H.J. Herrmann, Discrete element simulations of dense packings and heaps made of spherical and non-spherical particles, Powder Technol. 109 (1–3) (2000) 278–292, https://doi.org/10.1016/S0032-5910(99)00243-0.
[718] W.L. Lim, G.R. McDowell, Discrete element modelling of railway ballast, Granul. Matter 7 (1) (2005) 19–29, https://doi.org/10.1007/s10035-004-0189-3.
[719] F.Y. Fraige, P.A. Langston, G.Z. Chen, Distinct element modelling of cubic particle packing and flow, Powder Technol. 186 (3) (2008) 224–240, https://doi.org/10.1016/j.powtec.2007.12.009.
[720] H. Tangri, Y. Guo, J.S. Curtis, Packing of cylindrical particles: DEM simulations and experimental measurements, Powder Technol. 317 (2017) 72–82.
[721] S. Zhao, Nan Zhang, Xiaowen Zhou, Lei Zhang, Particle shape effects on fabric of granular random packing, Powder Technol. 310 (2017) 175–186, https://doi.org/10.1016/j.powtec.2016.12.094.
[722] Y. Wu, X. An, A. Yu, Dem simulation of cubical particle packing under mechanical vibration, Powder Technol. 314 (2017) 89–101.
[723] A.D. Rakotonirina, J.Y. Delenne, F. Radjai, A. Wachs, Grains3D, a flexible DEM approach for particles of arbitrary convex shape-part iii: extension to non-convex particles modelled as glued convex particles, Comput. Part. Mech. 6 (1) (2019) 55–84.
[724] J. Nam, J. Lyu, J. Park, Particle generation to minimize the computing time of the discrete element method for particle packing simulation, J. Mech. Sci. Technol. 36 (2022) 3561–3571, https://doi.org/10.1007/s12206-022-0632-6.
[725] X. Jia, R.A. Williams, A packing algorithm for particles of arbitrary shapes, Powder Technol. 120 (3) (2001) 175–186, https://doi.org/10.1016/S0032-5910(01)00268-6.
[726] S. Remond, J.L. Gallias, A 3D semi-digital model for the placing of granular materials, Powder Technol. 148 (1) (2004) 56–59, https://doi.org/10.1016/j.powtec.2004.04.045.
[727] T. Byholm, M. Toivakka, J. Westerholm, Effective packing of 3-dimensional voxel-based arbitrarily shaped particles, Powder Technol. 196 (2009) 139–146, https://doi.org/10.1016/j.powtec.2009.07.013.
[728] S. Rémond, J.L. Gallias, A. Mizrahi, Simulation of the packing of granular mixtures of non-convex particles and voids characterization, Granul. Matter 10 (2008) 157–170, https://doi.org/10.1007/s10035-007-0082-y.
[729] Z. Tian, Y. Tian, H. Ye, et al., VOX model: application of voxel-based packing algorithm on cementitious composites with 3D irregular-shape particles, Mater. Struct. 53 (2020) 75, https://doi.org/10.1617/s11527-020-01512-w.
[730] G.T. Nolan, P.E. Kavanagh, Random packing of nonspherical particles, Powder Technol. 84 (3) (1995) 199–205, https://doi.org/10.1016/0032-5910(95)98237-S.
[731] Y. Lee, C.T. Yang, C.S. Chien, A 3D ellipsoid-based model for packing of granular particles, International journal of computer applications in technology 17 (3) (2003) 148–155.
[732] C.R.A. Abreu, F.W. Tavares, M. Castier, Influence of particle shape on the packing and on the segregation of spherocylinders via Monte Carlo simulations, Powder Technol. 134 (1–2) (2003) 167–180, https://doi.org/10.1016/S0032-5910(03)00151-7.
[733] Y. Lee, C. Fang, Y.-R. Tsou, L.-S. Lu, C.-T. Yang, A packing algorithm for three-dimensional convex particles, Granul. Matter 11 (5) (2009) 307–315, https://doi.org/10.1007/s10035-009-0133-7.
[734] I. Pérez Morales, R. Roselló Valera, C. Recarey Morfa, et al., Dense packing of general-shaped particles using a minimization technique, Comput. Part. Mech. 4 (2017) 165–179, https://doi.org/10.1007/s40571-016-0103-x.
[735] M. Salemi, Hao Wang, Image-aided random aggregate packing for computational modeling of asphalt concrete microstructure, Constr. Build. Mater. 177 (2018) 467–476, https://doi.org/10.1016/j.conbuildmat.2018.05.139.
[736] Q.J. Zheng, Z.Y. Zhou, A.B. Yu, Contact forces between viscoelastic ellipsoidal particles, Powder Technol. 248 (2013) 25–33.
[737] A.K. Turner, Felix H. Kim, Dayakar Penumadu, Eric B. Herbold, Meso-scale framework for modeling granular material using computed tomography, Comput. Geotech. 76 (2016) 140–146, https://doi.org/10.1016/j.compgeo.2016.02.019.
[738] K. Kildashti, B. Samali Dong, An accurate geometric contact force model for super-quadric particles, CMAME 360 (2020) 112774.
[739] Qingchun Yuan, Xiaodong Jia, Richard Williams, Validation of a multi-component digital dissolution model for irregular particles, Powder Technol. 240 (2013) 25–30, https://doi.org/10.1016/j.powtec.2012.07.011.
[740] X. Jia, N. Gopinathan, R.A. Williams, Modeling complex packing structures and their thermal properties, Adv. Powder Technol. 13 (1) (2002) 55–71, https://doi.org/10.1163/15685520252900956.
[741] J. Lind Steven, D. Rogers Benedict, K. Stansby Peter, Review of smoothed particle hydrodynamics: towards converged Lagrangian flow modelling, Proc. R. Soc. (2020), https://doi.org/10.1098/rspa.2019.0801.
[742] C.K. Aidun, Jonathan R. Clausen, Lattice-Boltzmann method for complex flows, Annu. Rev. Fluid Mech. 42 (2010) 439–472, https://doi.org/10.1146/annurev-fluid-121108-145519.
[743] T. Krüger, Halim Kusumaatmaja, Alexandr Kuzmin, Orest Shardt, Goncalo Silva, Erlend Magnus Viggen, The Lattice Boltzmann Method: Principles and Practice, 2017. ISBN: 978-3-319-83103-9.
[744] Y. Han, P.A. Cundall, Lattice Boltzmann modeling of pore-scale fluid flow through idealized porous media, Int. J. Numer. Methods Fluids 67 (2011) 1720–1734.
[745] A.J.C. Ladd, Numerical simulations of particulate suspensions via a discretized Boltzmann equation Part I. Theoretical foundation, and Part II. Numerical results,

J. Fluid Mech. 271 (1994) 311–339, https://doi.org/10.1017/S0022112094001783, 285-309, and.
[746] A.J.C. Ladd, R. Verberg, Lattice-Boltzmann simulations of particle-fluid suspensions, J. Stat. Phys. 104 (2001) 1191–1251, https://doi.org/10.1023/A:1010414013942.
[747] P. Zhang, S.A. Galindo-Torres, Hongwu Tang, Guangqiu Jin, A. Scheuermann, Ling Li, Lattice Boltzmann simulations of settling behaviors of irregularly shaped particles, Phys. Rev. E 93 (2016) 062612, https://doi.org/10.1103/PhysRevE.93.062612.
[748] P. Adhav, Xavier Besseron, Bernhard Peters, Development of 6-way CFD-DEM-FEM momentum coupling interface using partitioned coupling approach, Results Eng. 22 (2024) 102214, https://doi.org/10.1016/j.rineng.2024.102214.
[749] Ante Munjiza, The Combined Finite-Discrete Element Method, Wiley, Chichester, 2004. ISBN 978-0-470-84199-0.
[750] J. Stránsky, Open source DEM–FEM coupling, in: PARTICLES III: Proceedings of the III International Conference on Particle-Based Methods: Fundamentals and Applications, CIMNE, 2013, pp. 46–57. http://hdl.handle.net/2117/188310. ISBN:978-84-941531-8-1.
[751] D. Wei, Ryan C. Hurley, Leong Hien Poh, Daniel Dias-da-Costa, Yixiang Gan, The role of particle morphology on concrete fracture behaviour: A Meso-scale modelling approach, Cem. Concr. Res. 134 (2020) 106096, https://doi.org/10.1016/j.cemconres.2020.106096.
[752] A. Farsi, Jiansheng Xiang, John-Paul Latham, Mikeal Carlsson, Hugh Stitt, Michele Marigo, Packing simulations of complex-shaped rigid particles using FDEM: An application to catalyst pellets, Powder Technol. 380 (2021) 443–461, https://doi.org/10.1016/j.powtec.2020.11.010.
[753] G. Ma, Wei Zhou, Richard A. Regueiro, Qiao Wang, Xiaolin Chang, Modeling the fragmentation of rock grains using computed tomography and combined FDEM, Powder Technol. 308 (2017) 388–397, https://doi.org/10.1016/j.powtec.2016.11.046.
[754] D. Wei, Budi Zhao, Yixiang Gan, Surface reconstruction with spherical harmonics and its application for single particle crushing simulations, J. Rock Mech. Geotech. Eng. 14 (1) (2022) 232–239, https://doi.org/10.1016/j.jrmge.2021.07.016.
[755] Y. Zheng, Chengzeng Yan, Hong Zheng, Modified joint element constitutive model for FDEM to simulate the nonlinear mechanical behavior of rocks, Comput. Geotech. 164 (2023) 105831, https://doi.org/10.1016/j.compgeo.2023.105831.
[756] Y. Tsuji, T. Kawaguchi, T. Tanaka, Discrete particle simulation of two-dimensional fluidized bed, Powder Technol. 77 (1) (1993) 79–87, https://doi.org/10.1016/0032-5910(93)85010-7.
[757] T. Tsuji, Keizo Yabumoto, Toshitsugu Tanaka, Spontaneous structures in three-dimensional bubbling gas-fluidized bed by parallel DEM–CFD coupling simulation, Powder Technol. 184 (2) (2008) 132–140, https://doi.org/10.1016/j.powtec.2007.11.042.
[758] J.E. Hilton, D.Y. Ying, P.W. Cleary, Modelling spray coating using a combined CFD–DEM and spherical harmonic formulation, Chem. Eng. Sci. 99 (2013) 141–160, https://doi.org/10.1016/j.ces.2013.05.051.
[759] Q. Hou, E. Dianyu, Shibo Kuang, Aibing Yu, A process scaling approach for CFD-DEM modelling of thermochemical behaviours in moving bed reactors, Fuel Process. Technol. 202 (2020) 106369, https://doi.org/10.1016/j.fuproc.2020.106369.
[760] X. Liu, Jieqing Gan, Wenqi Zhong, Aibing Yu, Particle shape effects on dynamic behaviors in a spouted bed: CFD-DEM study, Powder Technol. 361 (2020) 349–362, https://doi.org/10.1016/j.powtec.2019.07.099.
[761] A.P. Kieckhefen, S. Pietsch, R. Aguado, M. Olazar, S. Heinrich, Unresolved CFD-DEM simulation of spherical and ellipsoidal particles in conical and prismatic spouted beds, Powder Technol. 389 (2021) 493–506, https://doi.org/10.1016/j.powtec.2021.05.012.
[762] S. Golshan, R. Sotudeh-Gharebagh, R. Zarghami, N. Mostoufi, B. Blais, J.A. M. Kuipers, Review and implementation of CFD-DEM applied to chemical process systems, Chem. Eng. Sci. 221 (2020) 115646, https://doi.org/10.1016/j.ces.2020.115646.
[763] M.A. El-Emam, L. Zhou, W. Shi, et al., Theories and applications of CFD–DEM coupling approach for granular flow: A review, Arch. Computat. Methods Eng. 28 (2021) 4979–5020, https://doi.org/10.1007/s11831-021-09568-9.
[764] Dianyu E, Peng Zhou, Suya Guo, Jia Zeng, Jiaxin Cui, Youyuan Jiang, Yuanxiang Lu, Zeyi Jiang, Zhengquan Li, Shibo Kuang, Particle shape effect on hydrodynamics and heat transfer in spouted bed: a CFD–DEM study, Particuology 69 (2022) 10–21, https://doi.org/10.1016/j.partic.2021.11.009.
[765] D. Gou, Yansong Shen, GPU-accelerated CFD-DEM modeling of gas-solid flow with complex geometry and an application to raceway dynamics in industry-scale blast furnaces, Chem. Eng. Sci. 294 (2024) 120101, https://doi.org/10.1016/j.ces.2024.120101.
[766] M. Wang, Y.T. Feng, D.R.J. Owen, T.M. Qu, A novel algorithm of immersed moving boundary scheme for fluid–particle interactions in DEM–LBM, Comput. Methods Appl. Mech. Eng. 346 (2019) 109–125, https://doi.org/10.1016/j.cma.2018.12.001.
[767] Ali Abbas Zaidi, Particle resolved direct numerical simulation of free settling particles for the study of effects of momentum response time on drag force, Powder Technol. 335 (2018) 222–234, https://doi.org/10.1016/j.powtec.2018.04.058.
[768] K. Washino, L. Chan Ei, Giang T. Nguyen, Taichi Tsujimoto, Takuya Tsuji, Toshitsugu Tanaka, Fully resolved CFD–DEM coupling model for gas-liquid-solid flows with non-spherical particles, DEM9 (2023) 73. https://www.dem9.fau.de/.
[769] Mohammad Hassan Ahmadian, Wenbo Zheng, Simulating the fluid–solid interaction of irregularly shaped particles using the LBM-DEM coupling method, Comput. Geotech. 171 (2024) 106395, https://doi.org/10.1016/j.compgeo.2024.106395. ISSN 0266-352X.
[770] Ming Xia, Liuhong Deng, Fengqiang Gong, Tongming Qu, Y.T. Feng, Jin Yu, An MPI parallel DEM-IMB-LBM framework for simulating fluid-solid interaction problems, J. Rock Mech. Geotechn. Eng. 16 (6) (2024) 2219–2231, https://doi.org/10.1016/j.jrmge.2024.01.007. ISSN 1674-7755.
[771] F. Zhang, B. Damjanac, J. Furtney, DEM coupled with Lattice-Boltzmann Method (LBM), in: Coupled Thermo-Hydro-Mechanical Processes in Fractured Rock Masses, Springer, Cham, 2023, https://doi.org/10.1007/978-3-031-25787-2_5.
[772] S.L. Brunton, Bernd R. Noack, Petros Koumoutsakos, Machine learning for fluid mechanics, Annu. Rev. Fluid Mech. 52 (2020) 477–508, https://doi.org/10.1146/annurev-fluid-010719-060214.
[773] L. Lu, Xi Gao, Jean-François Dietiker, Mehrdad Shahnam, William A. Rogers, Machine learning accelerated discrete element modeling of granular flows, Chem. Eng. Sci. 245 (2021) 116832, https://doi.org/10.1016/j.ces.2021.116832.
[774] Z. Lai, Q. Chen, L. Huang, Machine-learning-enabled discrete element method: contact detection and resolution of irregular-shaped particles, Int. J. Numer. Anal. Methods 46 (2022) 113–140, https://doi.org/10.1002/nag.3293.
[775] T. Zhang, Shuang Li, Huanzhi Yang, Fanyu Zhang, prediction of constrained modulus for granular soil using 3D discrete element method and convolutional neural networks, J. Rock Mech. Geotech. Eng. (2024), https://doi.org/10.1016/j.jrmge.2024.02.005 (in press).
[776] L. He, Danesh K. Tafti, A supervised machine learning approach for predicting variable drag forces on spherical particles in suspension, Powder Technol. 345 (2019) 379–389, https://doi.org/10.1016/j.powtec.2019.01.013.
[777] S. Rushd, Mohammad Tanvir Parvez, Majdi Adel Al-Faiad, Mohammed Monirul Islam, Towards optimal machine learning model for terminal settling velocity, Powder Technol. 387 (2021) 95–107, https://doi.org/10.1016/j.powtec.2021.04.011.
[778] B. Ouyang, Li-Tao Zhu, Zheng-Hong Luo, Machine learning for full spatiotemporal acceleration of gas-particle flow simulations, Powder Technol. 408 (2022) 117701, https://doi.org/10.1016/j.powtec.2022.117701.
[779] S. Chen, Laurent A. Baumes, Aytekin Gel, Manogna Adepu, Heather Emady, Jiao Yang, Classification of particle height in a hopper bin from limited discharge data using convolutional neural network models, Powder Technol. 339 (2018) 615–624, https://doi.org/10.1016/j.powtec.2018.08.048.
[780] Fei-Liang Yuan, Combined 3D thinning and greedy algorithm to approximate realistic particles with corrected mechanical properties, Granul. Matter 21 (2019), https://doi.org/10.1007/s10035-019-0874-x.
[781] K. Giannis, Christoph Thon, Guoqing Yang, Arno Kwade, Carsten Schilde, Predicting 3D particles shapes based on 2D images by using convolutional neural network, Powder Technol. 432 (2024) 119122, https://doi.org/10.1016/j.powtec.2023.119122.
[782] B. Fauseweh, Quantum many-body simulations on digital quantum computers: state-of-the-art and future challenges, Nat. Commun. 15 (2024) 2123, https://doi.org/10.1038/s41467-024-46402-9.
[783] O. Hughes, 'Quantum-inspired' laser computing is more effective than both supercomputing and quantum computing, startup claims, in: LiveScience News, 14 May 2024, 2024. https://www.livescience.com/technology/computing/quantum-inspired-laser-computing-is-more-effective-than-either-supercomputing-or-quantum-computing-startup-claims.
[784] P. Henzler, J. Mitra Niloy, Tobias Ritschel, Escaping plato's cave: 3d shape from adversarial rendering, in: Proceedings of the IEEE/CVF International Conference on Computer Vision, 2019, pp. 9984–9993.
[785] X. Zhou, S. Xuanyuan, Y. Ye, Y. Sun, H. Du, L. Qi, C. Li, C. Xie, Predicting bulk density for agglomerated raspberry ketone via integrating morphological and size metrics using artificial neural networks, Processes 12 (5) (2024) 902, https://doi.org/10.3390/pr12050902.
[786] M. Batarfi, M. Mareboyana, Exploring the role of extracted features in deep learning-based 3D face reconstruction from single 2D images, in: 2023 3rd International Conference on Electrical, Computer, Communications and Mechatronics Engineering (ICECCME), Tenerife, Canary Islands, Spain 2023, 2023, pp. 1–7, https://doi.org/10.1109/ICECCME57830.2023.10252913.
[787] H. Diao, X. Jiang, Y. Fan, M. Li, H. Wu, 3D face reconstruction based on a single image: a review, in: IEEE Access vol. 12, 2024, pp. 59450–59473, https://doi.org/10.1109/ACCESS.2024.3381975.
[788] J. Ahn Dib, C. Thébault, P.H. Gosselin, L. Chevallier, S2F2: self-supervised high fidelity face reconstruction from monocular image, in: 2023 IEEE 17th International Conference on Automatic Face and Gesture Recognition (FG), Waikoloa Beach, HI, USA, 2023, pp. 1–8, https://doi.org/10.1109/FG57933.2023.10042713.
[789] X. Suo, Overview of 3D human face reconstruction techniques and a novel approach, in: 2023 Congress in Computer Science, Computer Engineering, & Applied Computing (CSCE), Las Vegas, NV, USA 2023, 2023, pp. 1975–1982, https://doi.org/10.1109/CSCE60160.2023.00325.
[790] D. Blatner, Spectrums: Our Mind-Boggling Universe from Infinitesimal to Infinity, Bloomsbury Pub Plc USA, 2014. Reprint edition (11 Feb. 2014) ISBN-10: 1620405202.
[791] Y. Li, 3 Dimensional Dense Reconstruction: A Review of Algorithms and Dataset. arXiv preprint arXiv:2304.09371 (2023).
[792] M. Bichsel, A.P. Pentland, A simple algorithm for shape from shading, in: Proceedings 1992 IEEE Computer Society Conference on Computer Vision and Pattern Recognition, IEEE Computer Society, 1992, January, pp. 459–460, https://doi.org/10.1109/CVPR.1992.223150.

[793] R. Zhang, Tsai Ping-Sing, J.E. Cryer, M. Shah, Shape-from-shading: a survey, IEEE Trans. Pattern Anal. Mach. Intell. 21 (8) (Aug. 1999) 690–706, https://doi.org/10.1109/34.784284.
[794] S. Augenstein, S. Rock, Simultaneous Estimaton of target pose and 3-D shape using the FastSLAM algorithm, in: AIAA Guidance, Navigation, and Control Conference, 2009, August, p. 5782, https://doi.org/10.2514/6.2009-5782.
[795] A. Rathinam, A.G. Dempster, 3D reconstruction of an asteroid shape using visual SLAM for autonomous navigation, in: Proc. 17th Autralian Space Res. Conf., 2017, pp. 87–96.
[796] L. Abada, Saliha Aouat, A machine learning approach for shape from shading, in: 2nd International Conference on Signal, Image, Vision and their Applications (SIVA'13), November 18–20, 2013 - Guelma, Algeria, 2013, https://doi.org/10.48550/arXiv.1607.03284.
[797] O.E.F. Bourahla, A.M. Debbah, L. Abada, S. Aouat, Shape from shading: a non-iterative method using neural networks, in: A. Abraham, T. Hanne, O. Castillo, N. Gandhi, T. Nogueira Rios, T.P. Hong (Eds.), Hybrid Intelligent Systems. HIS 2020. Advances in Intelligent Systems and Computing vol 1375, Springer, Cham, 2021, https://doi.org/10.1007/978-3-030-73050-5_74.
[798] X. Han, Todd Zickler, Curvature fields from shading fields, in: Proceedings of the NeurIPS Workshop on Symmetry and Geometry in Neural Representations 228, PMLR, 2023.
[799] Y. Kuroe, H. Kawakami, Shape from shading by model inclusive learning method with simultaneous estimation of parameters, in: A. Lintas, S. Rovetta, P. Verschure, A. Villa (Eds.), Artificial Neural Networks and Machine Learning – ICANN 2017. ICANN 2017. Lecture Notes in Computer Science( ) vol 10614, Springer, Cham, 2017, https://doi.org/10.1007/978-3-319-68612-7_20.
[800] C. Hernández, G. Vogiatzis, Shape from photographs: a multi-view stereo pipeline, in: R. Cipolla, S. Battiato, G.M. Farinella (Eds.), Computer Vision. Studies in Computational Intelligence vol 285, Springer, Berlin, Heidelberg, 2010, https://doi.org/10.1007/978-3-642-12848-6_11.
[801] C.B. Choy, D. Xu, J. Gwak, K. Chen, S. Savarese, 3D-R2N2: A unified approach for single and multi-view 3D object reconstruction, in: B. Leibe, J. Matas, N. Sebe, M. Welling, ECCV (Eds.), Lecture Notes in Computer Science, vol. 9912, Computer Vision - ECCV 2016. 14th European conference, Amsterdam, the Netherlands, October 11–14, 2016 : Proceedings, Springer, Cham, 2016, pp. 628–644.
[802] H. Xie, H. Yao, X. Sun, S. Zhou, S. Zhang, Pix2Vox: Context-Aware 3D reconstruction from single and multi-view images, in: 2019 IEEE/CVF International Conference on Computer Vision (ICCV), Seoul, Korea (South), 2019, pp. 2690–2698, https://doi.org/10.1109/ICCV.2019.00278.
[803] H. Xie, H. Yao, S. Zhang, et al., Pix2Vox++: multi-scale context-aware 3D object reconstruction from single and multiple images, Int. J. Comput. Vis. 128 (2020) 2919–2935, https://doi.org/10.1007/s11263-020-01347-6.
[804] A. Kar, C. Häne, J. Malik, Learning a multi-view stereo machine, in: NIPS, 2017, https://doi.org/10.48550/arXiv.1708.05375.
[805] M. Wang, L. Wang, Y. Fang, 3DensiNet: A robust neural network architecture towards 3D volumetric object prediction from 2D, Image (2017) 961–969, https://doi.org/10.1145/3123266.3123340.
[806] P. Huang, K. Matzen, J. Kopf, N. Ahuja, J. Huang, Deepmvs: learning multi-view stereopsis, in: CVPR, 2018, https://doi.org/10.48550/arXiv.1804.00650.
[807] D. Paschalidou, A.O. Ulusoy, C. Schmitt, L.V. Gool, A. Geiger, Raynet: Learning volumetric 3D reconstruction with ray potentials, in: CVPR, 2018, https://doi.org/10.48550/arXiv.1901.01535.
[808] B. Yang, S. Wang, A. Markham, et al., Robust attentional aggregation of deep feature sets for multi-view 3D reconstruction, Int. J. Comput. Vis. 128 (2020) 53–73, https://doi.org/10.1007/s11263-019-01217-w.
[809] B. Mildenhall, P.P. Srinivasan, M. Tancik, J.T. Barron, R. Ramamoorthi, R. Ng, Nerf: Representing scenes as neural radiance fields for view synthesis, Communications of the ACM 65 (1) (2021) 99–106.
[810] K. Gao, Y. Gao, H. He, D. Lu, L. Xu, J. Li, NeRF: Neural Radiance Field in 3D Vision, A Comprehensive Review. arXiv preprint arXiv:2210.00379 (2022).
[811] P. Wang, Lingjie Liu, Yuan Liu, Christian Theobalt, Taku Komura, Wenping Wang, NeuS: learning neural implicit surfaces by volume rendering for multi-view reconstruction, in: 35th Conference on Neural Information Processing Systems 2021, NeurIPS, 2021, https://doi.org/10.48550/arXiv.2106.10689.
[812] P. Wang, L. Liu, Y. Liu, C. Theobalt, T. Komura, W. Wang, NeuS: Learning neural implicit surfaces by volume rendering for multi-view reconstruction, in: M. Ranzato, A. Beygelzimer, Y. Dauphin, P.S. Liang, J. Wortman Vaughan (Eds.), Advances in Neural Information Processing Systems 34, Curran Assoicates, Inc, 2021, pp. 27171–27183. https://hdl.handle.net/21.11116/0000-0009-5276-6.
[813] Y. Wang, Q. Han, M. Habermann, K. Daniilidis, C. Theobalt, L. Liu, Neus2: Fast learning of neural implicit surfaces for multi-view reconstruction. in: Proceedings of the IEEE/CVF International Conference on Computer Vision (2023) pp. 3295-3306.
[814] Q. Fu, Qingshan Xu, Yew-Soon Ong, Wenbing Tao, Geo-neus: Geometry-consistent neural implicit surfaces learning for multi-view reconstruction, Adv. Neural Inform. Proc. Syst. (NeurIPS) (2022), https://doi.org/10.48550/arXiv.2205.15848.
[815] H. Jiang, C. Zeng, R. Chen, S. Liang, Y. Han, Y. Gao, C. Wang, Depth-neus: neural implicit surfaces learning for multi-view reconstruction based on depth information optimization, 2023, https://doi.org/10.48550/arXiv.2303.17088.
[816] Y.C. Cheng, H.Y. Lee, S. Tulyakov, A. Schwing, L. Gui, SDFusion: multimodal 3D shape completion, reconstruction, and generation, in: 2023 IEEE/CVF Conference on Computer Vision and Pattern Recognition (CVPR), Vancouver, BC, Canada, 2023, pp. 4456–4465, https://doi.org/10.1109/CVPR52729.2023.00433.
[817] P. Zheng, Y. Ding, J. Wang Shen, Z. Zhang, Research on 3D object reconstruction based on single-view RGB image, in: 2023 IEEE International Symposium on Broadband Multimedia Systems and Broadcasting (BMSB), Beijing, China, 2023, pp. 1–5, https://doi.org/10.1109/BMSB58369.2023.10211145.
[818] Z. Huang, V. Jampani, A. Thai, Y. Li, S. Stojanov, J.M. Rehg, ShapeClipper: scalable 3D shape learning from single-view images via geometric and CLIP-based consistency, in: 2023 IEEE/CVF Conference on Computer Vision and Pattern Recognition (CVPR), Vancouver, BC, Canada, 2023, pp. 12912–12922, https://doi.org/10.1109/CVPR52729.2023.01241.
[819] A. Radford, Jong Wook Kim, Chris Hallacy, Aditya Ramesh, Gabriel Goh, Sandhini Agarwal, Girish Sastry, Amanda Askell, Pamela Mishkin, Jack Clark, et al., Learning transferable visual models from natural language supervision, in: International Conference on Machine Learning, PMLR, 2021, pp. 8748–8763, https://doi.org/10.48550/arXiv.2103.00020.
[820] K.V. Alwala, Abhinav Gupta, Shubham Tulsiani, Pre-train, self-train, distill: A simple recipe for supersizing 3d reconstruction, in: Proceedings of the IEEE/CVF Conference on Computer Vision and Pattern Recognition, 2022, pp. 3773–3782.
[821] K.L. Navaneet, Ansu Mathew, Shashank Kashyap, Wei-Chih Hung, Varun Jampani, R. Venkatesh Babu, From image collections to point clouds with self-supervised shape and pose networks, in: Proceedings of the IEEE/CVF Conference on Computer Vision and Pattern Recognition, 2020, pp. 1132–1140.
[822] S. Wu, Christian Rupprecht, Andrea Vedaldi, Unsupervised learning of probably symmetric deformable 3d objects from images in the wild, in: Proceedings of the IEEE/CVF Conference on Computer Vision and Pattern Recognition, 2020, pp. 1–10.
[823] C.-H. Lin, Chaoyang Wang, Simon Lucey, Sdfsrn: Learning signed distance 3d object reconstruction from static images. NIPS'20: Proceedings of the 34th International Conference on Neural Information Processing Systems Article No.: 961, P. 11453–11464. https://doi.org/10.48550/arXiv.2010.10505.
[824] X. Yan, Jimei Yang, Ersin Yumer, Yijie Guo, Honglak Lee, Perspective transformer nets: Learning single view 3d object reconstruction without 3d supervision, NIPS (2016) 1696–1704, https://doi.org/10.48550/arXiv.1612.00814.
[825] A. Kanazawa, Shubham Tulsiani, Alexei A. Efros, Jitendra Malik, Learning category-specific mesh reconstruction from image collections, in: Proceedings of the European Conference on Computer Vision (ECCV), 2018, pp. 371–386.
[826] P. Henderson, Vittorio Ferrari, Learning single-image 3d reconstruction by generative modelling of shape, pose and shading, Int. J. Comput. Vis. (2019) 1–20.
[827] T. Monnier, Matthew Fisher, Alexei A. Efros, Mathieu Aubry, Share With Thy Neighbors: Single-View Reconstruction by Cross-Instance Consistency, ECCV, 2022.
[828] T. Samavati, M. Soryani, Deep learning-based 3D reconstruction: a survey, Artif. Intell. Rev. 56 (2023) 9175–9219, https://doi.org/10.1007/s10462-023-10399-2.
[829] A. Esteva, Katherine Chou, Serena Yeung, Nikhil Naik, Ali Madani, Ali Mottaghi, Yun Liu, Eric Topol, Jeff Dean, Richard Socher, Deep learning-enabled medical computer vision, NPJ Digit. Med. 4 (2021) 5, https://doi.org/10.1038/s41746-020-00376-2.
[830] X. Li, Lei Zhang, Jingsi Yang, Fei Teng, Role of artificial intelligence in medical image analysis: a review of current trends and future directions, J. Med. Biol. Eng. (2024), https://doi.org/10.1007/s40846-024-00863-x.
[831] X. Wang, H. Zhang, Z.-Y. Yin, D. Su, Z. Liu, Deep-learning-enhanced model reconstruction of realistic 3D rock particles by intelligent video tracking of 2D random particle projections, Acta Geotech. (2022) 1–24.
[832] S. Kench, I. Squires, A. Dahari, et al., MicroLib: A library of 3D microstructures generated from 2D micrographs using SliceGAN, Sci. Data 9 (2022) 645, https://doi.org/10.1038/s41597-022-01744-1.
[833] K.H. Lee, G.J. Yun, Multi-plane denoising diffusion-based dimensionality expansion for 2D-to-3D reconstruction of microstructures with harmonized sampling, NPJ Comput. Mater. 10 (99) (2024), https://doi.org/10.1038/s41524-024-01280-z.
[834] J. Phan, M. Sarmad, L. Ruspini, et al., Generating 3D images of material microstructures from a single 2D image: a denoising diffusion approach, Sci. Rep. 14 (2024) 6498, https://doi.org/10.1038/s41598-024-56910-9.
[835] K. He, X. Zhang, S. Ren and J. Sun, "Deep Residual Learning for Image Recognition," 2016 IEEE Conference on Computer Vision and Pattern Recognition (CVPR), Las Vegas, NV, USA, 2016, pp. 770-778, doi: 10.1109/CVPR.2016.90.
[836] Y. Liu, Teng Ran, Yuan Liang, Kai Lv, Guoquan Zheng, 3D face reconstruction from a single image based on hybrid-level contextual information with weak supervision, Comput. Graph. 118 (2024) 80–89, https://doi.org/10.1016/j.cag.2023.11.007.
[837] G. Ping, H. Wang, PushNet: 3D reconstruction from a single image by pushing, Neural Comput. & Applic. 36 (2024) 6629–6641, https://doi.org/10.1007/s00521-023-09408-w.
[838] G. Gkioxari, J. Johnson, J. Malik, Mesh R-CNN, in: 2019 IEEE/CVF International Conference on Computer Vision (ICCV), 2019, pp. 9784–9794, https://doi.org/10.1109/ICCV.2019.00988.
[839] S.S. Aremu, A. Taherkhani, C. Liu, S. Yang, 3D object reconstruction with deep learning, in: Z. Shi, J. Torresen, S. Yang (Eds.), Intelligent Information Processing XII. IIP 2024. IFIP Advances in Information and Communication Technology vol 704, Springer, Cham, 2024, https://doi.org/10.1007/978-3-031-57919-6_12.
[840] R. Dalai, N. Dalai, K.K. Senapati, An accurate volume estimation on single view object images by deep learning based depth map analysis and 3D reconstruction, Multimed. Tools Appl. 82 (2023) 28235–28258, https://doi.org/10.1007/s11042-023-14615-7.

[841] W. Chen, Jun Gao, Huan Ling, Edward J. Smith, Jaakko Lehtinen, Alec Jacobson, Sanja Fidler, Learning to predict 3D objects with an interpolation-based differentiable renderer, NeurIPS 2019 (2019), https://doi.org/10.48550/arXiv.1908.01210.
[842] T. Takikawa, Joey Litalien, Kangxue Yin, Karsten Kreis, Charles Loop, Derek Nowrouzezahrai, Alec Jacobson, Morgan McGuire, Sanja Fidler, Neural geometric level of detail: real-time rendering with implicit 3D Shapes, in: Proceedings of the IEEE/CVF Conference on Computer Vision and Pattern Recognition (CVPR), 2021, https://doi.org/10.48550/arXiv.2101.10994.
[843] Z. Li, Thomas Müller, Alex Evans, Russell H. Taylor, Mathias Unberath, Ming-Yu Liu, Chen-Hsuan Lin, Neuralangelo: High-Fidelity Neural Surface Reconstruction 2023, CVPR, 2023, https://doi.org/10.48550/arXiv.2306.03092.
[844] RapidScan Systems. https://www.rapiscansystems.com/en/products/920ct, 2024.
[845] A. Velten, T. Willwacher, O. Gupta, A. Veeraraghavan, M.G. Bawendi, R. Raskar, Recovering ThreeDimensional shape around a corner using ultra-fast time-of-flight imaging, Nat. Commun. (March 2012) (2012), https://doi.org/10.1038/ncomms1747.
[846] Andreas Velten, Di Wu, Adrián Jarabo, Belen Masia, Christopher Barsi, Chinmaya Joshi, Everett Lawson, Moungi Bawendi, Diego Gutiérrez, Ramesh Raskar, Femto-photography: capturing and visualizing the propagation of light, ACM Trans. Graph. (TOG). 32 (2013), https://doi.org/10.1145/2461912.2461928.
[847] G.W. Delaney, R.D. Morrison, M.D. Sinnott, S. Cummins, P.W. Cleary, DEM modelling of non-spherical particle breakage and flow in an industrial scale cone crusher, Min. Eng. 74 (2015) 112–122, https://doi.org/10.1016/j.mineng.2015.01.013. ISSN 0892-6875.
[848] Z.-K. Feng, Wen-Jie Xu, Retief Lubbe (2020) three-dimensional morphological characteristics of particles in nature and its application for DEM simulation, Powder Technol. 364 (2020) 635–646, https://doi.org/10.1016/j.powtec.2020.02.022.
[849] S.O. Farah, M. Guessasma, E. Bellenger, Digital twin by DEM for ball bearing operating under EHD conditions, Mechan. Industry 21 (2020) 506, https://doi.org/10.1051/meca/2020022.
[850] A. Feoktistov, Oleg Zolotarev, Digital twin in the mining industry: a grinding mill case study, 2021. https://youtu.be/91gc9iB1AhI.
[851] B. Jenkins, G. Lumay, F. Francqui, A.L. Nicusan, A. Neveu, J. Seville, C.R. K. Windows-Yule, Development and Applications of DEM Digital Twins of Powder Systems. https://mfix.netl.doe.gov/wp-content/uploads/2022/08/Jenkins-Ben.pdf, 2022.
[852] M. Moreno-Benito, Kai T. Lee, Denis Kaydanov, Hugh M. Verrier, Daniel O. Blackwood, Pankaj Doshi, Digital twin of a continuous direct compression line for drug product and process design using a hybrid flowsheet modelling approach, Int. J. Pharm. 628 (2022) 122336, https://doi.org/10.1016/j.ijpharm.2022.122336.
[853] A. Neveu, Geoffroy Lumay, Filip Francqui, Digital twins to improve the calibration of DEM simulation of powder processes, in: DEM9:119, 2023. https://www.dem9.fau.de/.
[854] M. Sakai, What technologies are essential in development of the DEM-based digital twin?, in: Plenary Talk, DEM-9 Erlangen, Germany, 18 September 2023, 2023.
[855] M. Wu, Jianfeng Wang, Adrian Russell, Zhuang Cheng, DEM modeling of mini-triaxial test based on one-to-one mapping of sand particles, Géotechnique 71 (8) (2021) 714–727, https://doi.org/10.1680/jgeot.19.P.212.
[856] M.S. Al-Sarouri, Ali Hassanpour, X. Jia, Virtual Reality Packing Optimisation for Nuclear Decommissioning, MEng Project Report, University of Leeds, 2024.
[857] O. Torgersrud, Hans Jodstad, Khoa Huynh, Santiago Quinteros, Ana Page, Suzanne Lacasse, Virtual reality testing for more reliable design in sand, in: 20th ICSMGE 2022, Sydney, Australia, 2022.
[858] J. Jumper, R. Evans, A. Pritzel, et al., Highly accurate protein structure prediction with AlphaFold, Nature 596 (2021) 583–589, https://doi.org/10.1038/s41586-021-03819-2.
[859] J. Abramson, J. Adler, J. Dunger, et al., Accurate structure prediction of biomolecular interactions with AlphaFold 3, Nature (2024), https://doi.org/10.1038/s41586-024-07487-w.
[860] W.M. Kincannon, Michael Zahn, Rita Clare, Jessica Lusty Beech, Ari Romberg, James Larson, Brian Bothner, Gregg T. Beckham, John E. McGeehan, Jennifer L. DuBois, Biochemical and structural characterization of an aromatic ring–hydroxylating dioxygenase for terephthalic acid catabolism, Proc. Natl. Acad. Sci. 119 (13) (2022) e2121426119, https://doi.org/10.1073/pnas.2121426119.
[861] K.T. Ko, F. Lennartz, D. Mekhaiel, et al., Structure of the malaria vaccine candidate Pfs48/45 and its recognition by transmission blocking antibodies, Nat. Commun. 13 (2022) 5603, https://doi.org/10.1038/s41467-022-33379-6.

Further-reading

[862] R. Cabiscol, J.H. Finke, A. Kwade, Calibration and interpretation of DEM parameters for simulations of cylindrical tablets with multi-sphere approach, Powder Technol. 327 (2018) 232–245.
[863] X. Lin, T.-T. Ng, Contact detection algorithms for three-dimensional ellipsoids in discrete element modelling, Int. J. Numer. Anal. Methods Geomech. 19 (1995) 653–659, https://doi.org/10.1002/nag.1610190905.